INVESTIGATING THE GROUNDWATER DEPENDENCE AND RESPONSE TO RAINFALL VARIABILITY OF VEGETATION IN THE TOUWS RIVER AND CATCHMENT USING REMOTE SENSING

By

SINETHEMBA DLIKILILI

A thesis submitted in fulfilment of the requirements for the degree Master of Arts in the Faculty of Arts, Department of Geography, Environmental Studies and Tourism, University of the Western Cape, Bellville

Supervisor: [1]Dr. Suzanne Grenfell

Co-supervisor: [2]Dr. Michael Grenfell

[1]University of the Western Cape, Department of Geography, Environmental Studies and Tourism, P/Bag X17, Bellville, 7535, South Africa

[2]University of the Western Cape, Department of Earth Sciences, P/Bag X17, Bellville, 7535, South Africa

2019

KEYWORDS

Climatic variability

Groundwater dependence

Semi-arid Karoo

NDVI

ABSTRACT

Changes in climate patterns have raised concerns for environmentalists globally and across southern Africa. The changes greatly affect the growth dynamics of vegetation to such an extent that climate elements such as rainfall have become the most important determinant of vegetation growth. In arid and semi-arid environments, vegetation relies on near-surface groundwater as the main source of water. Changes in the environment due to climate can be examined by using remotely sensed data. This approach offers an affordable and easy means of monitoring the impact of climate variability on vegetation growth. This study examined the response of vegetation to rainfall and temperature, and assessed the dependence thereof on groundwater in a climatically variable region of the semi-arid Karoo.

The methodology used included sampling plant species in the riparian and non-riparian areas over two plant communities in seven vegetation plots. The Normalised Difference Vegetation Index (NDVI) derived from the Landsat OLI and TM was used to measure vegetation productivity. This was compared with rainfall totals derived from the Climate Hazards Group InfraRed Precipitation with Station data (CHIRPS) and the mean monthly temperature totals. A drought index, (Standardised Precipitation Index – SPI) was an additional analysis to investigate rainfall variability. Object-based Image Analysis (OBIA) and Maximum Likelihood supervised classification approaches together with indicators of groundwater discharge areas (Topographic Wetness Index – TWI, and profile curvature) were used to map vegetation and surface water that depend on groundwater.

The findings showed that the study region is dominated by shrubland with most plant species characterized as drought-resistant. The NDVI trends and rainfall patterns displayed a weak association in most vegetation plots, with the former responding a few months after a major rainfall event. The rainfall showed a decreasing trend (-1.127 mm/year) over the years while temperatures showed an increasing trend, particularly maximum temperatures (0.057°C/year). A rainfall anomaly and an SPI-12 displayed a cycle of wet and dry seasons, approximating 4 to 6 years. Analysis showed that temperature is strongly related to NDVI (r = 0.47 and r = 0.45 for maximum and minimum temperatures respectively), while long-term rainfall was not significantly associated with NDVI (r = 0.10). At a vegetation community scale,

the NDVI responded differently to rainfall and temperatures in the floodplain woodland and the hillslope shrubland communities when compared with the immediately preceding rainfall (i.e. no lag) and the preceding 3-month rainfall totals. In the hillslope shrubland community the NDVI had a strong correlation with both climate elements and in the floodplain woodland, it only showed a strong correlation with temperatures in most vegetation plots. In assessing the combined effect of rainfall and temperature on vegetation productivity, the multiple regression model suggests that both climate elements are contributing factors to vegetation growth. The land cover classification results and indicators of groundwater discharge areas highlighted areas where vegetation and surface water may be considered groundwater dependent in that both consistently display greenness and wetness despite prolonged dry periods.

DECLARATION

I declare that *'Investigating the groundwater dependence and response to rainfall variability of vegetation in the Touws River and catchment using remote sensing'* is my own work, that it has not been submitted for any degree or examination in any other university, and that all the sources I have used or quoted have been indicated and acknowledged by complete reference. This thesis has been submitted to turnitin and the report checked by my supervisor.

Sinethemba Dlikilili Date……

Signed……

ACKNOWLEDGEMENTS

I would like to express my special appreciation and thanks of gratitude to my supervisors, Dr. S Grenfell and Dr. M Grenfell, for their great kindness, insights and generous guidance throughout the course of my research. Thank you for being more than supervisors, I feel incredibly fortunate to have been your mentee.

A genuine gratitude to the Non-perennial rivers research project, funded by anonymous donors, for funding this project, including fieldtrip and WorldView image expenses. A special thanks to my friend, Faeeza Fortune, who has helped and supported me unconditionally throughout the project.

I would also like to express my sincere appreciation to my family for moral support and for motivation throughout my studies.

LIST OF ABBREVIATIONS

ADEs	Aquifer Dependent Ecosystems
ARC-ISCW	Agricultural Research Council Institute for Soil, Climate, and Water
CHIRPS	Climate Hazards Group Infrared Precipitation with Station data
CV	Coefficient of Variation
DEM	Digital Elevation Model
DN	Digital Numbers
GIS	Geographical Information Systems
GPS	Global Positioning System
IPCC	Intergovernmental Panel on Climate Change
IWRM	Integrated Water Resource Management
MSS	Multispectral Scanner System
MSS	Multi-scale segmentation
NDVI	Normalized Difference Vegetation Index
NDWI	Normalised Difference Wetness Index
NIR	Near-Infrared
NN	Nearest Neighbor
OBIA	Object-based Image Analysis
OLI	Operational Land Imager
ROI	Region of Interest
SANBI	South African National Biodiversity Institute
SANSA	South African National Space Agency
SAWS	South African Weather Service
SPI	Standardized Precipitation Index
SR	Surface Reflectance
TM	Thematic Mapper
TOA	Top of the Atmosphere
TWI	Topographic Wetness Index
USGS	United States Geological Survey
VI_s	Vegetation Indices
WV-2	WorldView-2

TABLE OF CONTENTS

KEYWORDS ii

ABSTRACT iii

DECLARATION v

ACKNOWLEDGEMENTS vi

LIST OF ABBREVIATIONS vii

TABLE OF CONTENTS viii

LIST OF FIGURES xiii

LIST OF TABLES xvi

CHAPTER ONE – INTRODUCTION 1

1.1. Background 1

1.2. Aim and objectives 2

1.3. Description of the study area 2

1.3.1. Location 2

1.3.2. Climate 3

1.3.3. Geology 5

1.3.3.1. Table Mountain Group (TMG) 6

1.3.3.2. Bokkeveld and Witteberg Groups 7

1.3.3.3. Dwyka Group 7

1.3.3.5. Ecca Group 7

1.3.4. Vegetation 8

1.3.4.1. Fynbos biome 8

1.3.4.2. Succulent Karoo biome 9

1.4. The structure of the thesis 9

CHAPTER TWO – LITERATURE REVIEW 11

2.1. Introduction 11

2.2. The role of temperature and rainfall on plant growth and development: a broader overview 11

2.2.1. Temperature 11

2.2.2. Precipitation 12

2.3. The influence of climate on vegetation productivity in the Touws River catchment and the Klein Karoo 13

2.4. Groundwater Dependent Ecosystems (GDEs) 14

2.4.1. Defining GDEs 14

2.4.2. Types of GDEs 15

2.4.3. The importance of understanding GDEs 15

2.5. Application of remote sensing on monitoring vegetation and identifying GDEs 16

2.5.1. Vegetation Indices (VI_s) 16

2.5.1.1. The Normalized Difference Vegetation Index (NDVI) 17

2.5.1.2. The Normalized Difference Water Index (NDWI) 17

2.5.2. Data analysis with multiple sensors 17

2.5.3. Image classification 18

2.5.3.1. Supervised classification 19

2.5.3.2. Unsupervised classification 20

2.5.3.3. Object-based image analysis 20

2.5.4. Accuracy assessment 22

2.5.5. Limitations of remote sensing 23

2.5.6. Overcoming limitations of remote sensing 23

2.5.7. A review of studies on the use of remote sensing in vegetation mapping and identifying GDEs 23

CHAPTER THREE – RESEARCH METHODS 25

3.1. Introduction 25

3.2. Data and data sources 25

3.2.1. Field-based vegetation data 25

3.2.1.1. Survey design 25

3.2.1.2. Identifying plant communities 27

3.2.1.3. Grouping sample plots 27

3.2.2. Satellite data 27

3.2.2.1. Sensors 27

3.2.2.2. Criteria for image selection 27

3.2.2.3. Image pre-processing 28

3.2.3. Climate data 30

3.2.3.1. Rainfall data 30

3.2.3.2. Temperature data 30

3.3. Methods 31

3.3.1. Vegetation density assessment 31

3.3.1.1. Normalized Difference Vegetation Index (NDVI) 31

3.3.2. Climatic data analysis 32

3.3.2.1. Examining rainfall seasonality 32

3.3.2.2. Measuring variations in rainfall 32

3.3.2.3. Standardized precipitation Index (SPI) 33

3.3.2.4. Analyzing seasonal temperatures 33

3.3.3. Linear correlation and multivariate analysis 34

3.3.4. Assessing Groundwater Dependent Ecosystems (GDEs) 35

3.3.4.1. Image classification 36

3.3.4.2. Indicators of groundwater discharge areas 39

3.3.4.3. Validation 40

CHAPTER FOUR – THE IMPACT OF RAINFALL AND TEMPERATURE ON VEGETATION PRODUCTIVITY, AND THE SPATIAL RANGE OF GROUNDWATER DEPENDENT ECOSYSTEMS (GDEs) 42

4.1. Results 42

4.1.1. Introduction 42

4.1.2. Vegetation analysis 42

4.1.2.1. Description of plant communities 42

4.1.2.2. Plant species by vegetation community 44

4.1.3. Inter-annual variability of NDVI and precipitation 45

4.1.4. Intra-annual rainfall variability 62

4.1.5. Long-term climatic trends 64

4.1.5.1. Analysis of precipitation trends 64

4.1.5.2. Analysis of temperature trends 67

4.1.6. Relational trends between NDVI, rainfall and temperature 68

4.1.7. The relationship between vegetation productivity, precipitation and temperature 73

4.1.7.1. Inter-annual correlation 73

4.1.7.2. Correlation by plant community in riparian and non-riparian area 75

4.1.8. The spatial range of Groundwater Dependent Ecosystems (GDEs) 79

4.1.8.1. An overview of land cover classification results 79

4.1.8.2. Assessment of classification in July 2017 79

4.1.8.3. Assessment of classification in September 2017 81

4.1.8.4. Assessment of classification in October 2017 83

4.1.8.5. Quantitative assessment of classification results 85

4.1.8.6. Analysis of the indicators of groundwater discharge areas 86

4.2. Discussion 89

4.2.1. Analysis of plant species 89

4.2.2. The influence of rainfall and temperature on vegetation productivity 90

4.2.3. The occurrence of probable Groundwater Dependent Ecosystems (GDEs) 92

4.2.3.1. Uncertainties 93

CHAPTER FIVE - GENERAL DISCUSSION, CONCLUSION AND RECOMMENDATIONS 94

5.1. General discussion 94

5.1.1. The response of plant communities to rainfall and temperature 94

5.1.2. Riparian vs non-riparian areas, and potential GDEs 95

5.2. Conclusion 97

5.3. Recommendations 98

References 99

APPENDIX A - Samples of plant species collected during the survey 116

APPENDIX B - Spectral and spatial characteristics of the used satellite sensors with acquisition dates 118

LIST OF FIGURES

Figure 1.1: The location of the selected quaternary catchments in South Africa and in the Western Cape Province 3

Figure 1.2: Map of the Gouritz WMA. The study area is located in the south-west (indicated by the greyed out region) 4

Figure 1.3: The spatial distribution of rainfall patterns in the Touws River catchment in May 1995 (the wettest month between 1984 and 2017). The map is created using CHIRPS rainfall dataset 5

Figure 1.4: Schematic representation of the distribution of Cape Supergroup and the Karoo Supergroup (from Johnson *et al*., 2006) 6

Figure 1.5: The geological setting of the Touws River catchment area (from Department of Environmental Affairs, 2018). 6

Figure 1.6: The dominant vegetation biomes in the selected Touws quaternary catchments 8

Figure 2.1: GDEs and their locations (from Klove *et al*., 2011; WetlandInfo, 2014) 15

Figure 2.2: A schematic representation of the classification approaches in remote sensing 19

Figure 3.1: Setting up sample plots (quadrat) and collecting plant samples in the Touws River quaternary catchments 26

Figure 3.2: Map of the quaternary catchments showing the location of the paired vegetation plots 26

Figure 3.3: The location of the weather stations relative to the study region 31

Figure 3.4: Map of the quaternary catchments showing the boundary of the sub-region and sample plots 36

Figure 3.5: A flow diagram of the research methods from data acquisition to data analysis 41

Figure 4.1: Vegetation community types described and characterized in the Touws quaternary catchments 44

Figure 4.2: The Normalised Difference Vegetation Index (NDVI) and monthly precipitation for vegetation plot 1 (1984-2017) 49

Figure 4.3: The Normalised Difference Vegetation Index (NDVI) and monthly precipitation for vegetation plot 2 (1984-2017) 51

Figure 4.4: The Normalised Difference Vegetation Index (NDVI) and monthly precipitation for vegetation plot 3 (1984-2017) 53

Figure 4.5: The Normalised Difference Vegetation Index (NDVI) and monthly precipitation for vegetation plot 5 (1984-2017) 55

Figure 4.6: The Normalised Difference Vegetation Index (NDVI) and monthly precipitation for vegetation plot 4 (1984-2017) 57

Figure 4.7: The Normalised Difference Vegetation Index (NDVI) and monthly precipitation for vegetation plot 6 (1984-2017) 59

Figure 4.8: The Normalised Difference Vegetation Index (NDVI) and monthly precipitation for vegetation plot 7 (1984-2017) 61

Figure 4.9: Coefficient of variation in monthly precipitation amounts for vegetation plot 1 and 2, and 3 for the period between 1984 and 2017 62

Figure 4.10: Coefficient of variation in monthly precipitation amounts for vegetation plot 5, 4, 6 and 7 for the period between 1984 and 2017 63

Figure 4.11: CHIRPS total annual precipitation record for the study period (1984-2017)..... 65

Figure 4.12: The mean monthly rainfall conditions in the Touws quaternary catchments from 1984 to 2017 65

Figure 4.13: Rainfall anomaly with a 2-year moving average in the Touws quaternary catchments relative to 1984-2017 average 66

Figure 4.14: The Standardized Precipitation Index (SPI) at 12-month scale for the study record (1984-2017) 66

Figure 4.15: Average monthly temperatures of the Touws quaternary catchments from 1984 to 2017 67

Figure 4.16: Average annual maximum and minimum temperatures of the Touws quaternary catchments from 1984 to 2017 68

Figure 4.17: The relationship between average monthly NDVI and monthly maximum temperatures of the Touws quaternary catchments (1984-2017)..... 70

Figure 4.18: The relationship between average monthly NDVI and monthly minimum temperatures of the Touws quaternary catchments (1984-2017)..... 71

Figure 4.19: The relationship between average monthly NDVI and monthly rainfall of the Touws quaternary catchments (1984-2017) with lag time between rainfall peak and NDVI peak..... 72

Figure 4.20: Correlation coefficient between monthly NDVI and monthly rainfall for the period 1984-2017.....73

Figure 4.21: Correlation coefficient between monthly NDVI and monthly maximum temperatures, and between monthly NDVI and monthly minimum temperatures for the period 1984-2017.....74

Figure 4.22: Land cover classification results of SPOT 7 imagery taken on the 17th of July 2017 80

Figure 4.23: Sub-region of the pan-sharpened SPOT 7 image (17th July 2017).....81

Figure 4.24: Land cover classification results of SPOT 7 imagery taken on the 13th of September 2017.....82

Figure 4.25: Sub-region of the pan-sharpened SPOT 7 image (13th of September 2017) 83

Figure 4.26: Land cover classification results of WorldView-2 imagery taken on the 28th of October 2017 84

Figure 4.27: Sub-region of the pan-sharpened WorldView-2 image (28th of October 2017) .85

Figure 4.28: The Topographic Wetness Index (TWI) highlighting topographic depressions ..87

Figure 4.29: A profile curvature of the mapped region showing break of slope areas 88

Figure 4.30: The dominance of shrubland in the study region mostly located in hilly slope, with woodland vegetation located along the river channel or in a valley forming a linear shape.....89

Figure 5.1: Delineating the response and water availability for riparian and non-riparian vegetation 94

Figure 5.2: The sampled vegetation plots highlighting the location of riparian and non-riparian areas in the study region 95

LIST OF TABLES

Table 2.1: Types of South African GDEs that are relevant to the study (from Colvin *et al*., 2007; Colvin *et al*., 2002) 15

Table 3.1: The spectral properties of Landsat TM and OLI, WorldView-2 and SPOT 7 sensors 28

Table 3.2: A detailed summary of the weather stations 30

Table 3.3: Drought classification according to SPI values (from McKee *et al*., 1993) 33

Table 3.4: Annual precipitation by year during the study period (1984-2017) calculated from the CHIRPS rainfall dataset 35

Table 3.5: The land cover classes of GDEs used for classification (from Barron *et al*., 2012) 37

Table 3.6: Segmentation parameters and criterion 37

Table 3.7: Land cover classes and the random samples created in each image for classification 38

Table 3.8: Features considered for separating objects in object-based image classification. 38

Table 4.1: Plant species collected during the survey period in the floodplain woodland community 44

Table 4.2: Plant species collected during the survey period in the hillslope shrubland community 45

Table 4.3: Descriptive statistics of the sampled vegetation plots calculated from the full NDVI dataset 46

Table 4.4: Descriptive statistics of the sampled vegetation plots calculated from the CHIRPS rainfall dataset 46

Table 4.5: The units used in NDVI scatter plots and the corresponding Landsat image dates (1984-2017) 47

Table 4.6: The statistical summary of rainfall in the Touws quaternary catchments for the period (1984-2017) 64

Table 4.7: Descriptive statistical summary of the linear regression 73

Table 4.8: Multiple regression model summary 75

Table 4.9: Multiple regression ANOVA 75

Table 4.10: Multiple regression coefficients 75

Table 4.11: A zero-lag correlation matrix of NDVI versus rainfall and temperatures at a vegetation community scale 77

Table 4.12: A 3-month time lag correlation matrix of NDVI versus rainfall and temperatures at a vegetation community scale 78

Table 4.13: Error matrix of land cover classification in eCognition for July 2017 and September 2017, and in ENVI for October 2017 86

CHAPTER 1: INTRODUCTION

1.1. | Background

Vegetation is a significant component of our natural environment, so much so that other natural processes and livelihoods of some societies depend on vegetation. It provides a range of essential services many of which are of considerable economic value to society. However, due to the changes in climate patterns, the growth dynamics of vegetation are strongly affected by surface temperatures and variations in seasonal rainfall and long-term cycles.

In most catchments, rainfall is the most important determinant of vegetation growth (Xu *et al*., 2012; Huxman *et al*., 2004). As a result, variations in rainfall and the effects on vegetation growth has implications for catchment hydrological processes such as runoff, infiltration, evapotranspiration and consequently on river discharge and sediment availability. In highly variable rainfall environments, some vegetation (groundwater dependent ecosystem types) may rely on near-surface groundwater as the main source of water (Klove *et al*., 2011).

However, the dependence of vegetation on groundwater is temporal and spatially variable, depending on depths to groundwater (WetlandInfo, 2014). Therefore, this indicates a need for an improved understanding of how climate affects the spatiotemporal variability of Groundwater Dependent Ecosystems (GDEs). Temperature also plays a significant role in vegetation growth mainly through the impact on photosynthesis and respiration (Allen and Platt, 1990). Climate projections (IPCC, 2013) suggest that surface temperatures are increasing. Thus, increased temperatures beyond the norm can have a dire effect on vegetation growth, primarily during the developmental stages. It can also cause plant respiration rates to increase relative to photosynthesis, resulting in no gain net in biomass production (Turyahikayo, 2014).

In the Touws River catchment, vegetation is significantly influenced by climate variations. Dominant vegetation types in this area are vulnerable to declining rainfall and increasing temperatures (Midgley *et al*., 2001). Aridity and moisture stress has resulted in shrub-like vegetation rather than grasses. This is associated with drought events where dry periods are of longer duration than moist periods in this area (Milton *et al*., 1998). The importance of this study relates to the fact that there is limited research conducted on the influence of climate

on vegetation cover in the Touws River catchment and that research on GDEs in South Africa is at an early stage (Colvin *et al*., 2007). Ample research on the influence of climate on vegetation has been based in the Klein and Great Karoo at large (du Toit and O'Connor, 2014; Kraaij and Milton, 2006; Roux and Vorster, 1983). Hence, this study focuses on analyzing the response of vegetation to climate elements (i.e. rainfall and temperature) in order to determine whether groundwater dependent ecosystems occur in the Touws River catchment, and if so, what is their spatial and temporal occurrence. In essence, this is recorded through observations from remote sensing technologies that offer data archives of the earth's environment from present time to several decades back.

1.2. | Aim and objectives

Aim:

The primary aim of this study is to examine vegetation sensitivity to climate variables and assess the dependence of vegetation on groundwater in a climatically variable region of the semi-arid Karoo, South Africa.

Objectives:

This study has two main objectives: **1.**) to develop an understanding of spatiotemporal dynamics of rainfall in the Touws River quaternary catchments and provide a basis for assessing the role of rainfall and temperature variations on vegetation productivity, **2.**) to investigate the spatial occurrence of groundwater dependent ecosystems in 2017.

1.3. | Description of the study area

1.3.1. | Location

The Touws River catchment area lies in the Western Cape Province of South Africa (33° 20' 16" S; 21° 10' 55" E), approximately 183 km from Cape Town. The catchment forms part of the Klein Karoo and is a sub-catchment of the Gouritz River catchment system, and part of the Gouritz Water Management Area (WMA). The catchment is 95.81 km² in area. The Touws River is considered to be in a good ecological state (Gordon *et al*., 2004; River Health Programme, 2007). The river rises in the Matroosberg Mountains (Hex River Mountains), near the town of De Doorns and flows east through the Touws River town and south into the Klein

Karoo, where it joins the Groot River. However, considering the time and cost of field-work, this research focused on two quaternary catchments (J12L and J12H) as indicated in Figure 1.1.

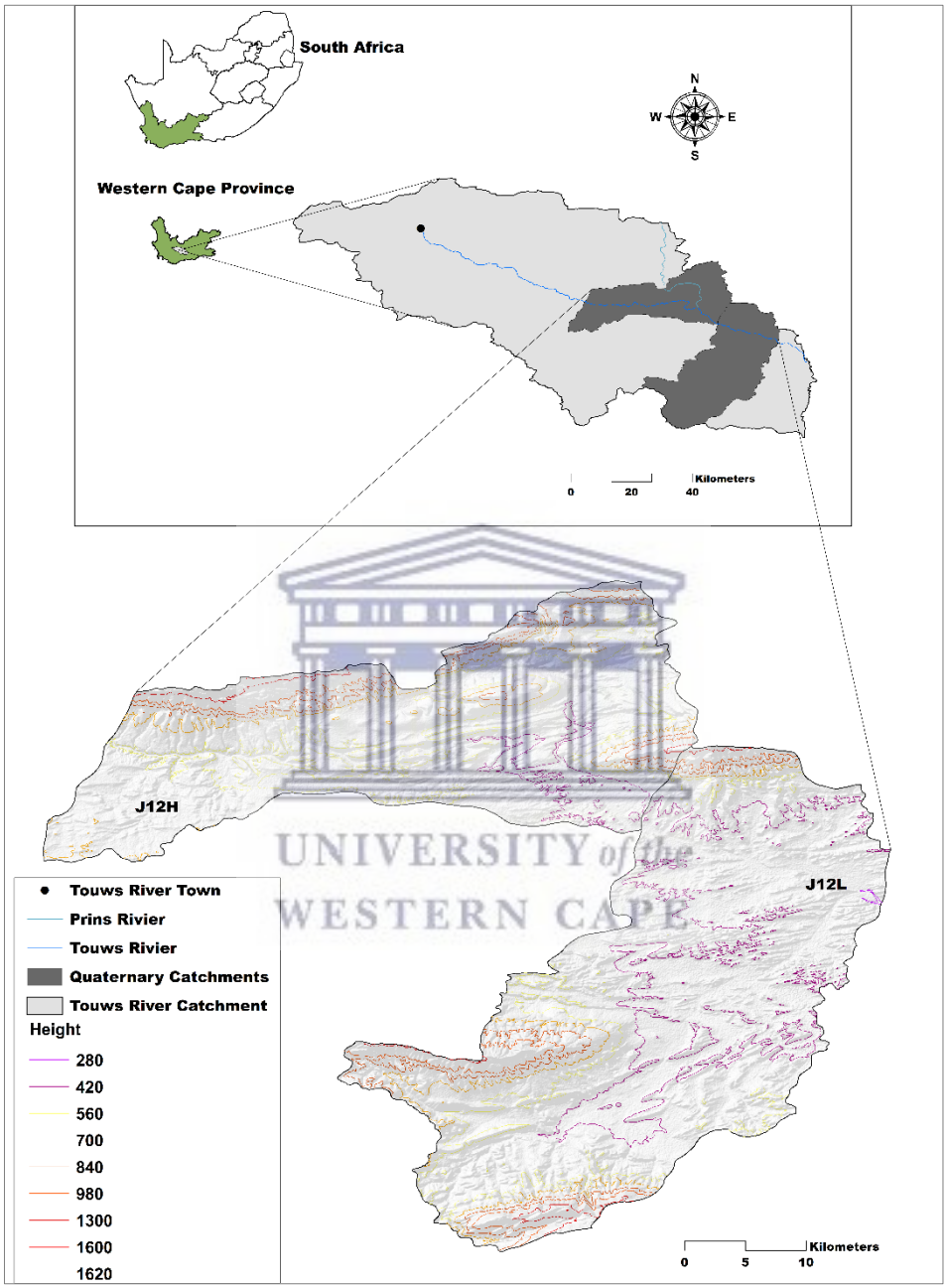

Figure 1.1: The location of the selected quaternary catchments in South Africa and in the Western Cape Province.

1.3.2. | Climate

Previous studies have looked at the climate of the entire Klein Karoo or the Gouritz WMA (Le Maitre *et al*., 2009; DWS, 2015) rather than individual catchment areas. In this study, the

description of climate is also based on that of the Klein Karoo and the Gouritz WMA. The Klein Karoo receives low rainfall of 100 mm to 450 mm/year (Le Maitre *et al*., 2009). The Gouritz WMA is divided into three areas (two inland zones and a coastal belt) with different climates. Rainfall varies from winter-dominant in the west to summer-dominant in the east (Le Maitre *et al*., 2009) (Figure 1.2). Winter rains are carried by cold fronts associated with low-pressure systems and westerly winds, while summer rainfall is dominated by moisture from the east and convective systems which are less affected by orographic gradients (Le Maitre *et al*., 2009).

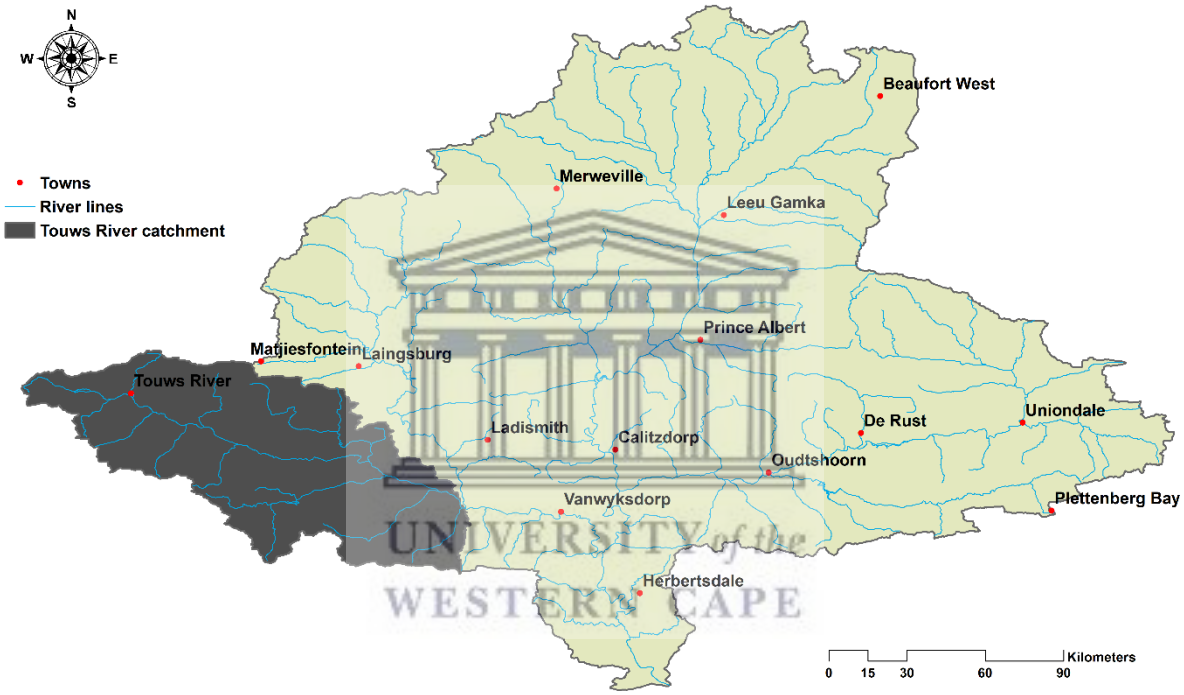

Figure 1.2: Map of the Gouritz WMA. The study area is located in the south-west (indicated by the greyed out region).

The rainfall pattern in the area is also characterized by extremely high rainfall events, associated with cut-off low-pressure systems, which can result in major floods. In hilly slopes, the rainfall ranges from 900-1 650 mm and the low-lying central valley receives 100-300 mm/year. Variation in rainfall patterns in the Gouritz WMA increases as the rainfall decreases (Le Maitre *et al*., 2009). Spatial variability in rainfall is demonstrated in Figure 1.3, which shows rainfall throughout the catchment in May 1995.

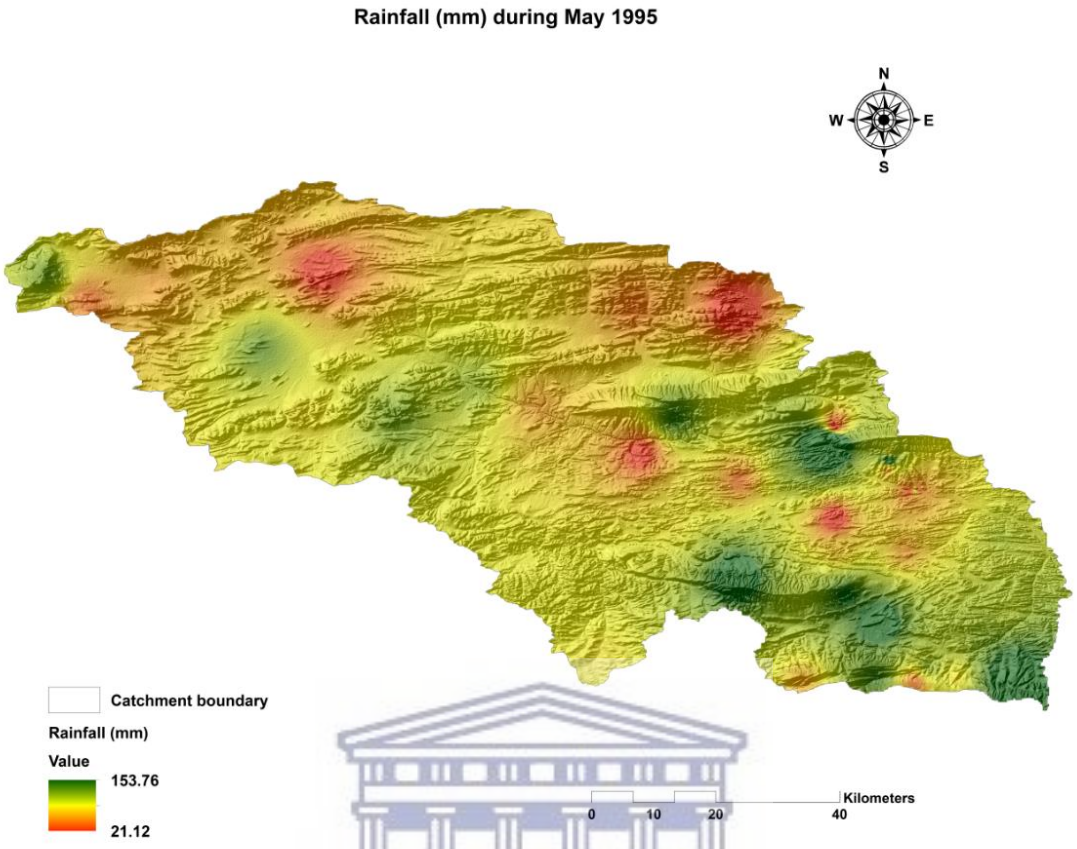

Figure 1.3: The spatial distribution of rainfall patterns in the Touws River catchment in May 1995 (the wettest month between 1984 and 2017). The map is created using CHIRPS rainfall dataset.

Temperatures in the summer season typically range from 22-25°C, exceeding 30°C in February and ranges between 18-21°C in winter (Petersen *et al*., 2017). Excessive temperatures results in high evaporation rates which exceed 2 250 mm/year (> 10 times than rainfall) in the dry central region (Le Maitre *et al*., 2009).

1.3.3. | Geology

The geological setting of the study area consists of a wide range of groups, sub-groups, and formations, which form part of the Cape Supergroup and the Karoo Supergroup (Figure 1.4 and 1.5). These consist of the Bokkeveld Group shale and sandstone; the Table Mountain Group (TMG) sandstone/quartzite; the Witteberg group; and the Ecca and Dwyka groups.

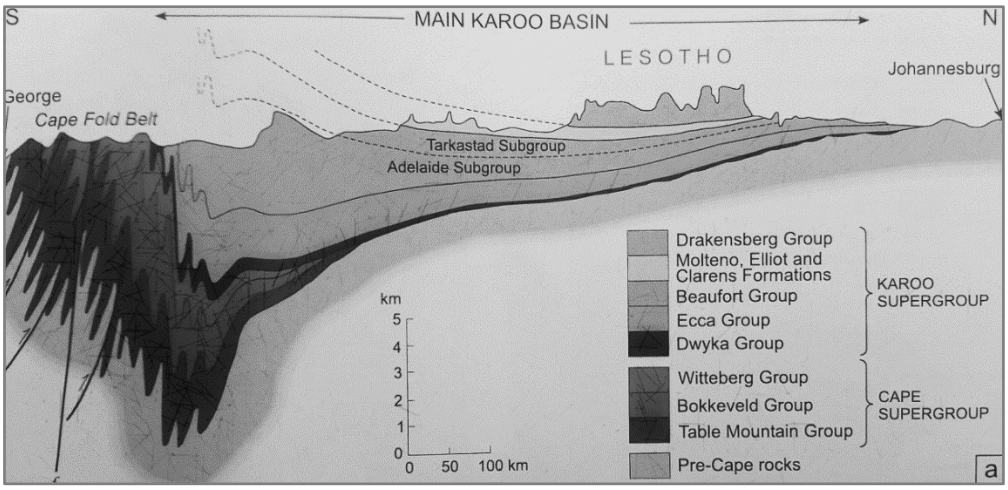

Figure 1.4: Schematic representation of the distribution of Cape Supergroup and the Karoo Supergroup. (***Source:*** *Johnson et al., 2006*).

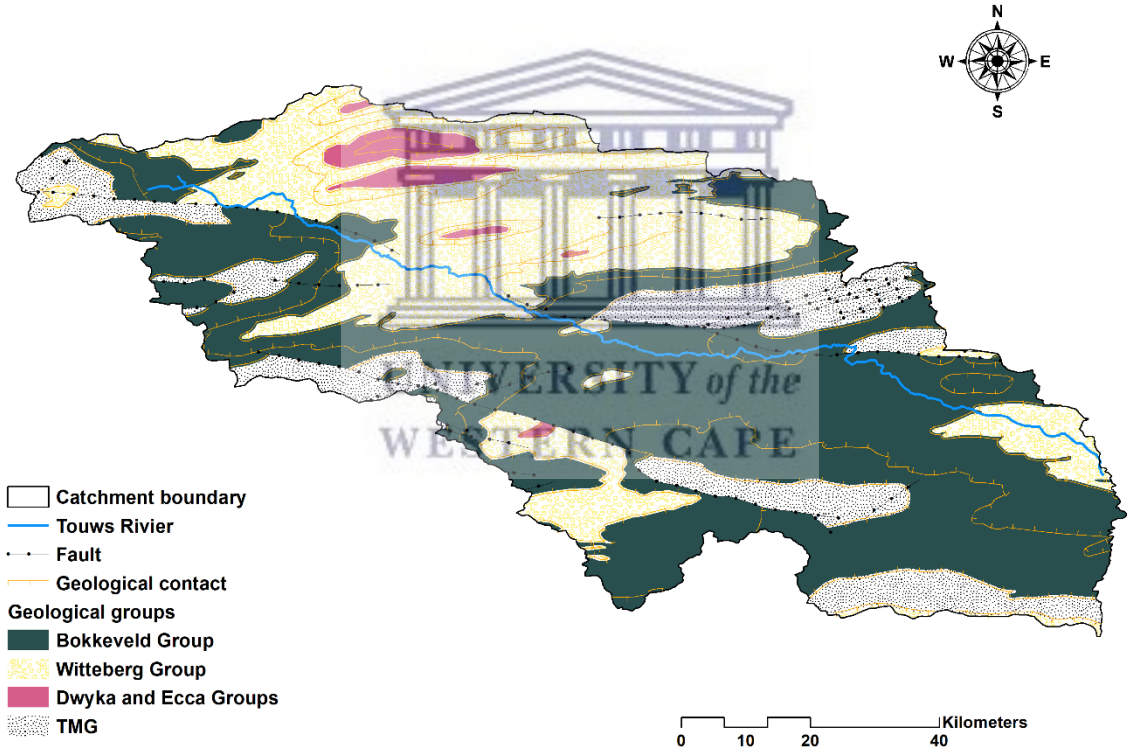

Figure 1.5: The geological setting of the Touws River catchment area. (***Source:*** *Department of Environmental Affairs, 2018*).

1.3.3.1. | Table Mountain Group (TMG)

The TMG is 520 million years old and consists of sediments deposited from early Ordovician to early Carboniferous times, approximately 500-340 million years ago (Duah, 2010). The TMG

forms the higher mountains (Swartberg, Kammanassie and Rooiberg mountains) and comprises resistant quartzitic sandstone (Midgley *et al*., 2005; River Health Programme, 2007).

1.3.3.2. | Bokkeveld and Witteberg Groups

The central part of the Touws River catchment is dominated by the Witteberg and Bokkeveld Groups (Figure 1.5). The Bokkeveld Group are predominantly mudstones. The Witteberg Group consists of quartzitic sandstone and micaceous mudrock and forms part of the uppermost layer of the Cape Supergroup (Buttner *et al*., 2016). The sandstones form a series of north-west to south-east trending ridges (Hiller and Dunlevey, 1978). The group consists of Weltevrede Subgroup, Weltevrede Formation, Witpoort Formation, Lake Mentz Subgroup, and Kommadagga Subgroup (Johnson *et al*., 2006).

1.3.3.3. | Dwyka Group

The Dwyka Group, also referred to as Dwyka Tillite, forms the lowermost and oldest deposit in the Karoo Basin. The Dwyka Group is divided into two facies: a valley highland facies and a shelf facies (Visser, 1986). Dwyka Group rocks rest directly on top of the Witterberg shales and consist of boulders, cobbles, and pebbles (Buttner *et al*., 2016). The rock was deposited by glaciers during a major ice age that affected the southern hemisphere supercontinent (Gondwana) during the late Carboniferous period.

1.3.3.4. | Ecca Group

Early deposition during the Cape Orogeny resulted in material being deposited into the Karoo basin to form the upper Ecca turbidites and prograding deltas (Geel *et al*., 2013). The Ecca Group comprises 16 formations which are grouped into three geographical areas (southern, western, north-western and north-eastern). In the western and north-western; Tierberg, Skoorsteenberg, Kookfontein, and Waterford Formations. (Smith, 1990; Hodgson *et al*., 2006; Johnson *et al*., 2006).

1.3.4. | Vegetation

The area has a rich biodiversity with two dominant vegetation biomes; Fynbos and the Succulent Karoo (Figure 1.6).

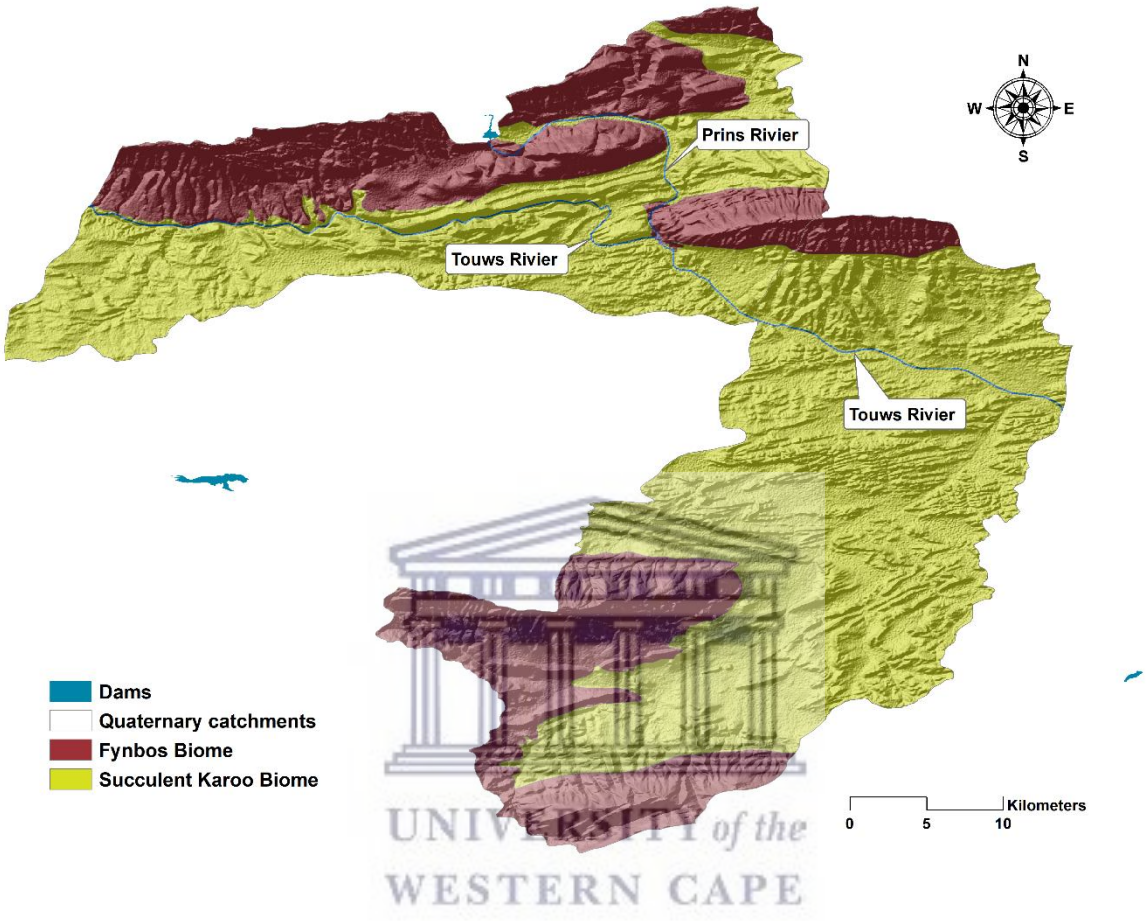

Figure 1.6: The dominant vegetation biomes in the selected Touws quaternary catchments.

1.3.4.1. | *Fynbos biome*

The Fynbos biome has the largest number of plant species of any biome in the country. The biome includes both Fynbos and Renosterveld vegetation. Fynbos tends to grow on poor soil and is extremely rich in plant species, while Renosterveld grows on richer soil (Rutherford and Westfall, 1994). Fynbos is a medium tall shrubland, comprising hard-leafed, evergreen, fire-prone shrubs, and is characterized by four major plant types: restioids, ericoids, proteoids and bulbs (River Health Programme, 2007). In addition, the Fynbos is also characterized by the presence of seven endemic or near-endemic plant families: Blacktips; Guyalone; Sillyberry; Brickleaf; Buttbush; Dewstick and Candlestick (Cowling *et al*., 2003). It grows in a 100-200 km

wide coastal belt from Clanwilliam on the west coast to Port Elizabeth on the southeast coast. The Fynbos in the western region is richer and more varied than in the eastern region of South Africa (Low and Rebelo, 1998). Renosterveld is dominated by shrubs from the Asteraceae family and is particularly known for its extraordinary diversity of geophytes, which during their spring flowering bring a profusion of colour (Curtis and Bond, 2013).

1.3.4.2. | *Succulent Karoo biome*

The Succulent Karoo biome is found mostly west of the western escarpment from Namibia through the western belt of the Northern Cape and Western Cape (Mucina and Rutherford, 2006). The biome is mostly flat with gently-curvy plain and hilly veld, situated to the west and south of the escarpment and north of the Cape Fold Belt. The biome is characterized by low winter rainfall, ranging between 20 mm and 290 mm. However, the biome adapts better to arid conditions and higher summer temperatures than the Fynbos vegetation type (Truc *et al*., 2013). The Succulent Karoo is characterized by a dwarf shrubland, succulent and non-succulent shrubs (Milton *et al*., 1998). Vygies (Mesembryanthemaceae) and Stonecrops (Crassulaceae) are prominent (Low and Rebelo, 1996). Extravagant mass flowering displays of annuals occur in the spring season, often on degraded or fallow lands (Low and Rebelo, 1996).

1.4. | The structure of the thesis

The thesis outline is as follows:

- **Chapter 1** provides an introductory background to the research, aim and objectives, climate and the physical environment of the Touws River catchment.
- **Chapter 2** presents a review of relevant literature to develop a strong theoretical background to investigate the influence of climate on vegetation productivity and vegetation dependency of groundwater.
- **Chapter 3** presents a description of datasets used and a detailed outline of the methods used in this study.
- **Chapter 4** examines the relationship between changes in vegetation vigor and variations in climatic elements. Presents image classification and assessment of indicators of groundwater discharge areas. This chapter contributes to achieving the objectives of this study.

- **Chapter 5** provides an overall general discussion, integrates key findings and formulates a conclusion for this study. Suggestions for future research directions are also provided**.**

CHAPTER 2: LITERATURE REVIEW

2.1. | Introduction

The aim of this chapter is to review previous research findings and methodologies that investigated the impact of climate on vegetation and the dependence of vegetation on groundwater. This chapter begins by describing the role of temperature and rainfall on vegetation productivity (Section 2.2). Section 2.3 reviews the impact of climate on vegetation in the Touws River catchment. This is followed by a description of GDEs in the context of South Africa (Section 2.4). A review of methodological approaches used in examining vegetation productivity and in identifying GDEs is provided, and a description of the limitations of remote sensing and ways of overcoming such limitations (Section 2.5). Finally, a review of previous studies on the use of remote sensing in vegetation studies is provided in Section 2.5.7.

2.2. | The role of temperature and rainfall on plant growth and development: a broader overview

Recent climate projections by the Intergovernmental Panel on Climate Change (IPCC) suggest that global warming will reach 1.5°C between 2030 and 2052, and 2°C by the end of the century if temperatures continue to increase at the current rate (IPCC, 2018). The report further suggests that limiting global warming to 1.5°C lowers the impacts on species loss and extinction. It is against this background that the impact of extreme temperatures and rainfall variations due to climate change on vegetation productivity should be considered.

2.2.1. | Temperature

Temperature plays a major role in plant growth and development. It influences plant growth (i.e. foliage, shoots, and stem wood) through the impact on photosynthesis and respiration (Allen and Platt, 1990). The response to temperature and demand for light varies amongst plant species throughout their life cycle, despite growing in the same environment (Tyler, 2001) primarily due to individual phenological responses and stages of plant development (Hatfield and Prueger, 2015). The differences are signified by a certain range of maximum, minimum and optimum temperatures, thus forming a boundary of observable growth (Hatfield and Prueger, 2015). Therefore, when temperature rise does not meet a certain

species' optimum level, plant development is significantly affected. This is illustrated by Hatfield and Prueger (2015, p.5) "Temperature which would be considered extreme and fall below or above specific thresholds at critical times during development can significantly impact productivity". Frost, for instance, results in leaf damage through freezing of external and internal plant water. An increase in air temperatures beyond the optimum level result in moisture stress and subsequently vegetation losses. The resulting net effect is the loss of above-ground biomass through top-kill (Whitecross *et al*., 2012).

The influence of temperature on vegetation growth has been observed in previous studies. Barlow *et al*. (2015) reviewed existing knowledge on the impacts of extreme heat and frost on crop production. It was found that temperature was a key factor determining the impact of heat shock and frost events on wheat production. Allen and Platt (1990) compared variations in seed crop size and climatic factors between Craigieburn Range and Mount Thomas Forest in New Zealand. A positive correlation between daily temperatures and seed production was found. However, the correlation varied between the two areas based on the elevation of the surrounding environment. Hatfield and Prueger (2015) assert that increasing climate change scenario will likely result in air temperatures exceeding the optimum range for many species. This will trigger constraints in plant species development because growth patterns will be negatively affected, and plant species will have to adapt to the changing climate, consequently, reducing production quantity and quality.

2.2.2. | Precipitation

Precipitation comes in many forms such as rain, snow, sleet, hail, and ice. Different forms of precipitation influence vegetation growth in several ways. In this study, the focus was explicitly based on water availability for vegetation growth through rain-water. The availability of water plays a major role in the growth stages of vegetation (Holding and Streich, 2013). However, water availability is influenced by several factors such as the type of precipitation, soil properties, temperature and wind (Enroth, 2014). Plants require a certain amount of water for growth, too much or too little water has major consequences on plant development. Too much water can reduce oxygen in the soil and heavy rain can damage plants, soil and can cause erosion (Enroth, 2014). Too little or no rain delays plant development and may cause plant death in the event of extremely dry conditions.

The southern Africa region is characterized by a high degree of rainfall variability (Ambrosino *et al*., 2011). The rainfall patterns in this region have shown strong inter-annual fluctuations since the 1970s, with persistent wet and dry periods (Rouault and Richard, 2003; Dieppois *et al*., 2016). According to Enroth (2014), variations in rain-water can permanently or temporarily influence vegetation productivity depending on how long the condition lasts. Richard *et al*. (2008) argue that in semi-arid African regions, characterized by annual rainfall between 200 and 600 mm, the vegetative photosynthetic activity is highly sensitive to inter-annual rainfall variability. Therefore, rainfall amount and intensity determine the availability of water for mechanisms that allow healthy plant growth. This further determines the type and density of plants that will grow. A study by Wessels (2008) showed that a decline in vegetation cover in arid and semi-arid lands could largely be attributed to variation in rainfall. Cisse *et al*. (2016) studied the influence of intra-seasonal spatiotemporal variability of rainfall on the seasonal variation of vegetation in the Ferlo region, Senegal. A stronger sensitivity of vegetation to rainfall was found two to three weeks after a rainfall anomaly. Dry spells of seven days' length were also found to significantly affect vegetation growth in the Ferlo region.

2.3. | The influence of climate on vegetation productivity in the Touws River catchment and the Klein Karoo

The Touws River catchment forms part of the Klein Karoo and is characterized as a water-stressed area (Le Maitre *et al*., 2009). Grass species respond to summer rainfall and the Karoo bushes are sensitive to autumn and spring rainfall (Milton *et al*., 1998). The seasonal rainfall variations stimulate plant phenological characteristics and this results in the physiognomy of the Karoo veld (False Upper Karoo) to change considerably from grassy to shrub-like (Milton *et al*., 1998). The dwarf Succulent shrubs decrease further inland in the Karoo due to low and seasonally variable rainfall (Milton *et al*., 1998). A similar trend has been detected by Masubelele *et al*. (2014) in the central semi-arid South Africa, dominated by shrubby vegetation.

The Klein Karoo is recognized as a biodiversity hotspot, with the meeting of three biomes; the Succulent Karoo, the Albany Thicket and the Fynbos biome (Mucina and Rutherford, 2006). However, the region is predicted to be affected by future incidences of drought, which will

cause intensive drying and loss of species richness (Murray, 2015). Limited rainfall in the Klein Karoo has meant that groundwater is an important water source (Le Maitre *et al*., 2009), particularly for irrigation. Shrubby vegetation on shallow soils is dependent on groundwater as the main source of water. This is because shrubs can outcompete grasses during drought periods where they have access to deeper soil water (Letts *et al*., 2010) which is stored and flows through fractures and fault systems (Le Maitre *et al*., 2009).

2.4. | Groundwater Dependent Ecosystems (GDEs)

2.4.1. | Defining GDEs

GDEs are defined as ecosystems that rely on near-surface groundwater or groundwater discharging from an aquifer to maintain their structure and ecosystem processes and services (Figure 4.1) on a permanent or irregular basis (Munch and Conrad, 2007; Klove *et al*., 2011; Richardson *et al*., 2011). Key characteristics of GDEs determine accessibility of groundwater: **1.)** the physical aquifer characteristics that regulate the amount of groundwater occurrence and discharge; **2.)** and biophysical characteristics that regulate dependency and uptake of water by the ecosystem (Colvin *et al*., 2007). In South Africa, the alternative term, Aquifer Dependent Ecosystems (ADEs) is increasingly preferred to GDEs because the term aquifer is more relevant or removes confusion about the primary water source (Colvin *et al*., 2007), but in this study, the term GDEs is used, as the water supply is not necessarily from an aquifer, but potentially from interflow sources. GDEs are normally found in water-scarce regions or areas that exhibit high rainfall variations. In South Africa, such ecosystems occur in areas where aquifer flows and discharge influence ecological patterns and processes (Colvin *et al*., 2007). In most environments, GDEs have a direct access to groundwater (direct dependence). However, indirect dependence may occur where species that can access groundwater sustain species that are unable to access groundwater (Colvn *et al*., 2002).

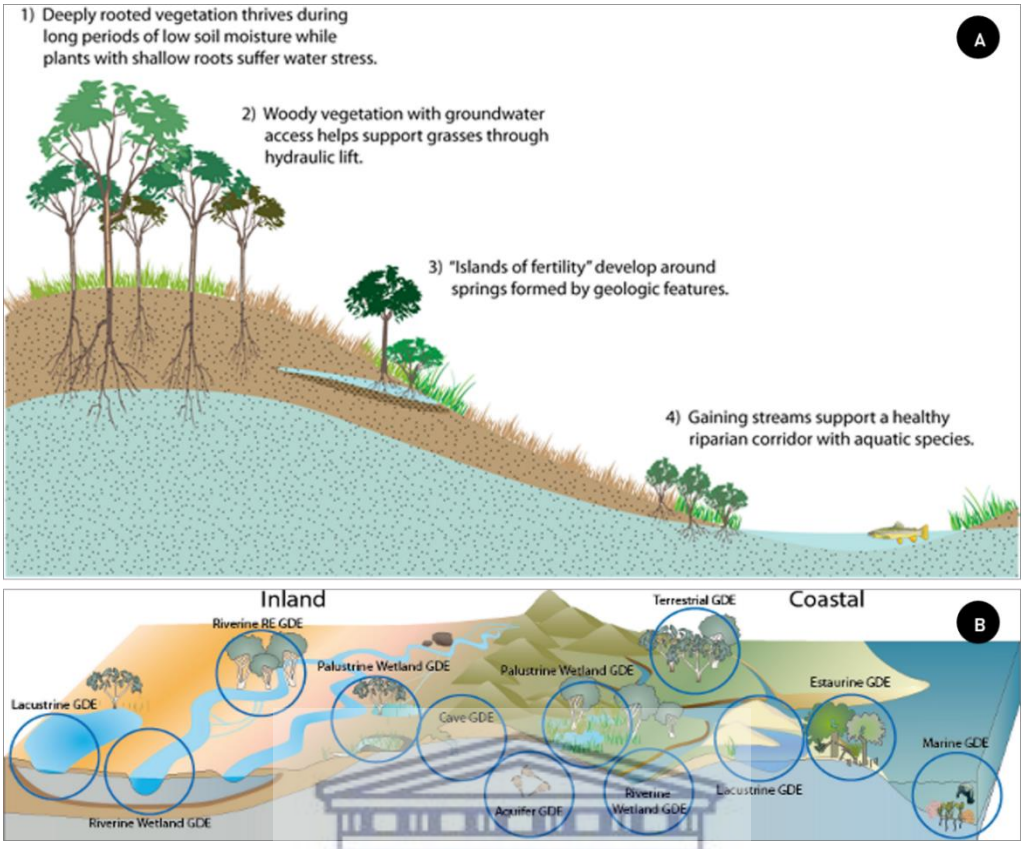

Figure 2.1: GDEs and their locations (**A** and **B**). (***Source:*** *Klove et al., 2011; WetlandInfo, 2014*).

2.4.2. | Types of GDEs

The examples of known South African GDEs that are relevant to the study are shown in the table below.

Table 2.1: Types of South African GDEs that are relevant to the study.

Surface/Sub-surface	GDEs	Example location
Surface	Terrestrial vegetation	Keystone species (Acacia erioloba) in the Kalahari.
	Riparian Zones	Seasonal alluvial systems of the Limpopo.
	Springs and seeps	In TMG sandstone in the Western Cape; on the Karoo dolerite sills.
Sub-surface	In-aquifer ecosystems	In the dolomites in the North Western Province.
	Riverbed	

Source: *Colvin et al. (2007) and Colvin et al. (2002).*

2.4.3. | The importance of understanding GDEs

GDEs are essential as they provide critical habitat for sensitive species in arid and semi-arid environments (Huntington *et al*., 2016). In several countries, GDEs are quantified and managed at a critical level. In South Africa, the protection and management of GDEs is an

essential water management policy initiative of the Integrated Water Resource Management (IWRM) programme. In addition, groundwater allocation has become an important issue in the country and, therefore, the identification of GDEs is important in defining what restrictions should be placed on the available groundwater allocation (Munch and Conrad, 2007; Rohde *et al*., 2017). An understanding of aquifers, of which GDEs depend on, and the nature of dependency is crucial before pumping groundwater (Colvin *et al*., 2007). In Australia, more than 50% of groundwater is used by vegetation that grows over shallower groundwater table (Zencich *et al*., 2002). Human exploitation exceeds natural recharge rates, and this affects GDEs, specifically in areas where dependency on groundwater increases with increased aridity (Hatton *et al*., 1997).

2.5. | Application of remote sensing on monitoring vegetation and identifying GDEs

Traditional methods of mapping vegetation have been criticized as time-consuming, date lagged, costly, and covering small areas (Mutanga *et al*., 2016). Remotely sensed data has replaced the traditional methods by providing appropriate and precise spatial information on a finer resolution to map vegetation over a short period of time (Vinod and Kamal, 2010). The availability of data archives, from several decades back, has prompted researchers and application specialists to use remote sensing in mapping vegetation (Xie *et al*., 2008). Remote sensing technology can extract meaningful phenological information such as growing period, date of the peak of greenness and end of the growing season (Wessels, 2008). This has provided users with a detailed analysis of vegetation properties such as quality, species, biomass etc. (Mutanga *et al*., 2016).

2.5.1. | Vegetation Indices (VI_s)

Vegetation can be assessed quantitatively and qualitatively by analyzing reflectance information from canopies using passive sensors (Xue and Su, 2017). However, climate and time influence solar varieties and this affects the quality of reflected information received. Therefore, remotely sensed data must be corrected before use. Jackson and Huete (1991) argue that a simple measure of light reflected from the surface is not enough to discriminate the surface in a repeatable manner. To overcome such limitation, data must be combined from two or more spectral bands to form a vegetation index with a single value that signifies the amount of vegetation within a pixel (Campbell and Wynne, 2011). VI_s record vegetation's

reactive contrast in the visible red and near-infrared (NIR) wavelengths, sometimes with additional channels included (Lanfri, 2010). VI_s can be calculated from sensor voltage output, radiance values, reflectance values and satellite digital numbers (DN) (Jackson and Huete, 1991). The commonly used VI_s in vegetation studies and in identifying GDEs are discussed below.

2.5.1.1. | *The Normalized Difference Vegetation Index (NDVI)*

The NDVI is one of the most widely used spectral reflectance indices in vegetation studies. The index has been previously used to discriminate sugarcane vegetation classes (Vinod and Kamal, 2010) and monitoring of GDEs in arid and semi-arid environments (Huntington *et al*., 2016). It is an indicator of vegetation phenology such as green-up, peak and offset of development (Beck *et al*., 2006). The NDVI is defined through absorption of red radiation by chlorophyll and leaf pigments and the scattering of near-infrared radiation by foliage (Beck *et al*., 2006). The values of this index range from -1.0 to +1.0

2.5.1.2. | *The Normalized Difference Water Index (NDWI)*

The NDWI measures vegetation liquid water content (Gao, 1996) and is derived from the near-infrared (NIR) and short-wave infrared (SWIR) channels. The SWIR spectral band is sensitive to both changes in vegetation water content and spongy mesophyll structure in the vegetation canopies while the NIR spectral band is sensitive to the leaf internal structure and the leaf dry matter content (Gao, 1996). The values of this index are similar to those of NDVI and range between -1.0 and +1.0 (Sanchez *et al*., 2016). Studies have demonstrated that both indices can be applied simultaneously. Barron *et al*. (2012) used the NDVI and NDWI to describe areas of greenness and surface moisture content. The results showed a classification of GDEs-related cover classes using the two indices.

2.5.2. | Data analysis with multiple sensors

In remote sensing, the integration of two or more satellite sensors is common when examining a common feature. The advantage of using multiple sensors is embedded in the idea of extracting better information and comparing the capabilities of different sensors while considering the characteristics (i.e. temporal and spatial resolution) of each satellite sensor. However, data needs to be consistent and synthesized before use to standardize sensor

characteristics such as pixel sizes, time of acquisition and scales (Thenkabail *et al*., 2004). Govender *et al*. (2008) compared the Hyperion hyperspectral sensor and multispectral Proba CHRIS (Compact High-Resolution Imaging Spectrometer) in classifying vegetation. The authors compared different classification techniques and degrees of accuracies varied between the two sensors, with an overall classification accuracy of 98%. Agapiou *et al*. (2014) compared the performance of seven satellite sensors (ALOS, ASTER, IKONOS, Landsat 4-7 and SPOT 5 HRV) in detecting archaeological remains. IKONOS produced significant results while other sensors showed comparatively similar accuracy and sensitivity. In assessing the ability of Landsat OLI imagery for mapping bracken fern weed, Matongera *et al*. (2017) found the OLI imagery to be comparative to the overall accuracy of WorldView-2 imagery.

2.5.3. | Image classification

Land cover change analysis can also be used to monitor vegetation. In essence, image classification is used by classifying images of a certain area taken in different dates to detect changes in vegetated surfaces. Image classification is the process of assigning pixels to classes based on values in several spectral bands (Campbell and Wynne, 2011). The classes represent regions in an image for further analysis. Two classification approaches; supervised and unsupervised have been traditionally followed. The object-based classification method has progressed over the years and is mostly preferred than the traditional classification methods (Figure 2.2).

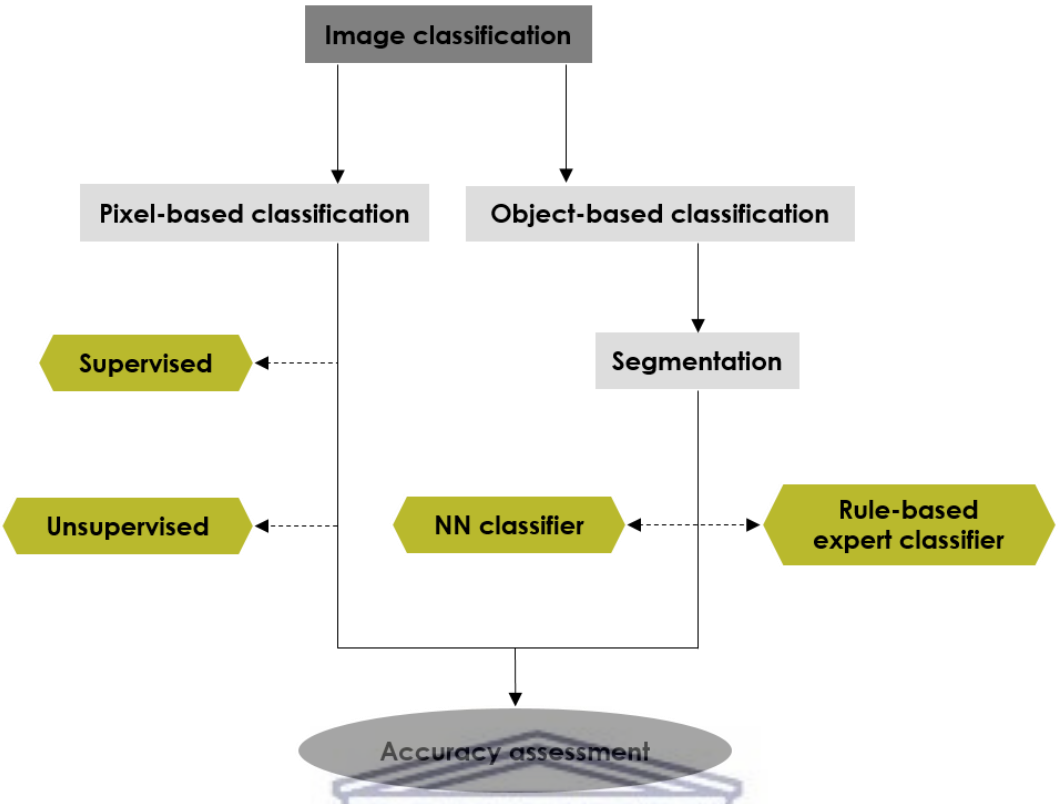

Figure 2.2: A schematic representation of the classification approaches in remote sensing.

2.5.3.1. | Supervised classification

The supervised classification approach follows a two-step process: 1.) **Defining training sites** - where a user directs the image processing software to assign pixels to land cover classes. The analyst can use common knowledge of the geographical area and familiarity of the actual surface cover types (through fieldwork or knowledge from the existing map) present in an image to determine the appropriateness of training sites (Levin, 1999); 2.) **A decision-making phase** - to assign class labels to all other image pixels by classifying each pixel to which of the trained classes the pixel is most familiar (Levin, 1999). Statistical characterizations of the information are then created and these are called signatures. The signatures guide the classification algorithm to assign specific values to relevant classes (Campbell and Wynne, 2011). The maximum likelihood classification is the most commonly used supervised classification method.

2.5.3.2. | *Unsupervised classification*

The unsupervised classification requires plotting of all pixels (spectral classes) of the image in a feature space and analyze feature space in other to group the feature vectors into clusters (Levin, 1999). Unsupervised classification incorporates no prior knowledge of the characteristics of the themes being studied (Xie *et al*., 2008). However, the user must specify the number of clusters to be obtained, the maximum cluster size (in the feature space) and the minimum distance that is allowed between different clusters. The process builds clusters as it scans through the image. When a cluster becomes larger than the maximum size, it is split into two clusters and when two clusters get nearer to each other than the minimum distance, they are merged into one (Levin, 1999). It is easy to apply and widely available in image processing and statistical software packages (Langley *et al*., 2001). The two most frequently used methods are the *K*-mean and the ISODATA clustering algorithms (Xie *et al*., 2008).

2.5.3.3. | *Object-based image analysis (OBIA)*

The OBIA is different from the traditional pixel-based approaches in that it classifies the spatial units or image objects by considering the neighboring and sub-image objects (Pauw, 2012). Object-based classifiers make use of the spatial context information around a pixel, thus considering the spectral, structural and hierarchical properties of each object (Bock *et al*., 2005). Additional information about objects such as the mean, median, minimum and maximum values are also provided (Blaschke, 2010). Object-based image classification uses a two-step procedure; image segmentation and the actual classification algorithm.

Segmentation algorithms

Image segmentation is the process of dividing an image into spatially continuous, disjoint and homogenous regions (Blaschke *et al*., 2004) based on spectral values of their pixels and analyst-determined constraints (Campbell and Wynne, 2011). The regions are then recognized by further processing steps and transferred into meaningful objects (Blaschke, 2010). In OBIA the analyst has the freedom of deciding on a set criterion that regulates the measures used to assess homogeneity and distinctness and the thresholds for a specific classification problem (Campbell and Wynne, 2011). Image segmentation methods have been

commonly divided into four categories; point-based, edge-based, region-based and combined (Blaschke, 2010).

The point-based method uses image thresholding (i.e. assigning a unique value) to identify homogenous pixels throughout an image. Elements that fall within the threshold are identified and these are grouped into regions considering they spatially connect (Pauw, 2012). Edge-based methods attempt to find an edge between regions and determine the segments as regions within these edges (Blaschke *et al*., 2004) by applying an edge-detection filter then transform to object outlines using a contour-generating algorithm (Pauw, 2012). Region-based methods compare image elements (pixels or regions) to identify similarities. Two approaches are used; region growing and region splitting. Region growing starts with seed pixels and combine neighboring pixels to regions and repeat the process until a certain threshold is reached (Blaschke *et al*., 2004). Region-spitting divides the image into sub-regions and these are further split into smaller objects based on spectral properties (Blaschke *et al*., 2004).

The most preferred and widely used segmentation algorithm is the region-based multiresolution segmentation method. The method merges input elements into a set of objects, ensuring that heterogeneity of pixels or object is minimized while homogeneity is significantly maximized (Pauw, 2012). The method uses a mutual-best-fitting approach where a seed object is evaluated in correspondence with the identified neighboring object. Once the best fitting is identified (in terms of meeting the required threshold), the objects are merged and if not, the neighboring object becomes the new seed (Pauw, 2012). The process is repeated until no more merges are allowed. Fitting is defined by the properties of homogeneity between objects such as spectral properties and shape (Pauw, 2012).

Classifiers in OBIA

There are several classifiers in OBIA that are available. The two commonly used methods include the rule-based expert systems and the nearest neighbor (NN) classification. In this study, the NN Fuzzy function classification method was used. The approach was found to be more accurate compared to the expert system by Pauw (2012). A detailed description of the rule-based classifiers is provided in Maxwell (2005) and Laliberte *et al*. (2006). The nearest neighbor classifier is an automatic generation based on sample objects (Wei *et al*., 2005).

Following image segmentation, the user selects object-based training samples for each class in the classification hierarchy and decides on appropriate features (Maxwell, 2005). Once the training samples have been identified, the remaining objects are assigned to the same class as the closest training object in feature space (Wei *et al*., 2005). The features are known as fuzzy logic membership functions and are used to define each class by assigning a membership value to each class that expresses the relationship between the class and the properties that describe it (Feizizadeh *et al*., 2017).

The membership value is calculated as a function of distance in feature space between the object being classified and the nearest training object for each class (Maxwell, 2005). When the difference between the two is small, the membership value will be higher and therefore, once the feature space becomes more stable the classification is likely to be more accurate (Laliberte *et al*., 2006). The final step is to run the classification process. In the case of misclassification or unclassified objects, training samples can be re-edited by assigning samples of the misclassified or unclassified classes to the correct classes and run the classification process again (Wei *et al*., 2005).

2.5.4. | Accuracy assessment

In remote sensing, the classification process is often followed by an accuracy assessment. This measures the correspondence between the presumed correct entity and the classified image of unknown quality (Campbell and Wynne, 2011). In essence, the user select samples of raster elements (image objects) which represents the classes used for classification and compare the classification results with real world classes (Kerle *et al*., 2004). The real world classes are derived from field observations or high-resolution imagery such as aerial photos (Kerle *et al*., 2004). The error matrix sometimes referred to as the confusion matrix, is a standard approach from which accuracy measures can be calculated. The error matrix identifies error and misclassification by category (Campbell and Wynne, 2011). Accuracy assessment is an important step when conducting a land cover classification as the precision of the map allow the user to make a reference about specific points on the map (Campbell and Wynne, 2011).

2.5.5. | Limitations of remote sensing

The use of remote sensing in vegetation studies is often associated with certain limitations. A mismatch between the resolution of remotely sensed imagery and the size of some ecosystems (i.e. spring groups, seeps, and individual springs) reduces the effectiveness of remote sensing approach in identifying GDEs (Perez Hoyos *et al*., 2016: Glanville *et al*., 2016). Despite the availability of finer resolution remote sensing imagery, a major problem is the cost, availability and huge volumes of such remote sensing datasets. Several issues are associated with NDVI and these include the influence of atmosphere, scaling problems, sensitivity to background variations, sensitivity to spectral effects, and asymptotic signals over high biomass conditions (Lanfri, 2010).

2.5.6. | Overcoming limitations of remote sensing

An approach that incorporates GIS techniques, spatial data and expert knowledge can offer a more comprehensive assessment of GDEs (Glanville *et al*., 2016). In addition, the inclusion of field studies and expert opinion provides validation of GDEs when remote sensing is applied, and this has been used in several studies (Doody *et al*., 2017; Tweed *et al*., 2007; Glanville *et al*., 2016). In South Africa, high scale datasets such as the SPOT series (SPOT 1-7) have become freely available to researchers. The Maximum Value Compositing (MVC) is a method used to eliminate atmospheric noise from NDVI and sensor errors such as line dropout (Beck *et al*., 2006). To account for soil background reflectance values, NDVI may be modified by indices such as SAVI or WDVI (Lanfri, 2010).

2.5.7. | A review of previous studies on the use of remote sensing in vegetation mapping and identifying GDEs

The application of remote sensing to quantify changes in vegetative surfaces and understand the impact of climate elements on the growth dynamics of vegetation has been observed at different spatial scales across the globe (Dube *et al*., 2014; Feng *et al*., 2017; Barbosa and Kumar, 2016). Dube and Mutanga (2016) combined a WorldView-2 dataset with environmental variables (rainfall, temperature, slope, aspect, total wetness index, elevation, insolation, and soil) to quantify aboveground biomass (AGB) and aboveground carbon stocks (AGCS) in a plantation forest in KwaZulu-Natal. The authors discovered that a combination of

remotely sensed data and environmental variables provide high accuracy to estimate and map AGB and AGCS than using each of the datasets separately.

The Moderate Resolution Imaging Spectroradiometer (MODIS) and Landsat imagery are commonly used to evaluate GDEs changes relative to climate variability (Doody *et al*., 2017: Huntington *et al*., 2016). Munch and Conrad (2007) combined aerial photography, remote sensing, GIS modeling, and field validation to identify riverine and wetland GDEs. In their study, Zhou *et al*. (2013) investigated the groundwater-surface water interactions using various methods such as hydrograph separation technique and analyzed vegetation dependency on groundwater using the NDVI. The authors discovered that vegetation sourced groundwater where the groundwater table was shallower.

Turyahikayo (2014) used the maximum likelihood classification to identify changes in vegetation density in the Molopo River catchment. Kotze and Fairall (2006) also used the supervised maximum likelihood classification to describe and map different plant communities and to determine the feasibility of using Landsat TM imagery for future vegetation mapping. Jumaat *et al*. (2018) mapped land cover change and detected major shifts in forest areas and built up areas using the object-based classification technique. Brooks *et al*. (2006) classified different agricultural crops using a combination of pixel-based unsupervised and object-based classification techniques. The object-based method had nearly identical accuracy to pixel-based approach. Adam *et al*. (2016) compared the performance of pixel-based and object-based classification algorithms by classifying land cover in Sudan. The pixel-based method performed slightly better than the object-based method.

CHAPTER 3: RESEARCH METHODS

3.1. | Introduction

The aim of this chapter is to present the research methods which seek to answer the objectives of this study. Different analytical techniques that were implemented to achieve the aim and objectives of this study are presented. The criteria for data selection, acquisition and preparation are first outlined. This is followed by an in-depth detail of the processes of relevant methods in the subsequent sub-sections.

3.2. | Data and data sources

3.2.1. | Field-based vegetation data

3.2.1.1. | *Survey design*

Prior to field survey, potential locations were identified using digital aerial photography (0.5 m) and remotely sensed imagery. During October 2017, sample plots of 10 m^2 in size were placed on hillslopes and along the floodplain to provide an indication of how plant species in different locations respond to rainfall and temperature variations. The plot size was chosen to accommodate some large tree species in the study area. Sample plots were placed on visually homogeneous stands of vegetation, in terms of composition, structure and habitat type. In total, 7 sample sites were selected, and these were paired into riparian and non-riparian plots, thus making a total of 14 vegetation plots (2 at each site, see Figure 3.2).

Geographic coordinates of each sampled vegetation plot were taken using a Garmin eTrex H hand-held Global Positioning System (GPS) receiver. In each sample plot, plant species were identified (Appendix A), and the percentage cover abundance was estimated for each dominant plant species in each quadrat.

Figure 3.1: Setting up sample plots (quadrat) and collecting plant samples in the Touws River quaternary catchments.

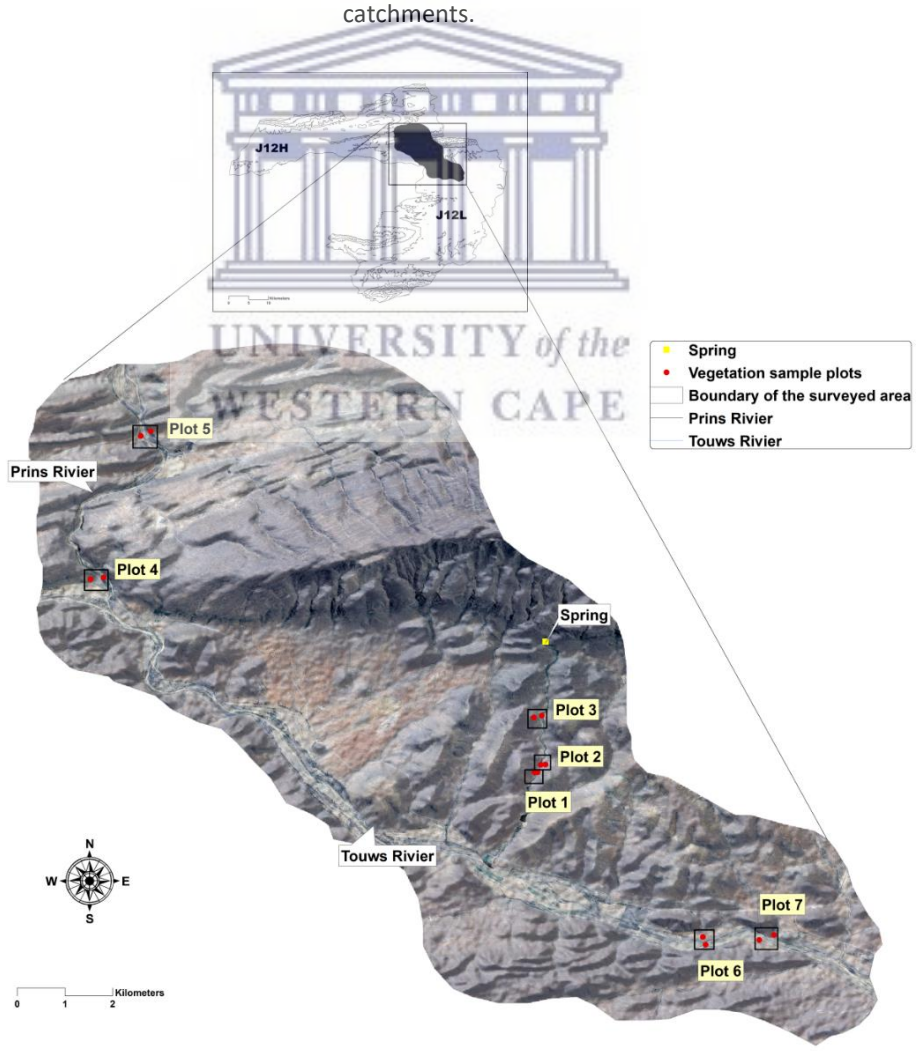

Figure 3.2: Map of the quaternary catchments showing the location of the paired vegetation plots.

3.2.1.2. | *Identifying plant communities*

In naming the plant communities, dominant species were used in conjunction with environmental variables (slope, aspect, and rockiness of the soil surface) gathered during the sampling period. Dominant species are those with greatest areal cover and occurrence (see Section 3.2.1.1).

3.2.1.3. | *Grouping sample plots*

Plant communities in combination with field observations and environmental variables were used to group the sample plots into hillslope shrubland and floodplain woodland groups. The hillslope shrubland group comprises plot 1, 2, 3 and 5 and the floodplain woodland group comprises plot 4, 6 and 7.

3.2.2. | Satellite data

3.2.2.1. | *Sensors*

The study used images from four satellite sensors: **1.**) Landsat Thematic Mapper (TM 4 and 5), **2.**) Landsat Operational Land Imager (OLI) both obtainable from the United States Geological Survey (USGS) Earth Explorer (https://earthexplorer.usgs.gov), **3.**) WorldView-2 obtainable and operated by DigitalGlobe Corporate, and **4.**) SPOT 7 obtainable from the South African National Space Agency (SANSA). Freely available historical multi-spectral image scenes and consistency motivated the selection of Landsat imagery. According to Xie *et al*. (2008), small-scale mapping requires high-resolution imagery. Hence, the application of WorldView-2 and SPOT 7 imagery to provide a finely detailed classification of GDEs. Table 3.1 indicates the spectral and spatial properties of the satellite sensors that were used in this study.

3.2.2.2. | *Criteria for image selection*

The decade beginning in 1984 was selected for this study because of the availability of cloudless, Landsat Surface Reflectance (SR) data which goes back until 1984 for the study region. A total of 132 Landsat SR images were utilized for a period of 34 years (1984-2017). The year 2012 was omitted because of missing data in the Landsat archive. The dates on which the images were acquired are listed in Appendix B. The WorldView-2 was selected to correspond with the exact dates of the field data collection.

Table 3.1: The spectral properties of Landsat TM and OLI, WorldView-2 and SPOT 7 sensors.

Satellite	Sensor	Bands	Wavelengths (µm)	Spatial resolution (m)	Temporal resolution	Launch date
Landsat 4 & 5	TM	B1 (blue)	0.45 – 0.52	30	16 days	1982 – 2012 (*no longer operational)
		B2 (green)	0.52 – 0.60	30		
		B3 (red)	0.63 – 0.69	30		
		B4 (near-IR)	0.76 – 0.90	30		
		B5 (SWIR-1)	1.55 – 1.75	30		
		B6 (Thermal)	10.40 – 12.50	30		
		B7 (SWIR-2)	2.08 – 2.35	30		
Landsat 8	OLI	B1 (coastal)	0.43 – 0.45	30		2013
		B2 (blue)	0.45 – 0.51	30		
		B3 (green)	0.53 – 0.59	30		
		B4 (red)	0.64 – 0.67	30		
		B5 (near-IR)	0.85 – 0.88	30		
		B6 (SWIR-1)	1.57 – 1.65	30		
		B7 (SWIR-2)	2.11 – 2.29	30		
		B8 (PAN)	0.50 – 0.68	15		
		B9 (cirrus)	1.36 – 1.38	30		
	TIRS	B10 (RIRS-1)	10.60 – 11.19	100		
		B11 (TIRS-2)	11.50 – 12.51	100		
WorldView-2		PAN	450 – 800	0.5	1.1 days	2009
		B1 (blue)	450 – 510	2.0		
		B2 (green)	510 – 580	2.0		
		B3 (red)	630 – 690	2.0		
		B4 (near-IR-1)	770 – 895	2.0		
SPOT 7		PAN	0.450 – 0.745	1.5	1 day	2014
		B1 (blue)	0.450 – 0.525	6.0		
		B2 (green)	0.530 – 0.590	6.0		
		B3 (red)	0.625 – 0.695	6.0		
		B4 (near-IR)	0.760 – 0.890	6.0		

3.2.2.3. | *Image pre-processing*

- **Landsat**

Traditionally, all Landsat data products were rescaled to Top of the Atmosphere (TOA) reflectance and/or radiance for analysis purposes. The reorganized Landsat archive consists of tiered (Tier 1, Tier 2) and Real-Time (RT) data collection structure, which represents a significant change in Landsat data. Landsat Collection 1 Level-2 data products include corrected SR data (Masek *et al*., 2006; Vermote *et al*., 2016) that do not require rescaling. Therefore, no pre-processing was applied to the Landsat images. SR image processing and subsequent image analysis were handled in ESRI ArcMap software (10.3.1).

- **SPOT and WV-2**

The SPOT 7 standard ortho-products are delivered application-ready: pan-sharpened, in most cases, and orthorectified imagery in natural colour (Parage *et al*., 2014). The standard ortho-products are georeferenced in earth geometry, corrected for acquisition and terrain off-nadir effects (Parage *et al*., 2014). DigitalGlobe provides 50 cm orthorectified imagery products that are application-ready. The images are radiometrically corrected, sensor corrected and orthorectified with a digital terrain model (DigitalGlobe, 2013b). DigitalGlobe offers three image band options; panchromatic, multispectral (4 or 8 bands) and pan-sharpened product in most cases. In this study, a 4-band multispectral image with the panchromatic band was used. Radiometric and geometric preprocessing processes were therefore not necessary in all images.

Mosaic and pan-sharpening

SPOT and WV-2 images were delivered in a tiled format, both multispectral and panchromatic. These were colour balanced and mosaiced in ENVI to give full seamless coverage. Pan-sharpening or data fusion was applied to create a high-resolution multispectral image. This yielded means to identify GDEs through change detection in a fine resolution imagery. Pan-sharpening refers to the process of integrating a high resolution one hand panchromatic image with a low resolution multispectral image (Campbell and Wynne, 2011). The technique is applicable when images are acquired on the same date or have close dates and they should register to each other (Campbell and Wynne, 2011). The process is computed on a pixel by pixel basis, thus changing the low-resolution image into a high-resolution colour image by fusing a co-registered fine spatial resolution image of the same area (Alimuddin *et al*., 2012). Different pan-sharpening methods have different capabilities. Alimuddin *et al*. (2012) found the Ehler method to be highly accurate when comparing different fusion methods using a WorldView-2 image. In this study, the Ehler technique, also known as intensity-hue-saturation (IHS) was compared with the Color Normalised (Brovey) and the Gram-Schmidt (GS) technique in ENVI. The Ehler method demonstrated to be a better option for pan sharpening the SPOT images, while the GS technique showed better results in the WV-2 image.

3.2.3. | Climate data

3.2.3.1. | *Rainfall data*

The monthly rainfall data for the period from 1984-2017 was obtained from the Climate Hazards Group InfraRed Precipitation with Station data (CHIRPS, available at http://chg.geog.ucsb.edu/data/chirps). CHIRPS is a 30+ year quasi-global rainfall dataset that incorporates a high-resolution satellite imagery (0.05°) with ground rainfall station data. The daily, pentadal (5-day rainfall) and monthly rainfall dataset cover all regions of the globe between 50°S - 50°N starting in 1981 to near-present (Funk *et al*., 2015).

3.2.3.2. | *Temperature data*

The daily and mean monthly temperature data for the study period (1984-2017) was sourced from both the Agricultural Research Council Institute for Soil, Climate, and Water (ARC-ISCW) and the South African Weather Service (SAWS). The data was recorded from neighboring stations in the study area (Figure 3.3). Table 3.2 provides a detailed summary of the weather stations.

Table 3.2: A detailed summary of the weather stations.

Station No	Station Name	Data period	Latitude (°)	Longitude (°)	Altitude (m)
20157	Rouxpos	1988 - 2017	-33,4049	21,06639	641
30906	Ladismith Buffelsvlei	1984 - 1987	-33,4991	21,21111	468

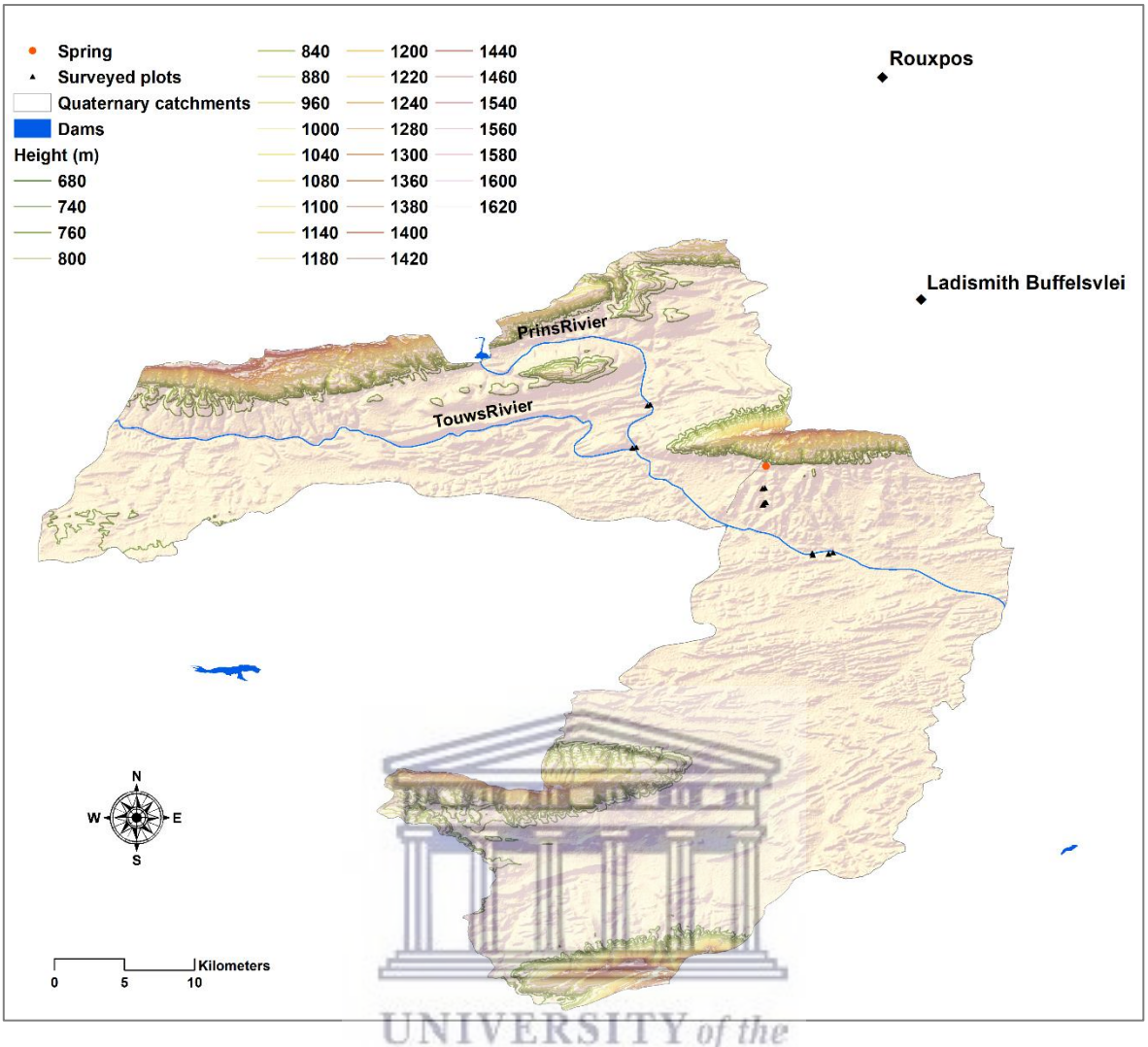

Figure 3.3: The location of the weather stations relative to the study region.

3.3. | Methods

3.3.1. | Vegetation density assessment

3.3.1.1. | Normalized Difference Vegetation Index (NDVI)

The NDVI is the most commonly used vegetation index that makes use of the red and near-infrared bands of the electromagnetic spectrum to determine vegetation status and photosynthetic activity in each area (Khosravi *et al*., 2017). The algorithm is explained through the equation:

$$NDVI = \frac{NIR - Red}{NIR + Red} \qquad (\mathbf{Eq.\ 1})$$

where *NIR* is the reflectance in the near-infrared band and *red* is the reflectance in the red visible channel. The resulting values range between -1 and +1. Where vegetation is dense, the index is close to +1 and it decreases with minimal vegetation cover till -1.

In the new Landsat SR products, values of spectral indices are different from the values of previous images. Pixel values with a spectral index of less than or equal to -1.0 are set to -10 000 and a spectral index greater than or equal to +1.0 are set to 10 000 in the output product (Masek *et al*., 2006; Vermote *et al*., 2016). However, for analysis purposes, the NDVI values were rescaled to values ranging between -1 and +1 to enable proper representation. Using a raster calculator in ArcMap, the scale factor of 0.0001 (mentioned in the USGS SR product guide) was used to convert the data range to -1 and +1 using the method:

$$(Calculated\ NDVI\ *\ 0.0001) \qquad (\mathbf{Eq.2})$$

3.3.2. | Climatic data analysis

3.3.2.1. | *Examining rainfall seasonality*

Average monthly rainfall totals were obtained by extracting the study area from the CHIRPS Africa monthly rainfall dataset using the extraction tool in spatial analyst tools, ArcMap toolbox. The monthly averages were used to analyze rainfall seasonality and anomaly for the study period (1984-2017). CHIRPS pixel values in each sample point were used to present rainfall record in each plot.

3.3.2.2. | *Measuring variations in rainfall*

The Coefficient of variation (CV) was used to test the level of variability of rainfall in each sampled vegetation plot. The CV (%) measures the probability of fluctuations by considering the mean and is independent of the original unit of measure in being expressed as a percentage (Schulze, 2011). A rule of thumb established by Conrad (1941) as cited by Schulze (2007) is that the higher the mean annual precipitation (MAP), the lower its inter-annual variability. The study area is characterized by low MAP and has high inter-annual rainfall variability, hence the need to measure variability. The CV is calculated as the standard deviation of the annual series divided by the mean (Chen *et al*., 2014):

$$CV = \frac{\sigma}{\mu} \times 100 \qquad (\mathbf{equ.3})$$

where *CV* is the coefficient of variation; σ is standard deviation, and μ is the mean precipitation. Low CV is represented by values less than 20 (CV <20), moderate (20 <CV <30) and high (CV >30) (Hare, 2003).

3.3.2.3. | *Standardized Precipitation Index (SPI)*

The SPI is a drought index that is explicitly based on precipitation data and can be used to identify the intensity and duration of droughts. The rainfall record is first fitted to a gamma distribution and transferred to a normal distribution using an equal probability transformation (Zargar *et al*., 2011). The mean is then set to zero and as such, values above zero indicate wet periods and values below zero indicate dry periods (Mckee *et al*., 1993). The MDM (Meteorological Drought Monitor) software from the AgriMetSoft (Agricultural and Meteorological Software) center was used to calculate the 12-month SPI from the CHIRPS average monthly rainfall totals. Further details on how to compute the SPI can be obtained from McKee *et al*. (1993) and Hayes *et al*. (1999). The SPI-12 was selected because it provides a reflection of long-term precipitation patterns (WMO, 2012).

Table 3.3: Drought classification according to SPI values.

SPI value	Classification description
≥ 2.00	Extremely wet
1.50 to 1.99	Very wet
1.00 to 1.49	Moderate wet
0 to -0.99	Near normal
-1.00 to -1.49	Moderate dry
-1.50 to -1.99	Severely dry
≤ -2.00 and less	Extremely dry

Source: *McKee et al. (1993).*

3.3.2.4. | *Analyzing seasonal temperatures*

The mean monthly maximum and minimum temperatures were analyzed to identify seasonal variations and for correlation determinations between temperature and vegetation productivity for a long-term series and for different seasons between 1984 and 2017.

3.3.3. | Linear correlation and multivariable analysis

The Pearson correlation coefficient was used to determine the strength of a linear relationship between monthly mean NDVI and monthly mean precipitation and between monthly mean temperature and NDVI. The correlations were computed for different seasons and for a long inter-annual time-series. A correlation coefficient is a statistical value used to measure the strength of a linear association between two variables:

$$r = \frac{n \sum xy - (\sum x)(\sum y)}{\sqrt{n(\sum x^2) - (\sum x)^2}\sqrt{n\,(\sum y^2) - (\sum y)^2}} \qquad (\mathbf{equ.4})$$

where *r* is a product correlation coefficient, *n* is the number of scores, *x* and *y* are variables, Σ xy is the sum of *x* and *y*, Σx is the sum of *x*, Σy is the sum of *y*.

The results range between -1 and +1. +1 in the case of a perfect positive linear relationship and -1 in the case of a perfect negative linear relationship. Values between -1 and +1 in all other cases indicate the degree of linear independence between the variables. A value near zero indicates a nonlinear relationship. The closer the coefficient is to either -1 or 1, the stronger the correlation between the variables (Turyahikayo, 2014) as indicated below:

$Negative$	$Small\ or\ none$	$Positive$
$r = -1$	$r = 0$	$r = +1$

Time lag analysis was carried out to consider the lag between vegetation productivity and changes in rainfall and temperature. A zero-month lag and 3-month lag relationships were investigated, and the results are presented in section 4.1.8.

A multivariate analysis refers to the impact of multiple variables to a single variable (Fox, 1997). It allows an analysis of the independent contribution of each variable to the dependent variable. In this study, a multiple regression model was used to observe the influence of rainfall and temperature on vegetation productivity and quantify the combined effect of independent variables on vegetation productivity. The multiple regression model was computed in the IBM Statistical Package for the Social Sciences (SPSS) software program using the stepwise method.

3.3.4. | Assessing Groundwater Dependent Ecosystems (GDEs)

The year 2017 was considered a suitable year for identifying potential GDEs. The year was extremely dry as indicated by low annual rainfall (Table 3.4). The dry conditions provided a basis to detect vegetation and water that rely on groundwater. For this section, a sub-region of the original study area was created and this consisted of the sampled vegetation plot sites and the center of the sampling region (Figure 3.4). The reasoning for creating a sub-region was to be able to map GDEs at a manageable scale and to avoid miss-classifications which were encountered during the initial classification using a map of the entire study area.

The mapping of GDEs comprised land cover classification using the supervised image classification approach, and identifying groundwater discharge areas. Eamus *et al*. (2006) have also argued that GDEs are likely to be situated in areas where groundwater is discharged to the surface. It is important to note that this section focused on surface GDEs, i.e. those reliant on a surface expression of groundwater with a specific focus on vegetation and water.

Table 3.4: Annual precipitation by year during the study period (1984-2017) calculated from the CHIRPS rainfall dataset.

Year	Annual precipitation (mm)	Year	Annual precipitation (mm)
1984	256.61	2001	298.07
1985	400.72	2002	349.02
1986	299.50	2003	317.73
1987	267.19	2004	336.62
1988	312.51	2005	301.52
1989	362.81	2006	346.99
1990	342.92	2007	358.94
1991	271.86	2008	267.12
1992	311.85	2009	318.12
1993	370.29	2010	237.67
1994	306.43	2011	326.41
1995	430.37	2012	346.80
1996	341.06	2013	344.95
1997	285.81	2014	266.79
1998	343.78	2015	301.34
1999	340.23	2016	270.80
2000	253.31	2017	200.68

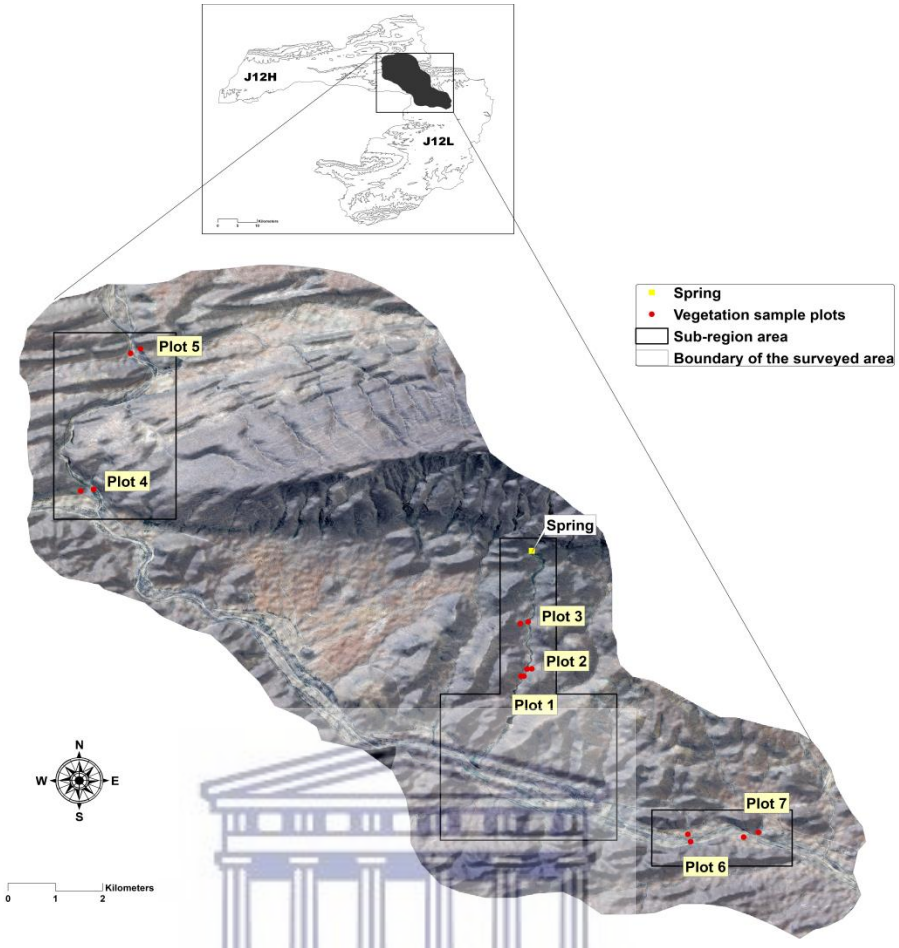

Figure 3.4: Map of the quaternary catchments showing the boundary of the sub-region and sample plots.

3.3.4.1. | Image classification

Three images were used for land cover classification; an ortho-corrected WorldView-2 image, which was taken during the period of data collection (28th October 2017), and two standard ortho-corrected SPOT 7 images taken on the 17th of July 2017 and 13th of September 2017. The SPOT image dates were the only available images in the South African National Space Agency (SANSA) online catalog for 2017, thus leading to a default selection.

Image classification was performed in Definiens eCognition version 9.0 and ENVI version 5.3 using the object-based and pixel-based classification methods respectively. The land cover classes used for classification are listed in Table 3.5. A true colour composite (red, green, blue) was used; bands (1, 2 and 3) for SPOT 7 and bands (3, 2 and 1) for WorldView-2.

Table 3.5: The land cover classes of GDEs used for classification.

Type	Land cover classes	
GDE related	LC 1	**Healthy green vegetation:** vegetation that has permanent access to water, shows consistent greenness and wetness even after a prolonged dry period.
	LC 2	**Water bodies:** consistent water content and wetness, with low greenness during the dry season.

Source: *Barron et al. (2012).*

Object-based classification

The object-based classification process can be divided into two main workflow steps as shown below; segmentation and classification of the resulting image objects.

- **Segmentation**

Image segmentation was carried out using the multi-scale segmentation (MSS) algorithm.

Spectral band selection and weighting

Each layer or image band is assigned a weight in the segmentation process. All bands were used in this study and these were assigned an equal weighting of 0.1 (default value in eCognition), expect the NIR band which was assigned a weight of 2. The reasoning for assigning the NIR band a different weight was that vegetation reflects high in the NIR band and this was considered important for delineating vegetation that relies on groundwater.

Scale, shape and compactness parameter selection

To produce visually pleasing segmentation results, the trial and error process was conducted. Three levels of scale (180, 100, and 60) combined with a shape factor of 0.1 and a compactness of 0.6 (Table 3.6) were tested in the error and trial process. At level 4, the scale factor of 40 combined with a shape factor of 0.1 and a compactness of 0.6 provided visually appealing segmentation results after costing a great deal of time.

Table 3.6: Segmentation parameters and criterion.

Segmentation level	Scale	Shape	Compactness
1	180	0.1	0.6
2	100	0.1	0.6
3	60	0.1	0.6
4	40	0.1	0.6

- **Classification**

The images were classified using a combination of user-defined fuzzy membership functions and the nearest neighbor classifier. Training samples were randomly created for each land cover class (Table 3.7). These differed in each image in order to identify surface changes in terms of vegetation and water, thus meeting the objective of classification (i.e. to identifying GDEs). The feature extraction and analysis function based on features listed in Table 3.8 were used to identify a suitable threshold value for separating classes. The feature properties, which are described through fuzzy rules, are mainly used for dealing with uncertainty and vagueness in cases where an image object belongs to more than one class (Feizizadeh *et al*., 2017). The selection of features was guided by the characteristics of surface features in the study area and the literature (Benz *et al*., 2004). The nearest neighbor classifier with the defined membership functions for each class was computed to classify the SPOT images.

Table 3.7: Land cover classes and the random samples created in each image for classification.

Land cover classes	Samples by image		
	SPOT 7 (17-July)	SPOT 7 (13-September)	WorldView-2 (28-October)
Healthy green vegetation	250	125	92
Water bodies	43	53	15

Table 3.8: Features considered for separating objects in object-based image classification.

Attribute		Properties
Spectral attributes		Mean
		Standard deviation
Geometric attributes	Extent	Area
	Shape	(Asymmetry, Border index, Compactness, and Shape index)
	Texture	Mean of sub-objects: standard deviation
		Average mean difference to neighbors of sub-objects

Pixel-based classification

The WorldView-2 image was initially classified in eCognition. However, the process was time-consuming and the results displayed enormous misclassification. To rectify the errors, other possible combinations of threshold values were required to separate the classes and samples needed to be reassigned to the misclassified areas. This was time-consuming and the software

eventually ran slow. Therefore, the WorldView-2 image was alternatively classified in ENVI using the traditional supervised maximum likelihood method.

- **Defining training sites and classifying**

The same classes in Table 3.7 were used to create training sites by assigning pixels to these land cover classes. A signature file which contains statistical information about the reflectance values of the pixels within the training sites for each class was created. A maximum likelihood algorithm was used to classify the image based on the signature file.

Classification problems encountered

In segmenting image objects, the major challenge experienced was choosing the appropriate segmentation parameters. The mapped area consists of objects that vary in size substantially. For instance, the size of shrubs is significantly small compared to the size of water bodies or bare land. Therefore, some small individual shrubs were merged with bare land or unclassified area. The mapped area is located in the Karoo, a semi-desert environment, and therefore some vegetated areas have similar reflectance signatures to bare land due to their composition and texture. The classification algorithm classified such features as a single class, thus resulting in misclassification.

3.3.4.2. | Indicators of groundwater discharge areas

A 30 m SRTM Digital Elevation Model (DEM) obtained from the USGS Earth Explorer website was used to create profile curvature, Topographic Wetness Index (TWI) and the hill-shade which was used to visualize elevation. A threshold value of 0.01 derived from Tweed *et al*. (2007) was used to calculate the profile curvature.

As demonstrated by Tweed *et al*. (2007), topographic depression can be used to detect potential zones of groundwater discharge. In this study, the TWI was used to identify potential zones of saturation. The modified wetness index (w) was calculated using the following equation (Moore *et al*., 1991):

$$w = 1\mathrm{n}\left(\frac{1}{\tan\beta}\right), \qquad (\mathbf{equ.\ 5})$$

where β is the slope gradient (in degrees). A threshold technique of >10, adopted from Tweed *et al*. (2007), was used on the wetness index to map topographic depressions and areas of potential groundwater discharge.

3.3.4.3. | *Validation*

The classification results were assessed through the producer and user accuracy, overall accuracy, and Kappa coefficient derived from the confusion matrix. Producer accuracy determines the degree of accurately classified reference data and user accuracy is a descriptive summary of how much of the entire classified area was correct (Barron *et al*., 2012). The Kappa coefficient measures the agreement between classification and reference data. Accuracy assessment of the classified WorldView-2 image was computed using the ground truth region of interest (ROIs) approach in ENVI. Training samples of the same classes as those in the classified image were created using the random sampling method which is recommended by Kerle *et al*. (2004).

The classified SPOT 7 images were assessed by comparing the location and class of each ground truth sample of the reference image with the corresponding location and class of the same sample in the classified image. The natural colour image that was used for classification was also used for accuracy. 300 sample points were randomly created in ArcGIS. These were converted to a raster file and imported in eCognition. The points were linked with corresponding classes by manually creating samples where a pixel correspond with a point and saving the results as a TTA mask which was used to calculate the accuracy assessment. The method has been previously used by Kongo and Pavlique (2015).

GDEs were further validated by examining the characteristics of the dominant plant species in both the floodplain woodland and the hillslope shrubland plant communities (Chapter 5). This was guided by the literature.

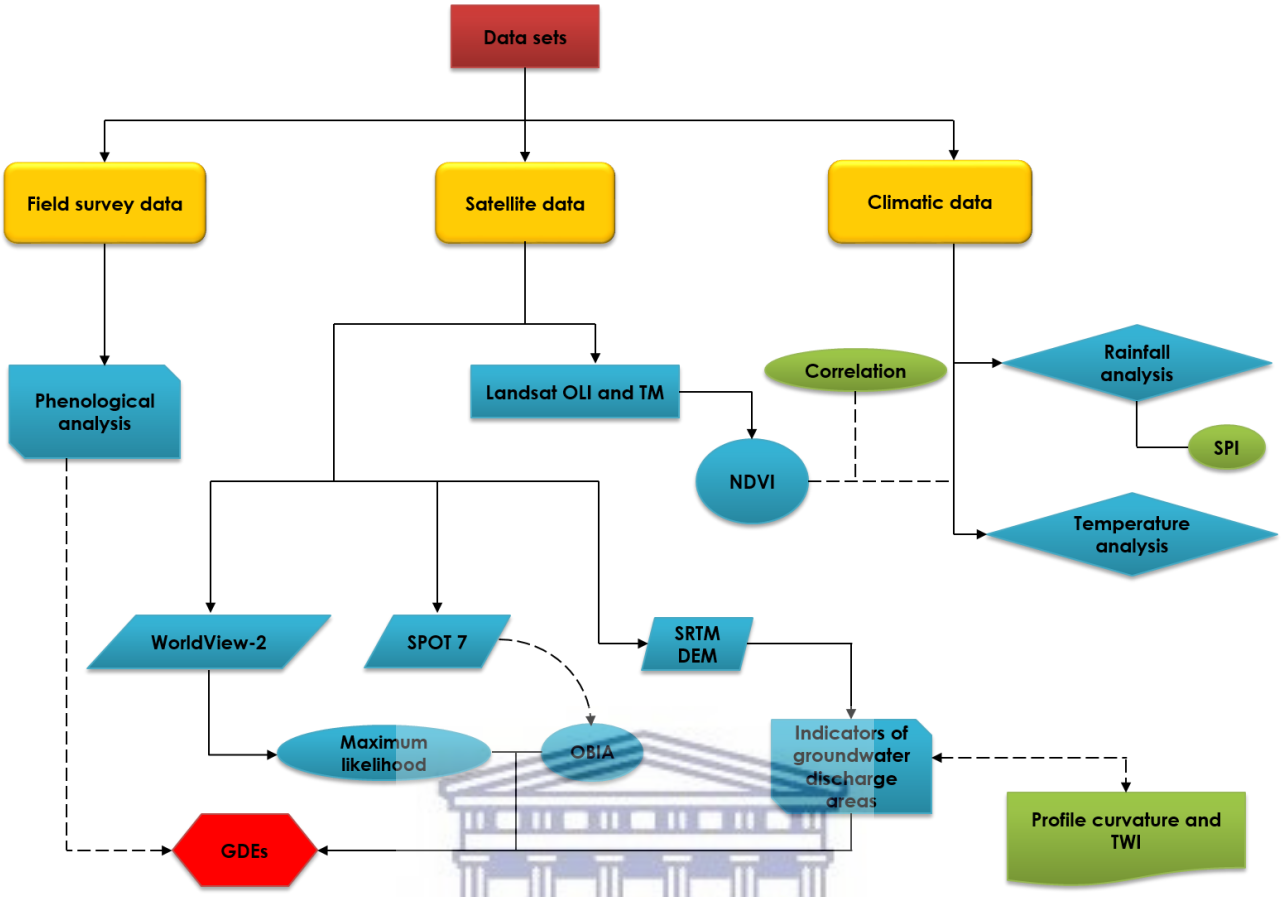

Figure 3.5: A flow diagram of the research methods from data acquisition to data analysis.

CHAPTER 4: THE IMPACT OF RAINFALL AND TEMPERATURE ON VEGETATION PRODUCTIVITY, AND THE SPATIAL RANGE OF GROUNDWATER DEPENDENT ECOSYSTEMS (GDEs)

4.1. | Results

4.1.1. | Introduction

The aim of this chapter is to present the results used to address the objectives of this study; *"To develop an understanding of spatiotemporal dynamics of rainfall in the Touws River quaternary catchments and provide a basis for assessing the role of rainfall and temperature variations on vegetation productivity"* and *"To investigate the spatial occurrence of groundwater dependent ecosystems in 2017"*. Extensive analysis of the generated findings and a detailed discussion is carried out. This chapter starts by delineating the plant species gathered in each sampled vegetation plot, and their communities. This is followed by a presentation of inter-annual variation of vegetation productivity and precipitation at plot scale. Analysis of temperature and rainfall data on different time scales is performed, followed by a correlation analysis. The results of image classification are presented followed by a detailed analysis of the indicators of groundwater discharge areas and lastly, a comprehensive discussion is carried out.

4.1.2. | Vegetation analysis

4.1.2.1. | *Description of plant communities*

The plant communities of the study area can be grouped as follows:

1. Floodplain woodland community
2. Hillslope shrubland community
    2.1. *Vygie*-open succulent sub-community

1. Floodplain woodland community (Figure 4.1 a & b)

The floodplain woodland community grows along the river banks and along the edges of the floodplain, where the soil is poorly developed. The alluvium is sand, or gravel and the water

is slightly saline. The deposited material in the floodplain also consists of medium to large pebbles and small boulders. The vegetation in this community is dominated by a 9-12 m *Vachellia karroo* trees (Table 4.1). Other species present include *Veronica anagallis-aquatica* subsp. *anagallis-aquatica*, an annual macrophyte of 30-120 cm tall, *Mesembryanthemum guerichianum*, *Gomphocarpus fruticosus* subsp. *fruticosus*, a perennial plant, and *Calpurnia aurea* subsp. *aurea*, which grows on moist sandy soil. The floodplain woodland community is found in vegetation plot 4, 6 and 7.

2. Hillslope shrubland community (Figure 4.1 c & e)

The hillslope shrubland community is commonly found in rocky flats and hilly arid surfaces. The substrate is dominated by gravel on hard ground, made up of stones and fines of less than 2 cm in size. The community is composed of drought-resistant low growing shrubs, which mostly flower in spring. Plant species in this community include *Pteronia pallens*, *Rhigozum obovatum*, *Drosanthemum micans*, *Searsia crenata*, *Salsola aphylla*, *Indigofera aspalathoides*, *Ruschia muricata*, *Euclea undulata*, *Monsonia camdeboensis,* and *Anchusa capensis* (Table 4.2). The hillslope shrubland community is found in vegetation plot 1, 2, 3 and 5.

2.1. *Vygie*-open succulent sub-community (Figure 4.1 d)

The *Vygie* is a sub-community of the hillslope shrubland community and is found on a gentle to flat open surface, with undulating sand deposits along the floodplain. It is characterized by sandy soils, with exposed pebbles ranging from 20% to 80%. The vegetation forms scattered groups of low to short shrubs. The dominant species in this community is the *Mesembryanthemaceae fenzl*, a succulent dwarf shrub. This sub-community is found in vegetation plot 5.

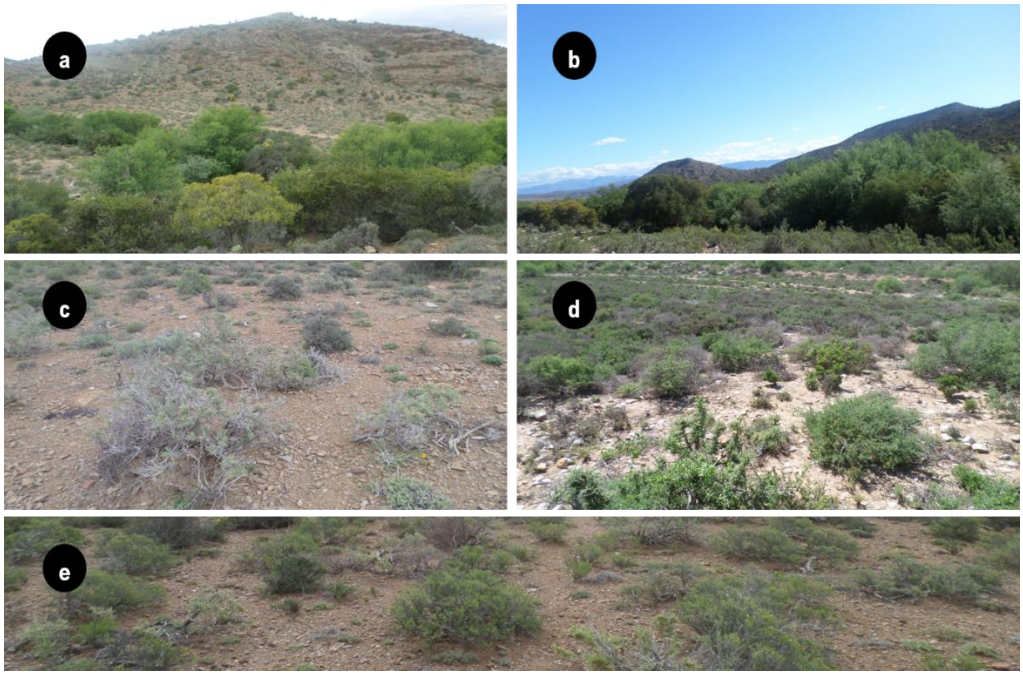

Figure 4.1: Vegetation community types described and characterized in the Touws quaternary catchments: (**A** and **B**) Floodplain woodland community, (**C** and **E**) Hillslope shrubland community, and (**D**) *Vygie* – open succulent sub-community.

4.1.2.2. | Plant species by vegetation community

The plant species gathered at sample plots in the study site are presented in Table 4.1 and 4.2. Each vegetation plot is paired into a riparian (A) and non-riparian area (B) and the percentage cover is based on the dominant plant species in each plot, denoted by the asterisk (*):

Table 4.1: Plant species collected during the survey period in the floodplain woodland community.

Plots	Location of occurrence	Scientific name	Family name	Cover (%)
Plot 4	A riparian	*Ruschia muricate* *	Aizoaceae	50-70
		Anchusa capensis	Boraginaceae	
		Pteronia pallens	Asteraceae	
	B non-riparian	*Vachellia karroo* *	Fabaceae	70-90
		Calpurnia aurea subsp. *aurea*	Fabaceae	
Plot 6	A riparian	*Indigofera aspalathoides* *	Fabaceae	60-90
		Pteronia pallens	Asteraceae	
		Ruschia muricata	Aizoaceae	
	B non-riparian	*Vachellia karroo* *	Fabaceae	45-60
		Euclea undulata	Ebenaceae	
		Indigofera aspalathoides	Fabaceae	
Plot 7	A riparian	*Pteronia pallens*	Asteraceae	
		Ruschia muricate *	Aizoaceae	35-60
	B non-riparian	*Vachellia karroo* *	Fabaceae	65-80
		Mesembryanthemum guerichianum	Aizoaceae	

*indicates dominant plant species in each area.

Table 4.2: Plant species collected during the survey period in the hillslope shrubland community.

Plots	Location of occurrence	Scientific name	Family name	Cover (%)
Plot 1	A (riparian)	*Vachellia karroo* *	Fabaceae	75-80
		Euclea undulata	Ebenaceae	
		Searsia crenata	Anacardiaceae	
	B (non-riparian)	*Pteronia pallens*	Asteraceae	
		Salsola aphylla	Amaranthaceae	
		Drosanthemum micans	Aizoaceae	
		Indigofera aspalathoides	Fabaceae	30-50
		Ruschia muricata	Aizoaceae	
Plot 2	A (riparian)	*Veronica anagallis-aquatica* subsp. *anagallis-aquatica* *	Plantaginaceae	60-70
	B (non-riparian)	*Monsonia camdeboensis* *	Geraniaceae	20-45
		Rhigozum obovatum	Bignoniaceae	
		Euclea undulata	Ebenaceae	
Plot 3	A (riparian)	*Vachellia karroo* *	Fabacea	50-70
		Gomphocarpus fruticosus subsp. *fruticosus*	Apocynaceae	
	B (non-riparian)	*Euclea undulata* *	Ebenaceae	70-80
Plot 5	A (riparian)	*Euclea undulata* *	Ebenaceae	60-90
		Rhigozum obovatum	Bignoniaceae	
	B (non-riparian)	*Vachellia karroo* *	Fabaceae	40-65
		Ruschia muricata	Aizoaceae	
		Rhigozum obovatum	Bignoniaceae	
		Mesembryanthemaceae fenzl	Aizoaceae	

*indicates dominant plant species in each area.

4.1.3. | Inter-annual variability of NDVI and precipitation

This section shows the variations of vegetation productivity and precipitation in the sampled plot sites for the study period (1984-2017). The two areas in each vegetation plot, (i.e. area A and area B) represent riparian (shown in green, area A) and non-riparian (shown in red, area B) areas respectively. It is worth noting that within the CHIRPS rainfall dataset, plot 1 and 2 are within the same pixel and have the same rainfall values. Plots 6 and 7 are also within the same pixel and have the same rainfall values. The vegetation plots are presented in the following order: plot 1, 2, 3 and 5 (hillslope shrubland community) and plot 4, 6 and 7 (floodplain woodland community). Descriptive statistics of rainfall and NDVI for each plot site were calculated (Table 4.3 and Table 4.4).

Table 4.3: Descriptive statistics of the sampled vegetation plots calculated from the full NDVI dataset.

Plots	Location of occurrence	Community name	Average	Maximum	Minimum	Standard deviation
Plot 1	Area A (riparian)	**Hillslope shrubland community**	0,2715	0,3363	0,1479	0,03747
	Area B (non-riparian)		0,2582	0,3498	0,1125	0,03966
Plot 2	Area A (riparian)		0,2708	0,3661	0,1919	0,03657
	Area B (non-riparian)		0,2546	0,3466	0,1817	0,03215
Plot 3	Area A (riparian)		0,2683	0,3328	0,1318	0,03547
	Area B (non-riparian)		0,2550	0,3634	0,1000	0,04051
Plot 4	Area A (riparian)	**Floodplain woodland community**	0,2924	0,4173	0,1987	0,03907
	Area B (non-riparian)		0,2860	0,8940	0,1037	0,11968
Plot 5	Area A (riparian)	**Hillslope shrubland community**	0,3707	0,4740	0,1292	0,05286
	Area B (non-riparian)		0,2542	0,8610	0,1574	0,07238
Plot 6	Area A (riparian)	**Floodplain woodland community**	0,4518	0,6390	0,1915	0,07690
	Area B (non-riparian)		0,3327	0,4391	0,1703	0,05601
Plot 7	Area A (riparian)		0,4046	0,5062	0,1074	0,06028
	Area B (non-riparian)		0,2886	0,4256	0,1451	0,05243

Table 4.4: Descriptive statistics of the sampled vegetation plots calculated from the CHIRPS rainfall dataset.

Plots	Location of occurrence	Average (mm)	Maximum (mm)	Minimum (mm)	Standard deviation (mm)
PLOT 1 & 2		7.17	10.16	2.56	1.37
PLOT 3		10.30	13.55	3.61	2.02
PLOT 4	Area A (riparian)	8.65	12.54	3.07	1.71
	Area B (non-riparian)	7.19	10.77	2.60	1.41
PLOT 5		7.31	11.07	2.56	1.46
PLOT 6 & 7		7.40	10.55	2.66	1.41

Table 4.5: The units used in NDVI scatter plots and the corresponding Landsat image dates (1984-2017).

No.	Date		No.	Date		No.	Date	
1	04-Jul	**1984**	129	30-Apr	**1995**	269	24-Dec	**2006**
5	25-Nov		131	01-Jun		275	02-Jun	**2007**
29	01-Dec	**1986**	132	19-Jul		276	04-Jul	
30	18-Jan	**1987**	134	05-Sep		277	05-Aug	
31	03-Feb		139	12-Feb	**1996**	283	13-Feb	**2008**
54	23-Jan	**1989**	143	03-Jun		298	06-May	**2009**
56	28-Mar		143.5	19-Jun		298.5	22-May	
57	29-Apr		144	21-Jul		309	07-Apr	**2010**
58	15-May		145	22-Aug		321	10-Apr	**2011**
59	16-Jun		148	10-Nov		350	06-Sep	**2013**
61	03-Aug		150	13-Jan	**1997**	350.5	22-Sep	
64	07-Nov		150.5	29-Jan		351	24-Oct	
65	09-Dec		151	14-Feb		352	25-Nov	
67	27-Feb	**1990**	152	02-Mar		356	17-Mar	**2014**
71	19-Jun		154	21-May		357	18-Apr	
72	05-Jul		156	08-Jul		359	21-Jun	
72.5	21-Jul		158	10-Sep		360	07-Jul	
73	06-Aug		158.5	26-Sep		361	24-Aug	
75	25-Oct		161	15-Dec		362	25-Sep	
76	26-Nov		163	01-Feb	**1998**	363	11-Oct	
77	28-Dec		164	21-Mar		365	14-Dec	
78	13-Jan	**1991**	168	11-Jul		366	15-Jan	**2015**
80	02-Mar		174	19-Jan	**1999**	368	20-Mar	
81	19-Apr		175	04-Feb		370	07-May	
82	21-May		178	11-May		371	08-Jun	
85	09-Aug		179	12-Jun		372	10-Jul	
88	29-Nov		186	22-Jan		373	27-Aug	
94	07-May	**1992**	190	13-May		376	01-Dec	
95	08-Jun		195	20-Oct	**2000**	376.5	17-Dec	
97	27-Aug		196	05-Nov		377	02-Jan	**2016**
100	15-Nov		197	23-Dec		380	07-Apr	
101	17-Dec		235	02-Feb		381	25-May	
104	07-Mar	**1993**	236	21-Mar		384	29-Aug	
104.5	23-Mar		239	09-Jun	**2004**	385	14-Sep	
108	13-Jul		239.5	25-Jun		388	03-Dec	
109	14-Aug		240	11-Jul		389	04-Jan	**2017**
113	20-Dec		252	14-Jul	**2005**	391	25-Mar	
114	21-Jan	**1994**	256	19-Nov		392	10-Apr	
117	11-Apr		261	12-Apr		394	13-Jun	
118	13-May		261.5	28-Apr		394.5	29-Jun	
122	02-Sep		264	01-Jul	**2006**	397	01-Sep	
127	09-Feb	**1995**	265	18-Aug		398	03-Oct	
128	13-Mar		267	05-Oct		399	04-Nov	
129	30-Apr		268	06-Nov		400	06-Dec	

The gaps in NDVI scatter plots (Figure 4.2 to 4.8) show the missing data from the Landsat archive and the excluded images because of cloud cover. The numbers on the x-axes of each NDVI scatter plot represents the dates of Landsat images converted to numbers based on the length of the dataset and these are displayed in Table 4.5. This was to provide a clear visualization of the missing data and to make the scatter plots more readable. In plot sites (1, 2, 3 and 4), the NDVI display a similar trend throughout the years, with minimal difference between the two areas. However, the riparian area is consistently greener in all plot sites as indicated by high NDVI values. Differences between the riparian and the non-riparian area

are most noticeable in plots 5, 6 and 7 (Figure 4.5, 4.7 and 4.8). This is further illustrated in the statistics; firstly, the difference in average and maximum values between plot 1 and plot 4 is minimal compared to the difference between plot 5, 6 and 7. Secondly, the difference between the minimum and the maximum values from plot 5 to 7 is comparatively high, thus indicating very little overlap in terms of NDVI values for riparian and non-riparian areas.

Figure 4.2 display the spread of NDVI and precipitation in the riparian and non-riparian area in vegetation plot 1 for the observed time series 1984-2017. The NDVI is low in both areas, and this is demonstrated by fairly low maximum values, 0.3362 in the riparian area and 0.3498 in the non-riparian area (Table 4.3). However, vegetation productivity in the riparian area is generally higher (0.2715 on average) than in the non-riparian area (0.2582 on average), except where the latter surpasses the former most notably in July 1997 as indicated in Figure 4.2a. This plot also experiences low precipitation, and this is highlighted by the monthly average of 20.62 mm and a maximum precipitation of just above 80 mm (Table 4.4). April 1989 and April 1993 are the only months with rainfall of more than 80 mm (Figure 4.2b). Precipitation is predominantly below the average (20.62 mm). Most precipitation is received between autumn (March – May) and summer (December – February), while precipitation is low in winter (June – August). The NDVI displays a similar pattern, where values are low during winter and high in spring and in summer (Figure 4.2a and Table 4.5).

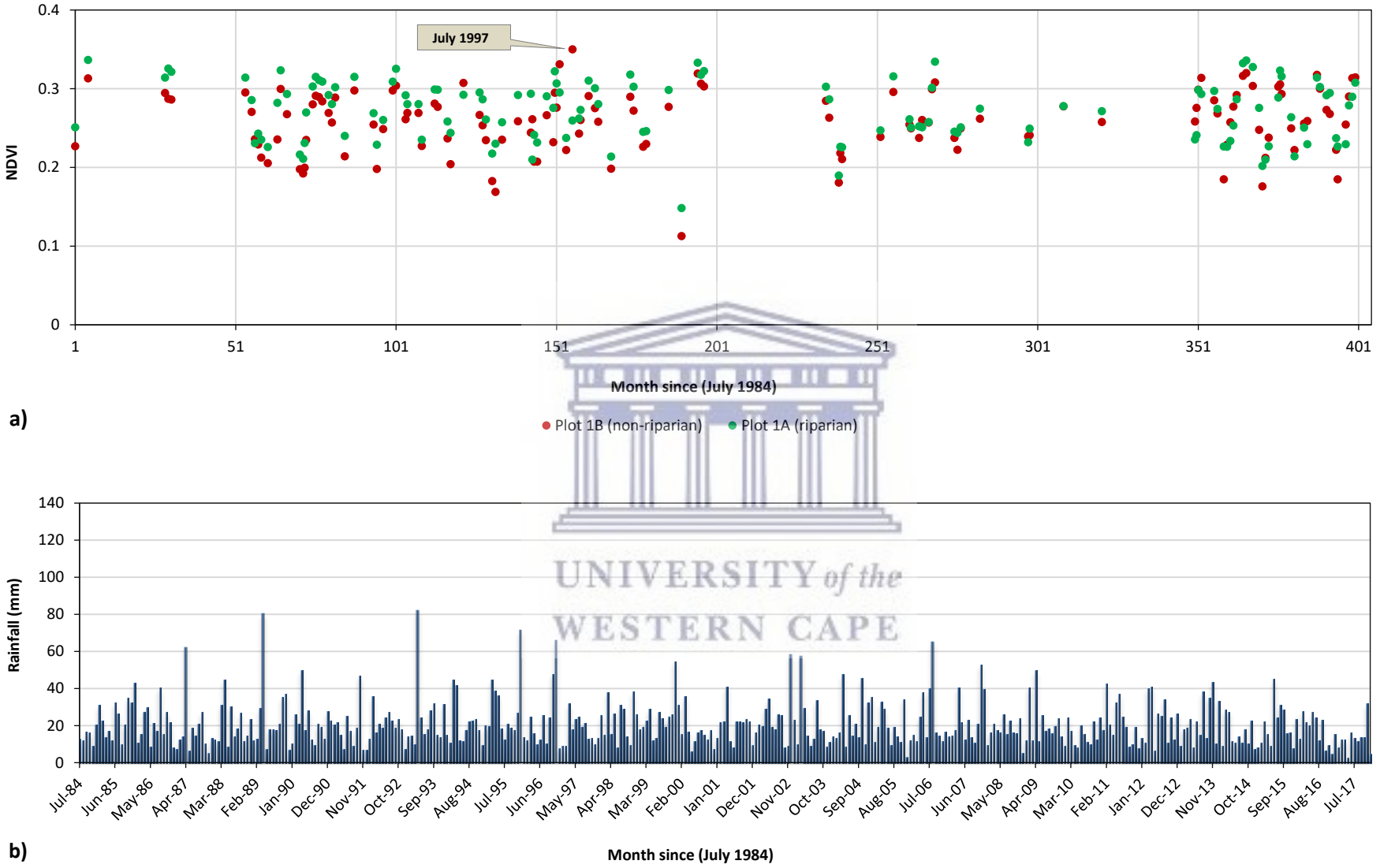

Figure 4.2: The Normalised Difference Vegetation Index (NDVI) (**a**) and monthly precipitation (**b**) for vegetation plot 1 (1984-2017).

Vegetation plot 1 and 2 are comparatively similar, both displaying low NDVI throughout the years. A similar NDVI pattern is observed in both plots where the riparian and non-riparian areas overlap almost every month. In Figure 4.3a most of NDVI is clustered between the range of 0.2 and 0.3 from January 1989 to December 2000 as indicated. This shows a uniform linear pattern and indicates less dispersal of NDVI values (standard deviation of 0.03657 in the riparian area and 0.03215 in the non-riparian area, Table 4.3). However, the difference in average values between the riparian and non-riparian area is statistically significant. This was tested using a student t-test at 0.05 probability level.

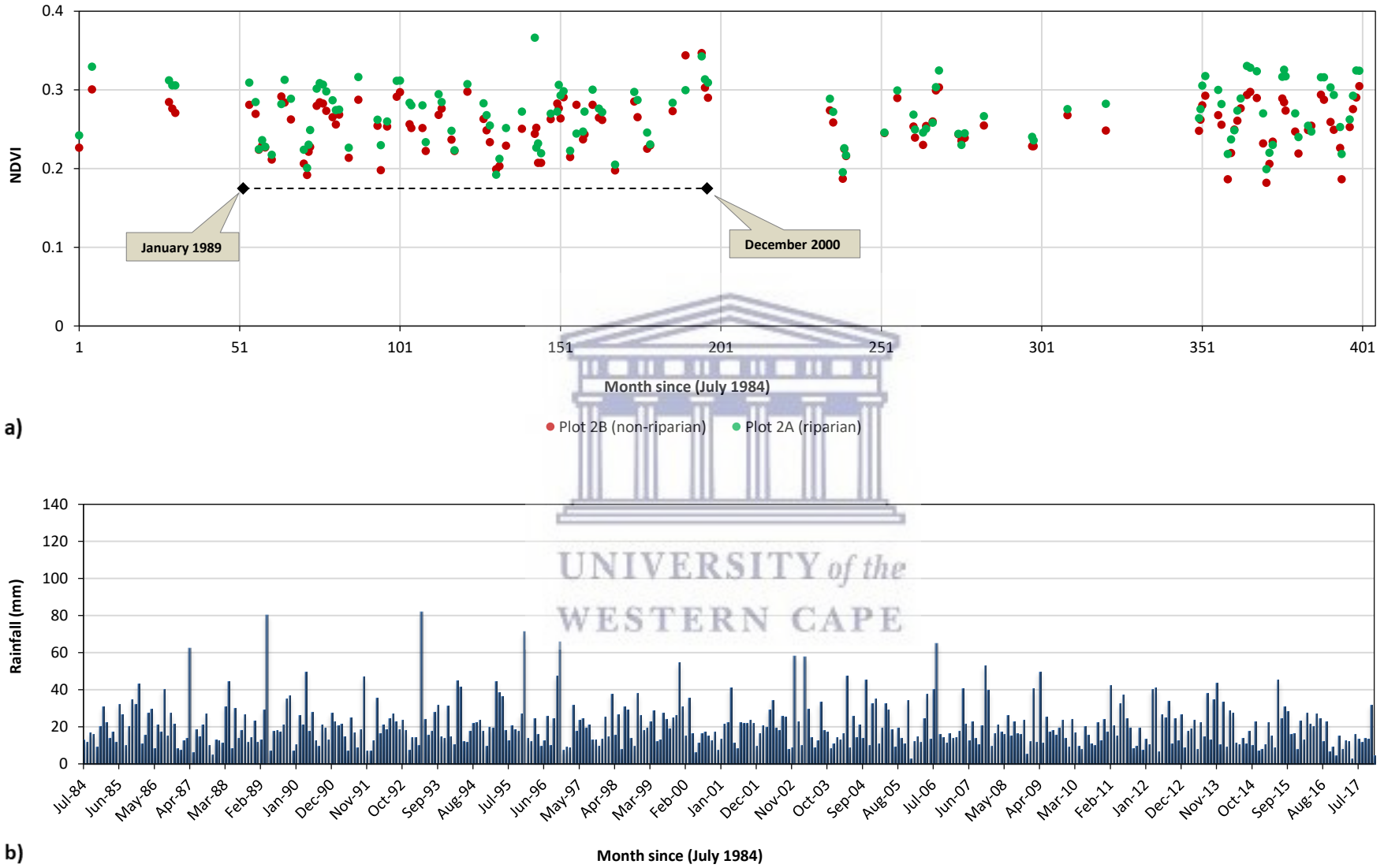

Figure 4.3: The Normalised Difference Vegetation Index (NDVI) (**a**) and monthly precipitation (**b**) for vegetation plot 2 (1984-2017).

In vegetation plot 3, the riparian and non-riparian areas are clustered in the same way as in plots 1 and 2. This makes the separation between the two areas challenging, especially when identifying patterns over the years. Plot 3 experienced the lowest NDVI value (0.1) in the non-riparian area in May 2000 (Figure 4.4a). Plot 3 has the highest monthly precipitation average (29.61 mm), the highest maximum precipitation value (133.40 mm), but also the highest standard deviation (18.89 mm) of all plots (Table 4.4). Precipitation in this plot is highly variable. A substantial number of months have precipitation of more than 40 mm, indicating sporadic, large rainfall events in this plot (Figure 4.4b). However, the NDVI has low values and therefore shows little response to these conditions.

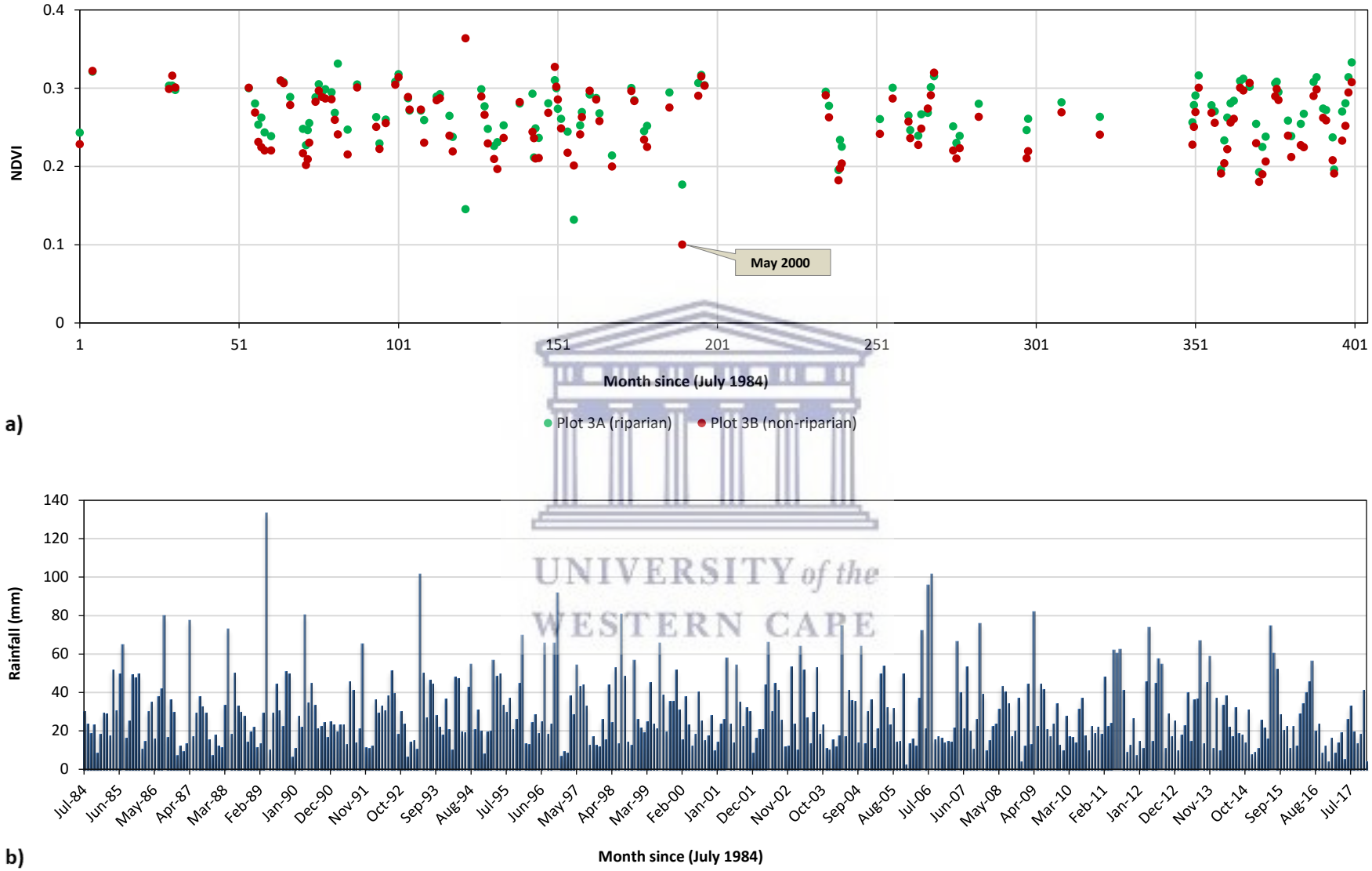

Figure 4.4: The Normalised Difference Vegetation Index (NDVI) (**a**) and monthly precipitation (**b**) for vegetation plot 3 (1984-2017).

In vegetation plot 5 the spread of NDVI is strong in both the riparian and non-riparian area, with the former consistently higher. May 1991 is the only time the NDVI was lowest in the riparian area (0.1292) and November 1984 emerges with an exceptional NDVI value (0.8610) in this plot (Figure 4.5a). Only a few months have precipitation of more than 50 mm in plot 5 (Figure 4.5b). Most of the precipitation received between 1984 and 2017 is less than the average. Some years are characterized by extremely low precipitation, most notably 2017 where November is the only month with precipitation of (34.37 mm) more than the average. Other years, such as 1999 and 2011, received precipitation of more than the average for most months and rainfall occurred almost throughout the entire year.

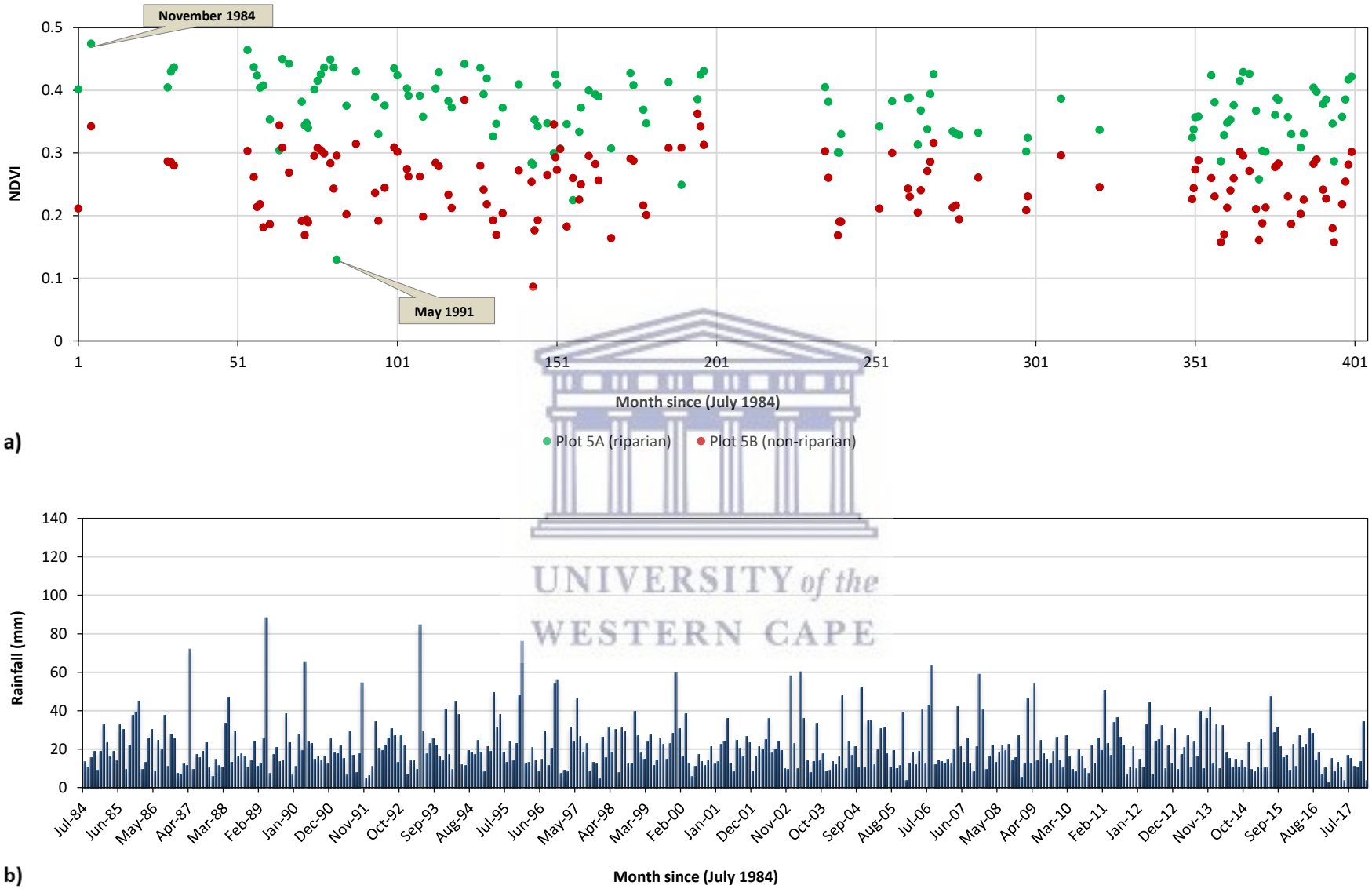

Figure 4.5: The Normalised Difference Vegetation Index (NDVI) (**a**) and monthly precipitation (**b**) for vegetation plot 5 (1984-2017).

In plot 4 (Figure 4.6a) the NDVI values for the non-riparian area are more dispersed than the riparian area and this is indicated by the high standard deviation of 0.11968 (Table 4.3). The riparian area, on the other hand, shows an almost linear pattern and low variability (SD of 0.03907). The overlap between February 2004 and December 2017 (indicated in Figure 4.6a) demonstrate a minimal difference between the two areas and this is further indicated by the slight difference in NDVI average values, 0.2871 in the riparian area and 0.2667 in the non-riparian area. In addition, the difference in average values was found to be statistically insignificant. Both areas have varying rainfall totals in plot 4 and the riparian area has increasingly high precipitation (Figure 4.6b). This area also has a maximum monthly rainfall value of 105.82 mm and an average monthly rainfall of 24.88 mm. The non-riparian area has a maximum monthly rainfall value of 84.16 mm and average monthly rainfall of 20.66 mm (Table 4.3).

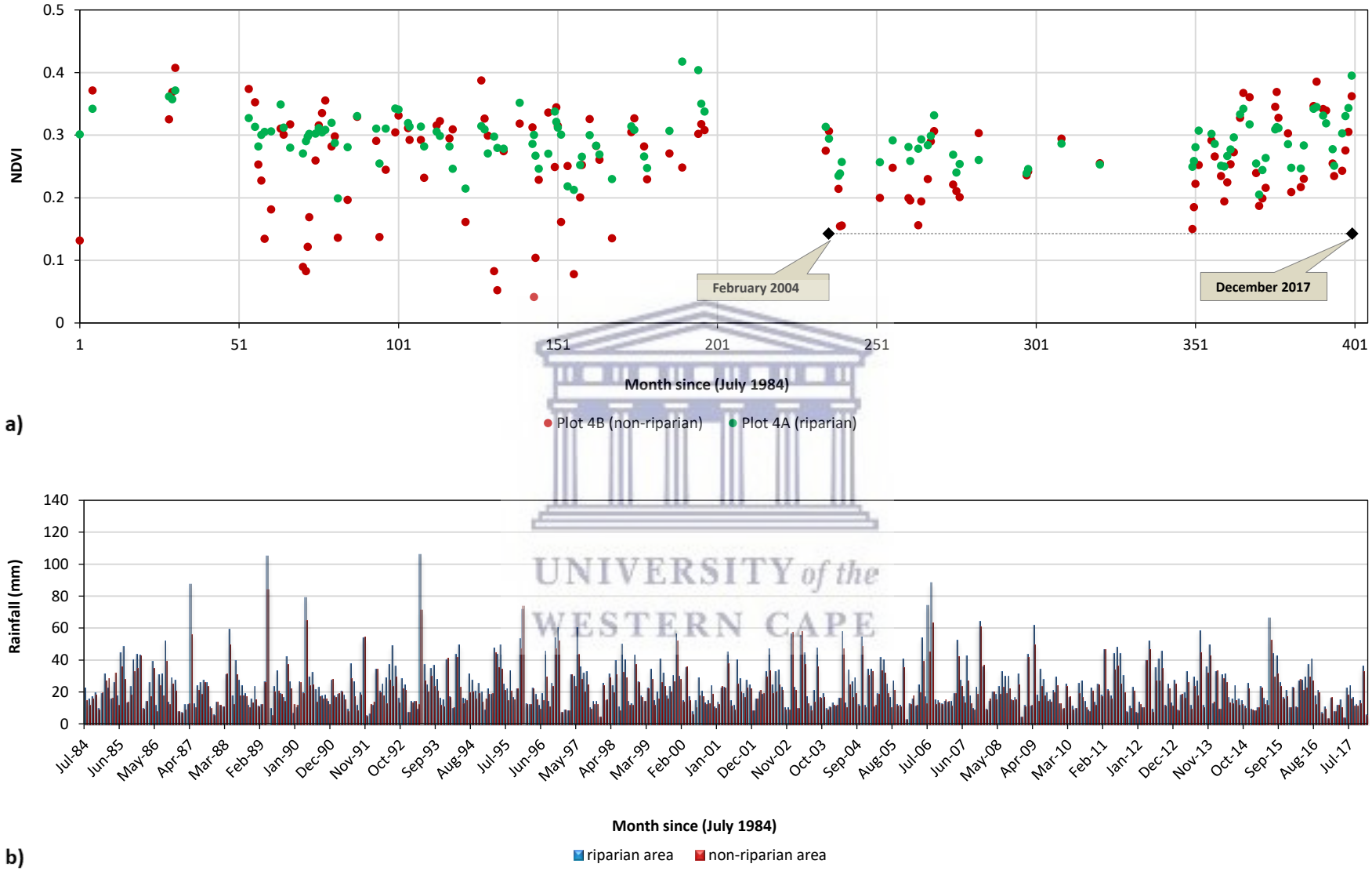

Figure 4.6: The Normalised Difference Vegetation Index (NDVI) (**a**) and monthly precipitation (**b**) for vegetation plot 4 (1984-2017).

Figure 4.7a reveals that vegetation plot 6 has high NDVI values (a maximum value of 0.3690) and the spread in riparian and non-riparian areas is wide. The difference between the two areas is more visible and can be detected by average values (Table 4.3). The difference in average values was found to be statistically significant. However, the pattern between February 2004 and December 2017 is quite similar to the pattern in plot 4 where the riparian and non-riparian areas overlap substantially. The distribution of rainfall in plot 6 (Figure 4.7b) suggests that only a few months have rainfall totals of more than the monthly average (21.27 mm) and this is comparable with rainfall conditions in vegetation plot 5. The average monthly rainfall is 21.27 mm, the maximum is 79.03 mm and the minimum rainfall total is 2.87 mm.

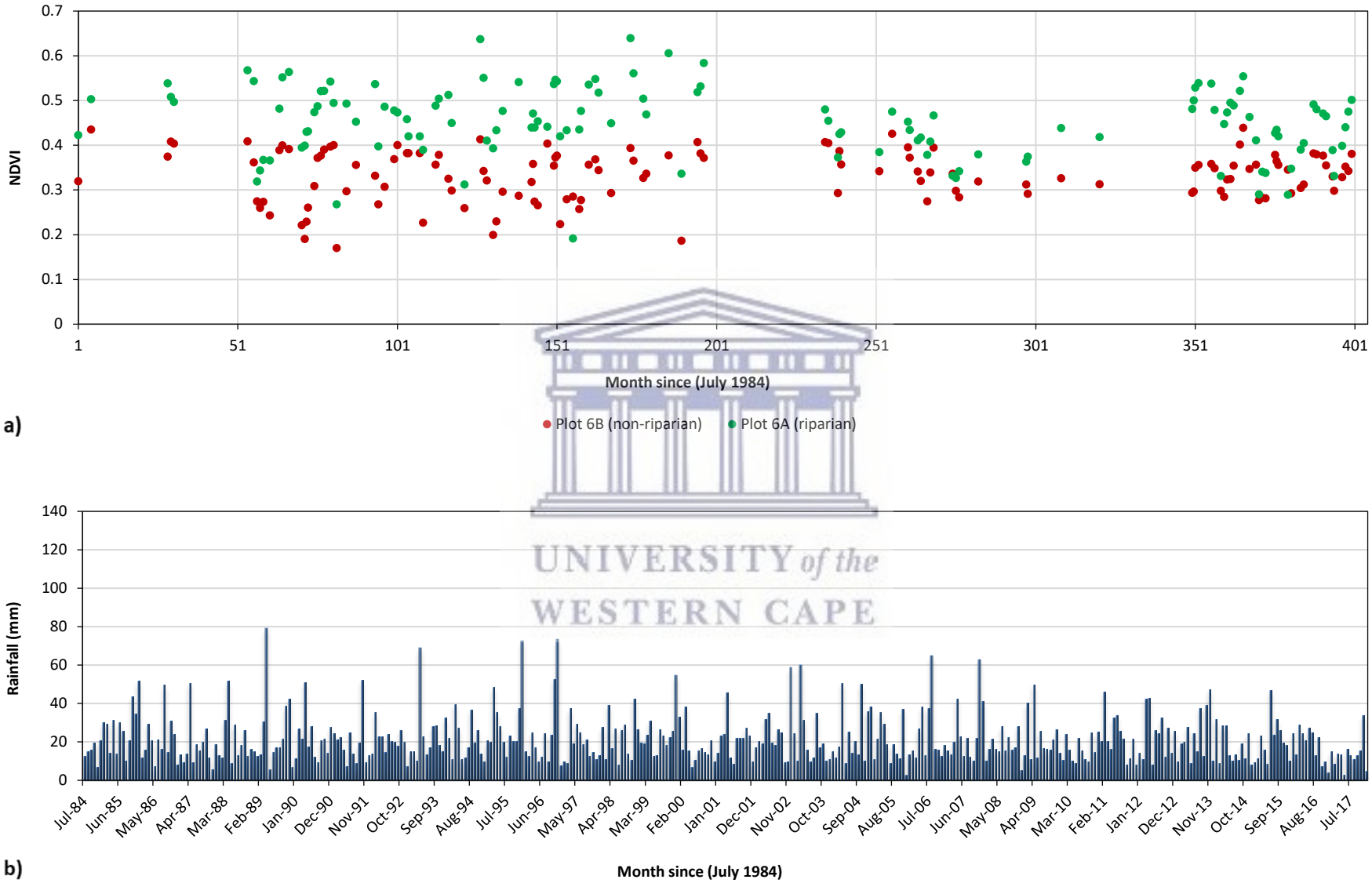

Figure 4.7: The Normalised Difference Vegetation Index (NDVI) (**a**) and monthly precipitation (**b**) for vegetation plot 6 (1984-2017).

In vegetation plot 7 the overlap between the riparian and non-riparian area is infrequent, and the difference is immense. The difference can also be comprehended by the huge difference in average NDVI values, which was found to be significant using the t-test. The difference between standard deviations of the two areas is minimal; 0.06028 and 0.05243 in the riparian and non-riparian area respectively. This means both areas almost have the same pattern and the spread of NDVI is quite similar. Both riparian and non-riparian areas display a declining trend over the years, where NDVI decreases from July 1984 to December 2017.

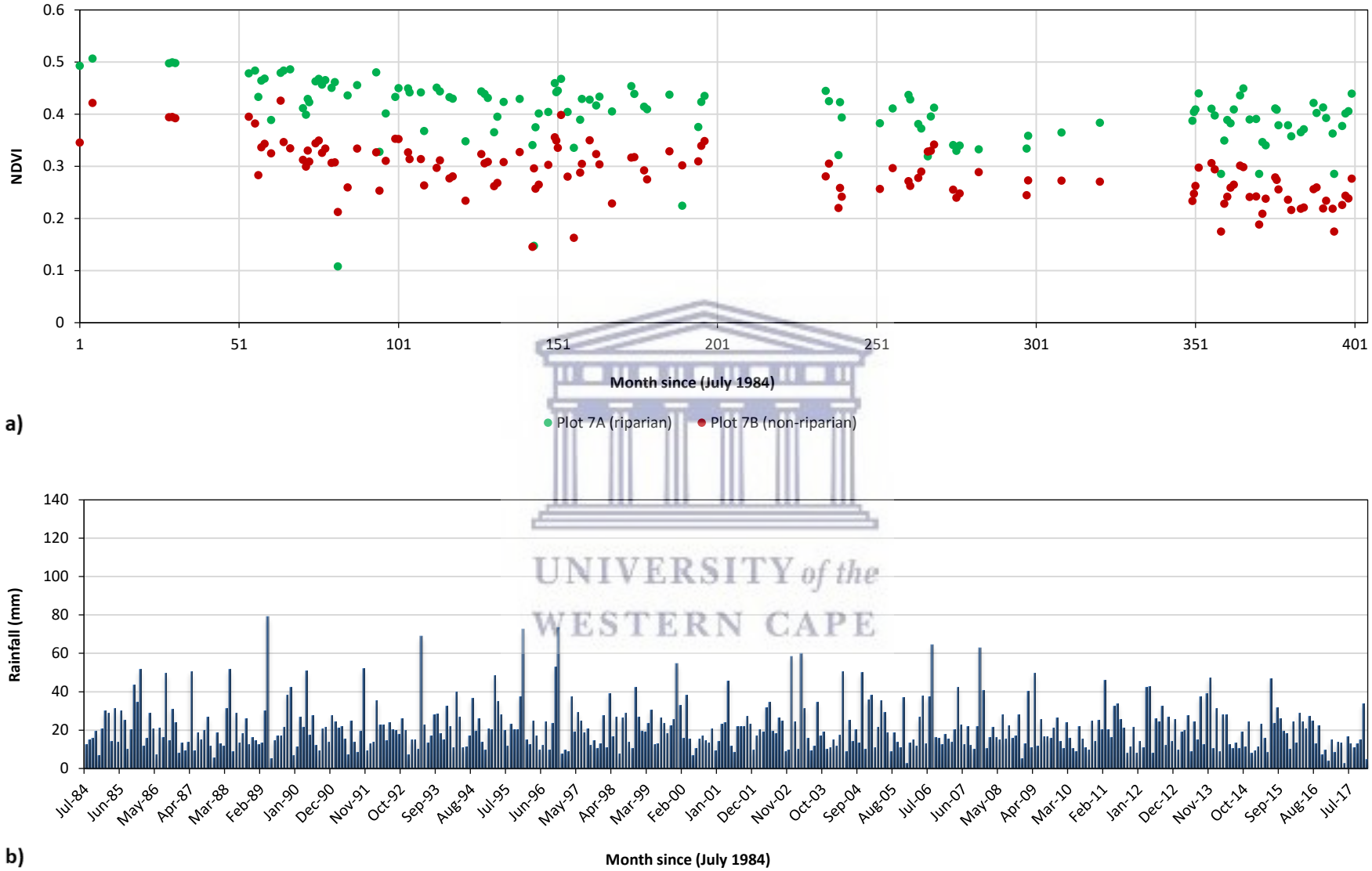

Figure 4.8: The Normalised Difference Vegetation Index (NDVI) (**a**) and monthly precipitation (**b**) for vegetation plot 7 (1984-2017).

4.1.4. | Intra-annual rainfall variability

The coefficient of variation (CV) was used to evaluate the variability of precipitation in each sampled vegetation plot (Figure 4.9 and 4.10). It is to be noted here that vegetation plot 1 and 2 have the same CV because the two plots have the same precipitation totals. Plots 6 and 7 also have the same CV. The results demonstrate that all vegetation plots received highly seasonal precipitation, except in 1984 where precipitation occurred throughout the year as indicated by a low to moderate CV (20-30%). The rainfall shows major seasonal variability prior to 1997 and between 2002 and 2009 in all vegetation plots. However, from 2010 to 2017 there is less variability, indicating that rainfall commonly occurs throughout the year. This is similar in all sampled vegetation plots.

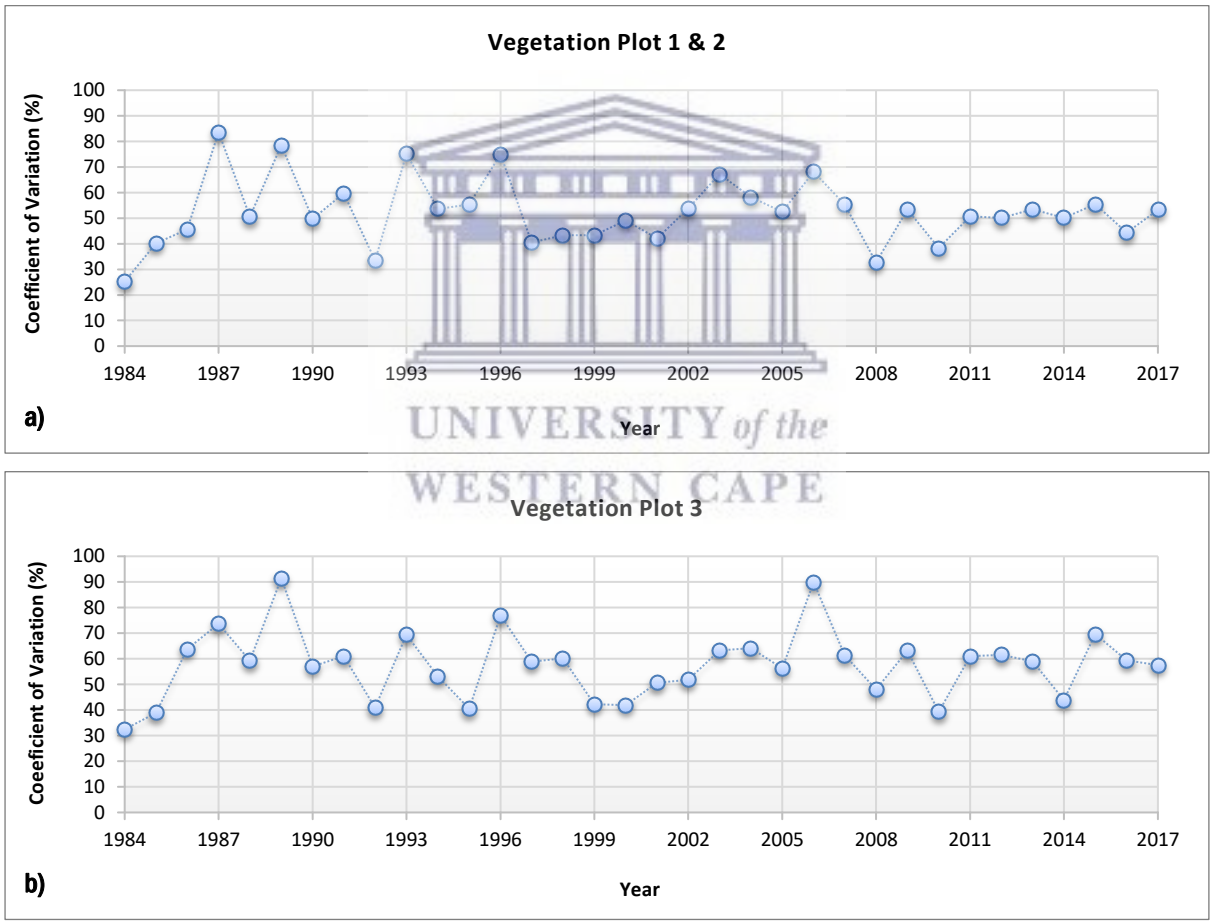

Figure 4.9: Coefficient of variation in monthly precipitation amounts for vegetation plot 1 and 2 (**a**), and 3 (**b**) for the period between 1984 and 2017.

In vegetation plot 4 (Figure 4.10b) and 5 (Figure 4.10a), the highest coefficient of variation can be noticed in 1987 and 1989 (CV > 90%). In Figure 4.10b the riparian area experiences

slightly more variable precipitation than the non-riparian area. However, the difference in CV values between the two areas is minimal. Plot 6 and 7 (Figure 4.10c) displayed the highest variability in 1996 (CV > 80%) and 1989 (CV of 79.25%).

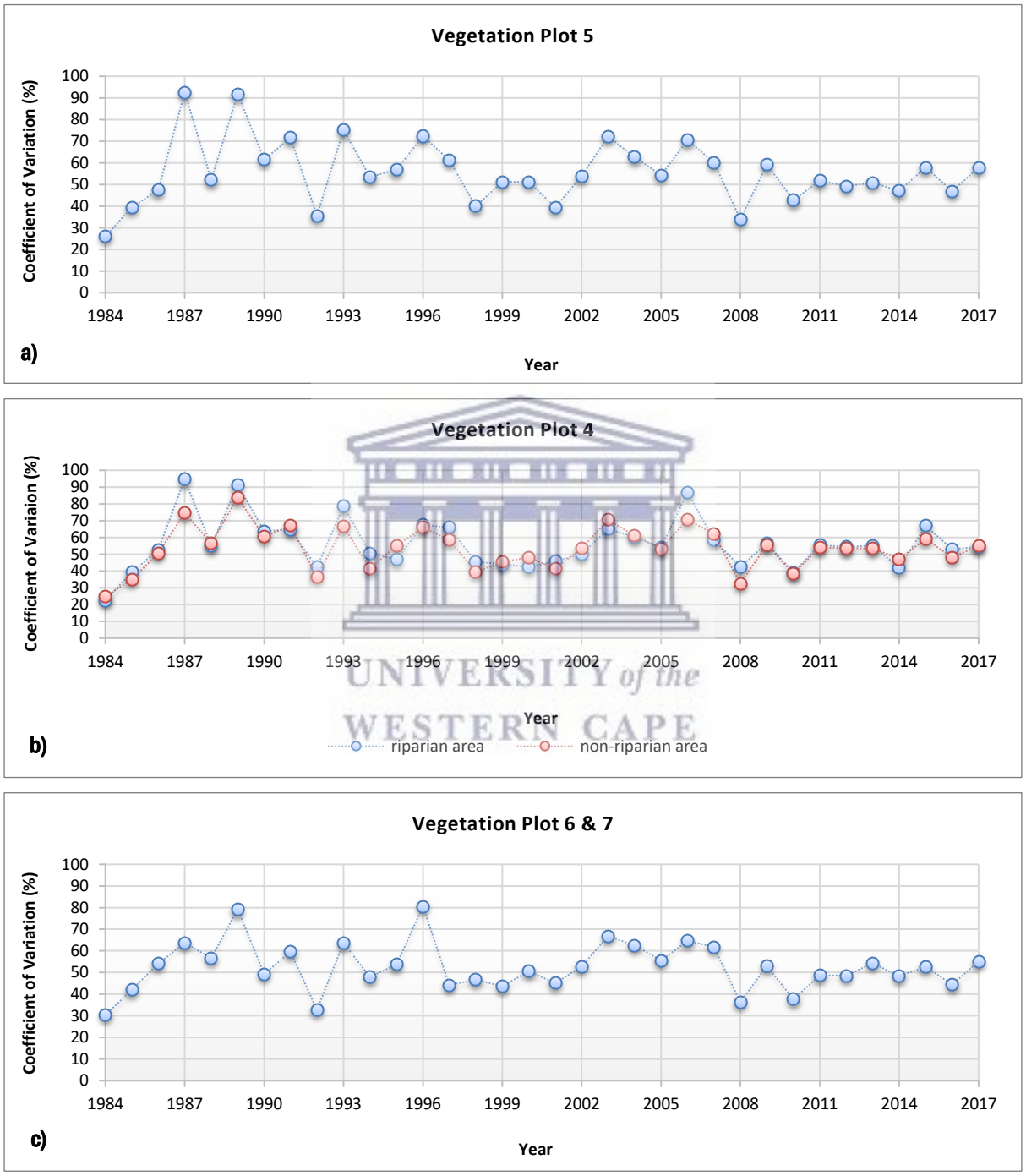

Figure 4.10: Coefficient of variation in monthly precipitation amounts for vegetation plot 5 (**a**), 4 (**b**), 6 and 7 (**c**) for the period between 1984 and 2017.

4.1.5. | Long-term climatic trends

4.1.5.1. | *Analysis of precipitation trends*

The average annual rainfall for the 34-year data is 314.34 mm with an annual coefficient of variance of 48.80% (Table 4.6). The annual maximum and minimum rainfall totals are 754.67 mm and 117.26 mm respectively. Figure 4.11 demonstrates that the year 1995 is the wettest year (430.37 mm) and 2017 is the driest year (200.68 mm) on record. This is further illustrated in Figure 4.13. Some months are significantly more variable than the annual record (CV 48.80%). For instance, the rainfall variability is extremely high in December (CV 77.38%), November (60.19%), May (58.24%) and April (54.09%). The rainfall historical trend shows that most years received rainfall totals that were below the average (Figure 4.11). Furthermore, the rainfall recorded above the average is less than 450 mm and thus, leading to the conclusion that the region has received tremendously less precipitation. This statement is similar to what Le Maitre *et al*. (2009) asserted, i.e. that the Klein Karoo receives low rainfall of 100 mm to 450 mm per year. The slope of regression line also suggests that the annual rainfall is declining by -1.127 mm/year (Figure 4.11). However, the declining trend is insignificant (r^2 = 0.0535).

Table 4.6: The statistical summary of rainfall in the Touws quaternary catchments for the period (1984-2017).

Month	Min	Max	Mean	SD	CV %
January	11.06	44.30	20.21	8.86	43.84
February	9.12	51.97	20.93	9.96	47.61
March	13.72	71.06	30.01	12.88	42.93
April	13.91	95.91	39.96	21.61	54.09
May	4.10	48.61	22.01	12.82	58.24
June	11.27	61.88	26.01	10.31	39.63
July	13.44	58.09	29.75	9.14	30.71
August	10.83	75.66	27.65	13.37	48.35
September	8.67	26.98	17.36	4.72	27.19
October	10.10	69.60	30.60	16.03	52.40
November	7.12	77.36	28.38	17.08	60.19
December	3.92	73.25	21.47	16.62	77.38
Annual	**117.26**	**754.67**	**314.34**	**153.40**	**48.80**

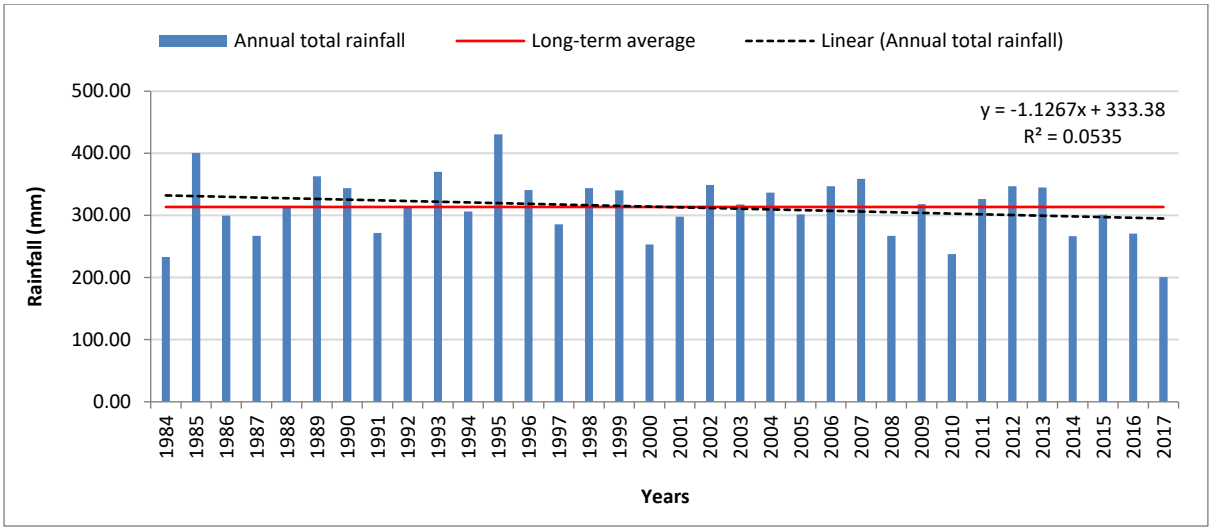

Figure 4.11: CHIRPS total annual precipitation record for the study period (1984-2017).

As depicted in Table 4.6 and Figure 4.12, the rainfall trend also displays a random or sporadic pattern where rainfall is scattered and falls in various seasons throughout the years. The highest precipitation has been received mainly in autumn (March to May), with April having the highest average (39.96 mm) and maximum rainfall (95.91 mm) of all months (Table 4.6). Winter (June to August) also displays high rainfall followed by spring (September to November), specifically in October and November (Figure 4.12). Rainfall is generally low in summer (December to February).

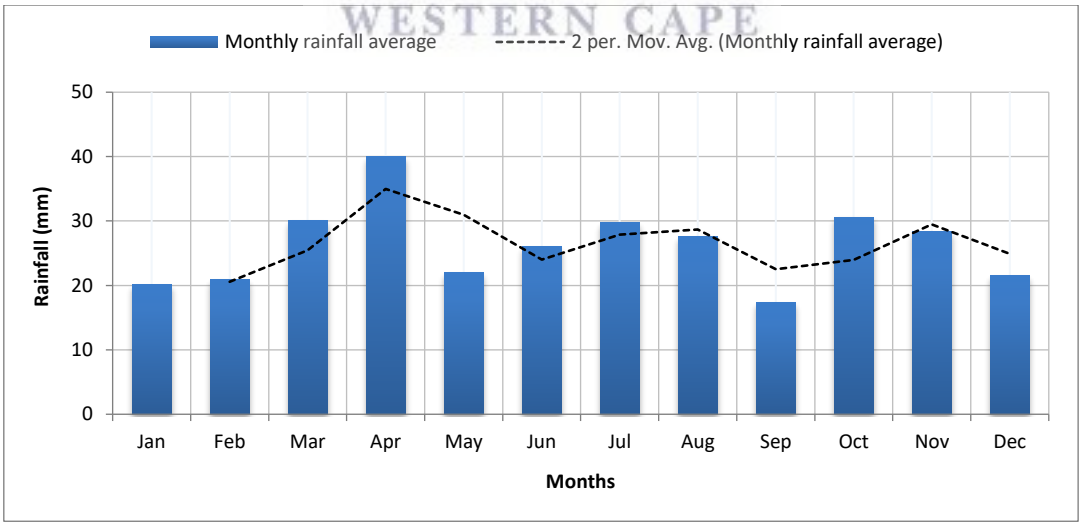

Figure 4.12: The mean monthly rainfall conditions in Touws quaternary catchments from 1984 to 2017.

Figure 4.13 displays the presence of inter-annual rainfall variability, a cycle of wet and dry conditions, where some years have received high rainfall while other years have experienced

dry spells. This suggests a 4 to 6-year cycle where a period of 2-3 years is characterized by floods and 2-3 years is characterized by drought (Figure 4.14). The variation of SPI-12 is identical to the variation of rainfall anomaly. Both graphs demonstrate that the year 1995 experienced the highest rainfall, while the dry period from 2014 to 2017 was the longest drought. 2017 stand out as the year with the most intensive drought as indicated in Figure 4.13 and 4.14.

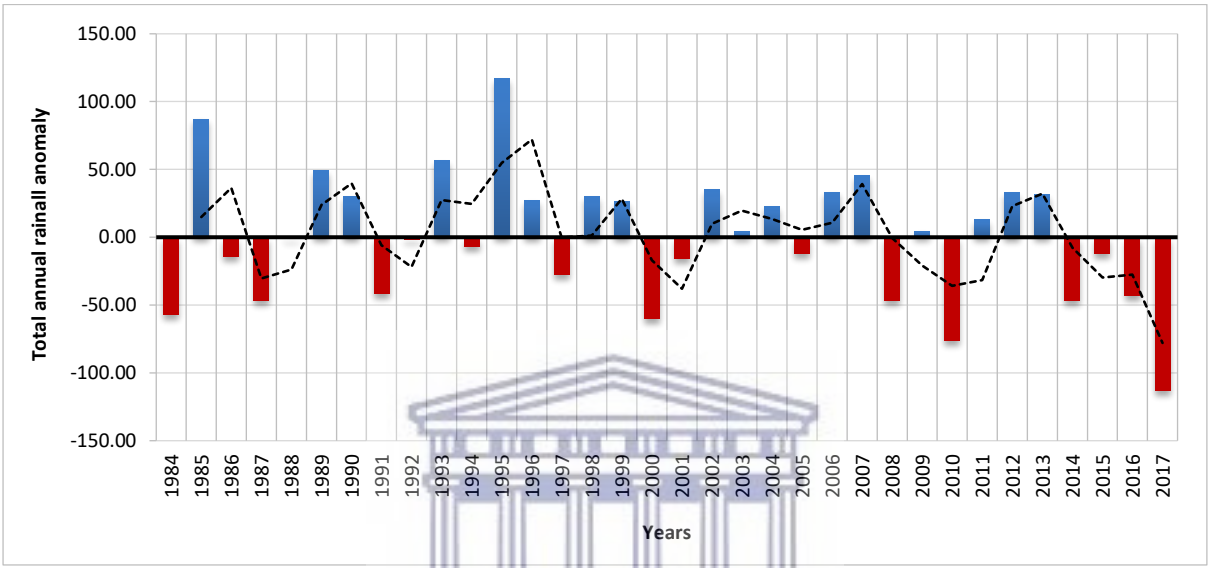

Figure 4.13: Rainfall anomaly with a 2-year moving average in the Touws quaternary catchments relative to 1984-2017 average.

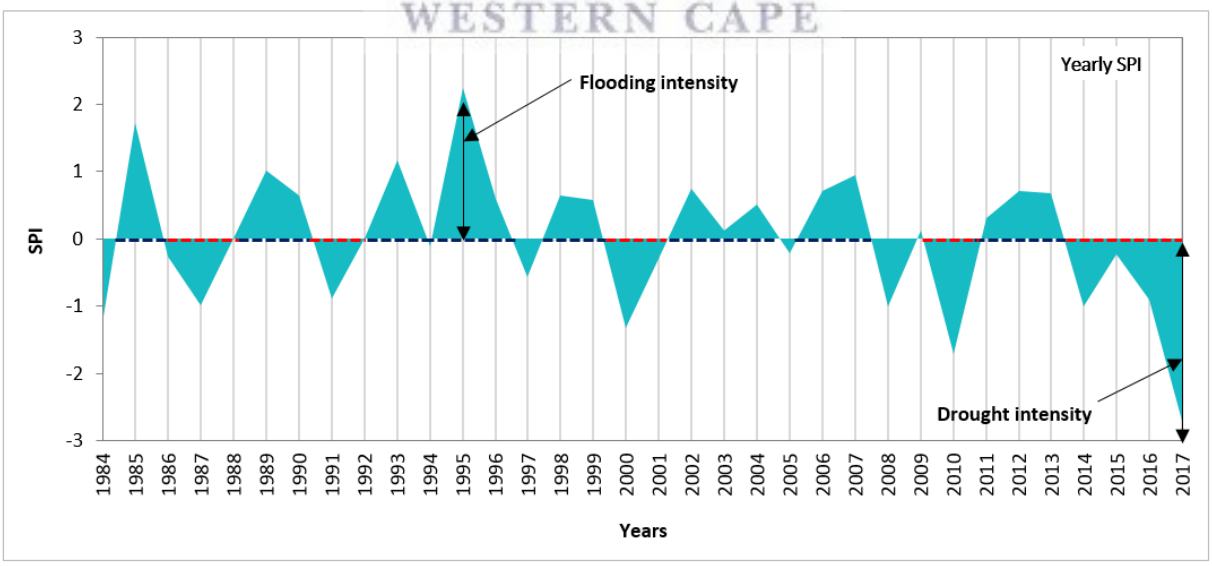

Figure 4.14: The Standardized Precipitation Index (SPI) at 12-month scale for the study record (1984-2017).

4.1.5.2. | Analysis of temperature trends

This section examines the temperature trends in the study region for the period of 1984-2017. In Figure 4.15, the maximum temperatures show greater variability than the minimum temperatures throughout the years. Temperatures are extremely high in summer (December to February) and begin to decline in autumn (March to May). They reach low levels during winter (June to August) and begin to intensify in spring (September to November). Figure 4.16 depicts that the highest annual average maximum temperature between 1984 and 2017 is 26.73°C in 2016, while the lowest is 23.88°C in 1984. The highest annual average minimum temperature is 12.94°C in 1999 and the lowest is 8.89°C in 1984.

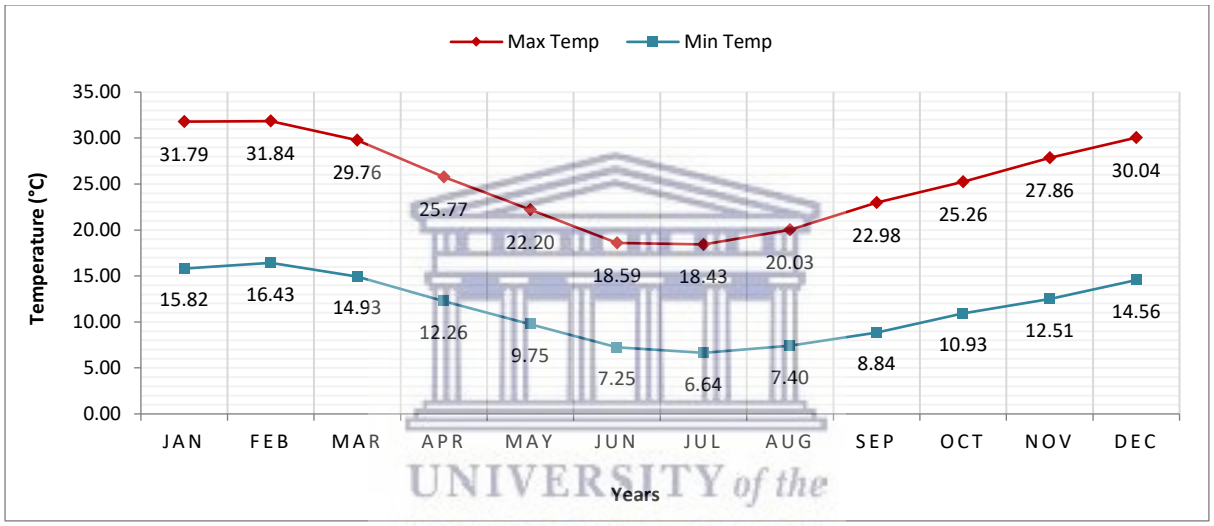

Figure 4.15: Average monthly temperatures of the Touws quaternary catchments from 1984 to 2017.

Overall, both minimum and maximum temperatures indicate an increasing trend since 1984 and this is further illustrated by the slope of regression line where temperatures have increased at a rate of 0.020°C/year and 0.057°C/year for minimum and maximum temperature respectively during the period from 1984 to 2017 (Figure 4.16). The increasing trend in maximum temperatures was found to be statistically significant ($r^2 = 0.55$ at $p < 0.01$), while that of minimum temperatures was not.

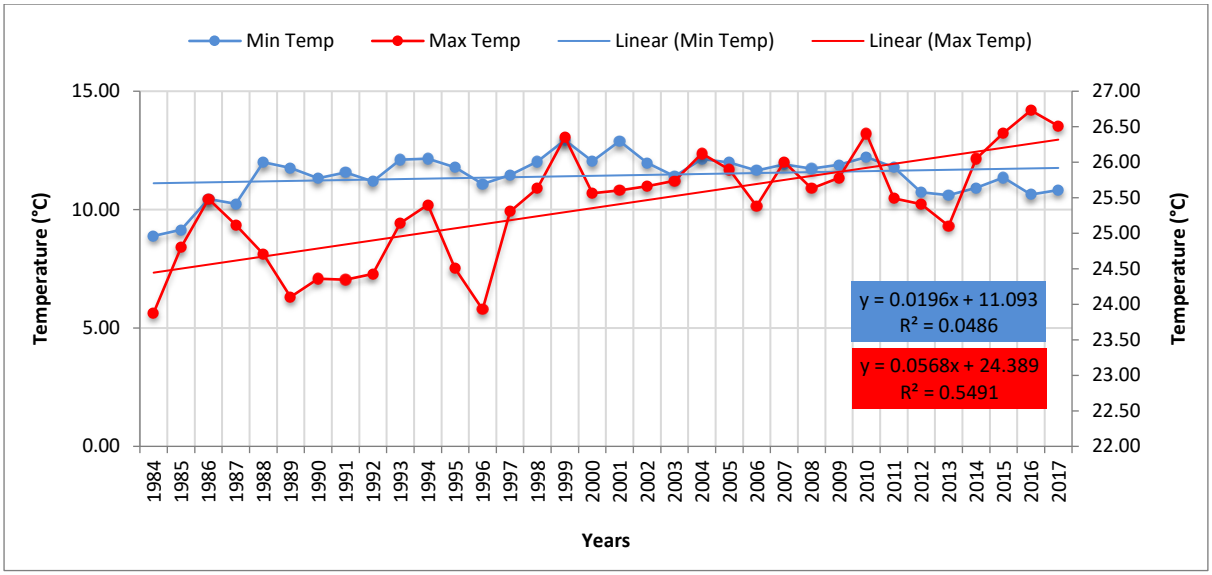

Figure 4.16: Average annual maximum and minimum temperature of the Touws quaternary catchments from 1984 to 2017.

4.1.6. | Relational trends between NDVI, rainfall, and temperature

Figure 4.17-4.19 display the relationship between average monthly NDVI, monthly temperatures and monthly rainfall for the study period (1984-2017). A decrease in maximum temperatures corresponds with a decrease in NDVI and an increase in maximum temperatures corresponds with an increase in vegetation productivity (Figure 4.17). This is further illustrated by the significant correlation between average monthly NDVI and monthly maximum temperatures between August 1989 and August 1991 (r = 0.79; p < 0.01), and September 2013 and June 2015 (r = 0.66; p < 0.01). The minimum temperatures and NDVI displays a similar pattern and this is statistically significant (r = 0.57; p < 0.01) between July 2006 and June 2015 (Figure 4.18). A correlation matrix between NDVI and temperature for the full study record (1984-2017) is provided in Section 4.1.8.2.

In contrast, the trend between rainfall and NDVI is inconsistent (Figure 4.19). In some years an increase in rainfall may result in an immediate increase in vegetation productivity. For instance, during April 1989 both rainfall and NDVI display a drastic increase compared to previous months of 1989 and 1987. However, in some years the NDVI responds a few months after a major rainfall event. This is indicated in Figure 4.19 where vegetation productivity took long (roughly 6 months) to increase following a major rainfall in November 2013, while it took

a month during 2015. 2013 was the last year of an anomalously wet season, while 2015 was during a drought phase (Figure 4.19).

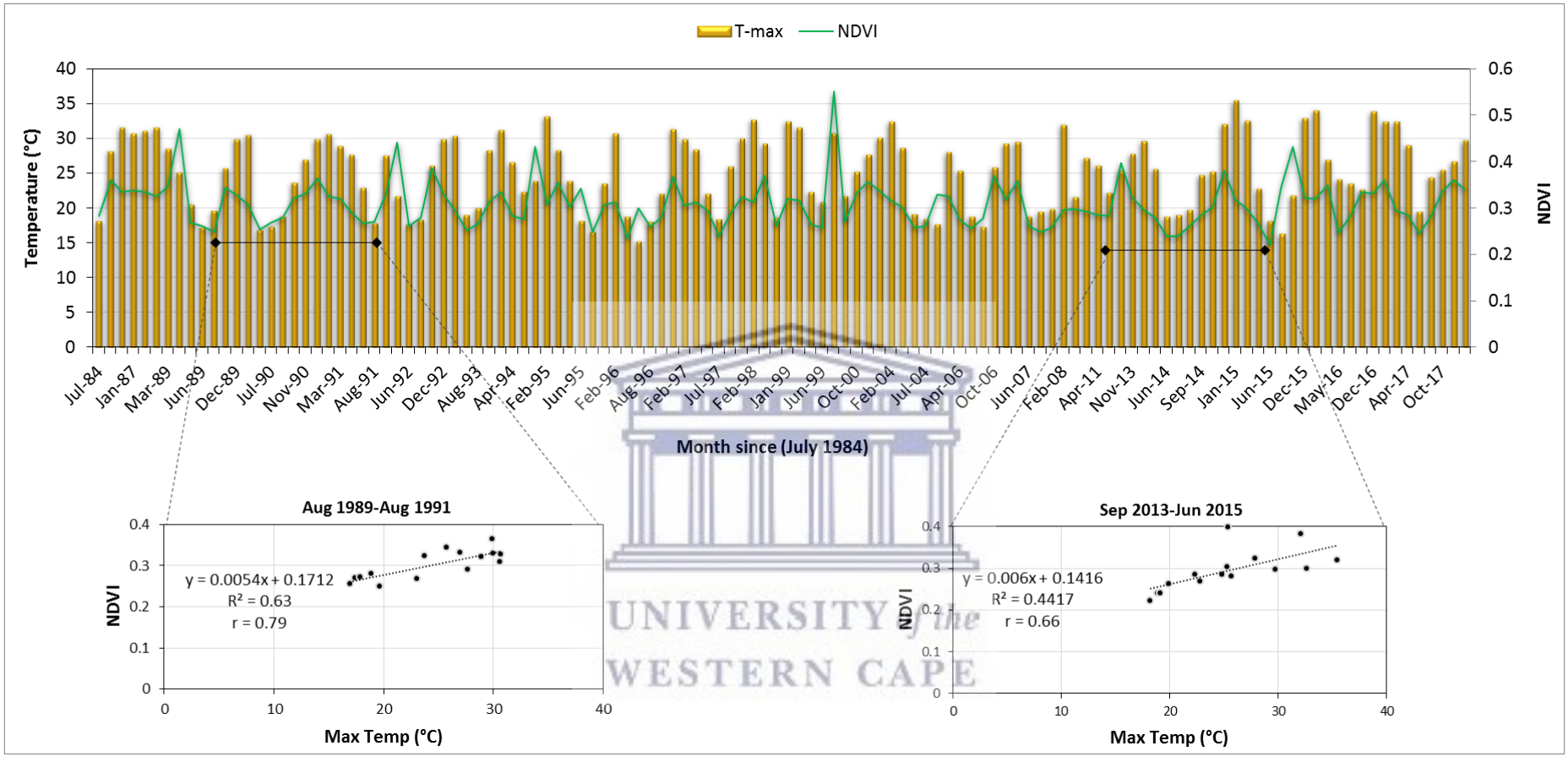

Figure 4.17: The relationship between average monthly NDVI and monthly maximum temperatures of the Touws quaternary catchments (1984-2017).

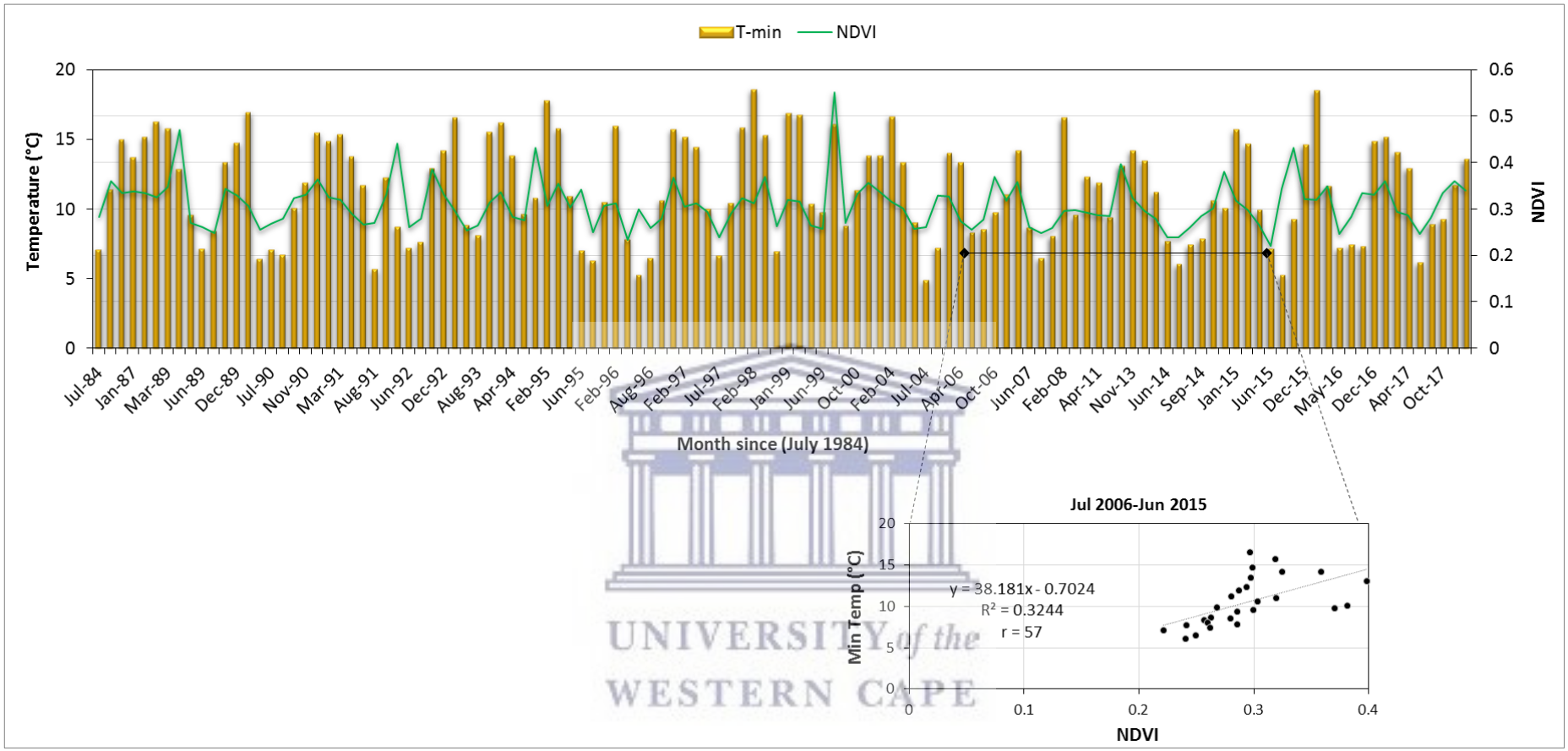

Figure 4.18: The relationship between average monthly NDVI and monthly minimum temperatures of the Touws quaternary catchments (1984-2017).

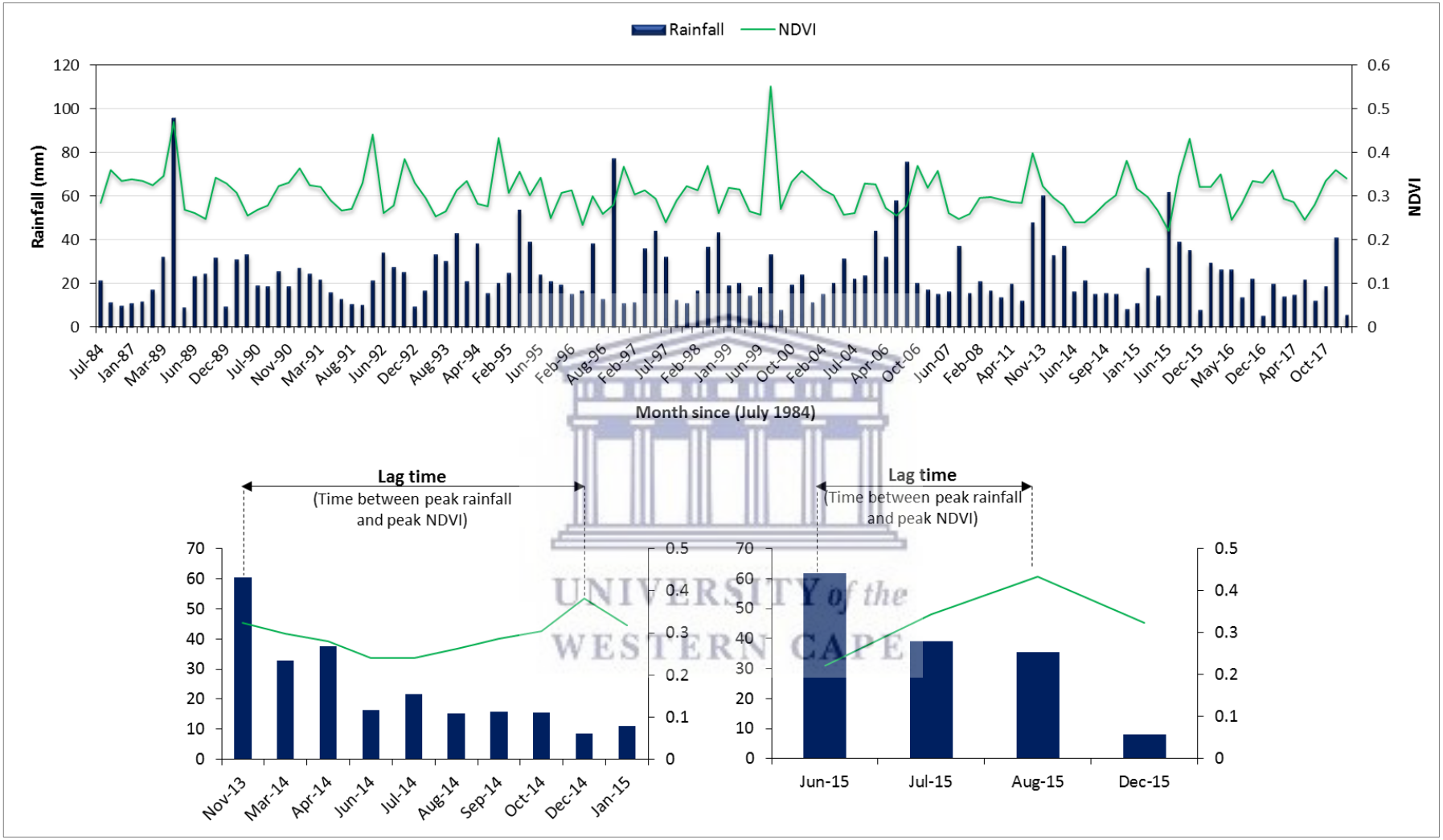

Figure 4.19: The relationship between average monthly NDVI and monthly rainfall of the Touws quaternary catchments (1984-2017) with lag time between rainfall peak and NDVI peak.

4.1.7. | The relationship between vegetation productivity, precipitation, and temperature

This section provides a detailed statistical analysis of the relationship between NDVI, temperature and rainfall. An analysis using average monthly totals with all vegetation plots is provided first. This is followed by an analysis by vegetation community and by riparian versus non-riparian area.

4.1.7.1. | Inter-annual correlation

A correlation coefficient (*r*0) and a multiple regression model in SPSS using the stepwise method were computed to examine the relationship between NDVI, rainfall, and temperature using average monthly totals with all vegetation plots for the study period (1984-2017). Table (4.7 to 4.10) summarizes the descriptive statistics and analysis results. Both maximum and minimum temperatures are positively associated with NDVI and this is statistically significant (p <0.01) at 99% level (Table 4.7). Rainfall also displays a positive association with NDVI (0.10), but the relationship is not statistically significant (Figure 4.20). The relationship between NDVI and minimum and maximum temperatures is demonstrated visually in Figure 4.21.

Table 4.7: Descriptive statistical summary of the linear regression.

		Rainfall	T-max	T-min
NDVI	Pearson Correlation	.102	**.474****	**.456****
	Sig. (1-tailed)	.133	.000	.000
	N	120	120	120

Note: ** statistically significant at the 0.01 alpha level (1-tailed).

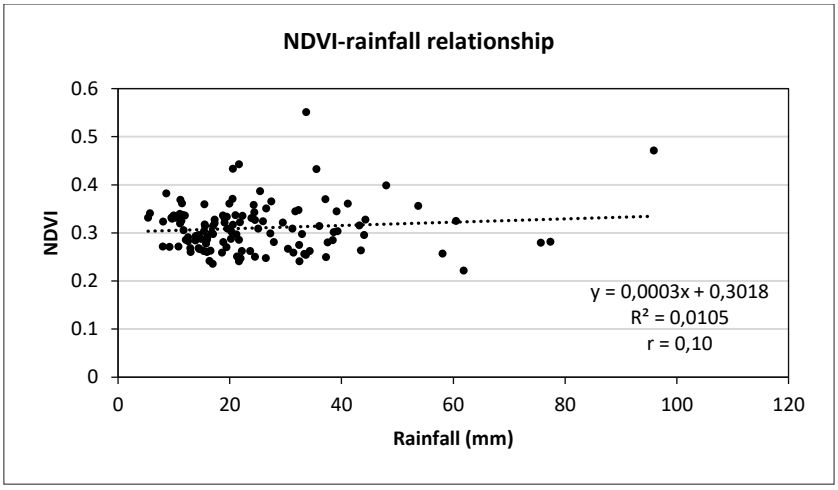

Figure 4.20: Correlation coefficient between monthly NDVI and monthly rainfall for the period 1984-2017.

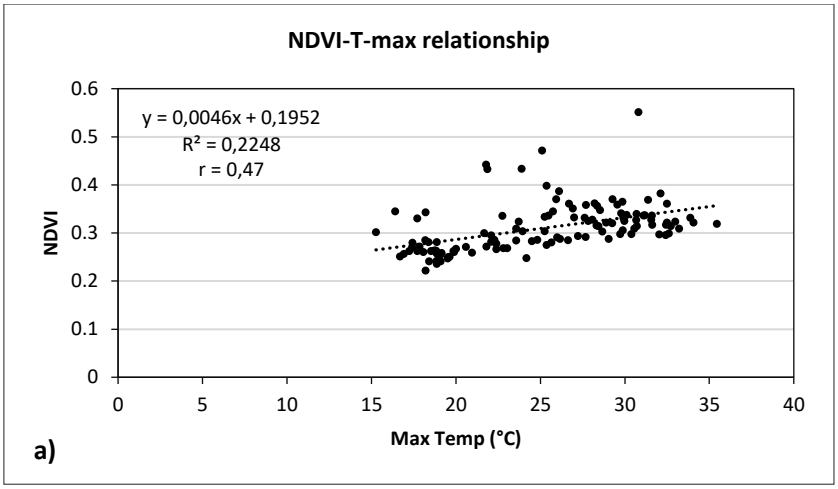

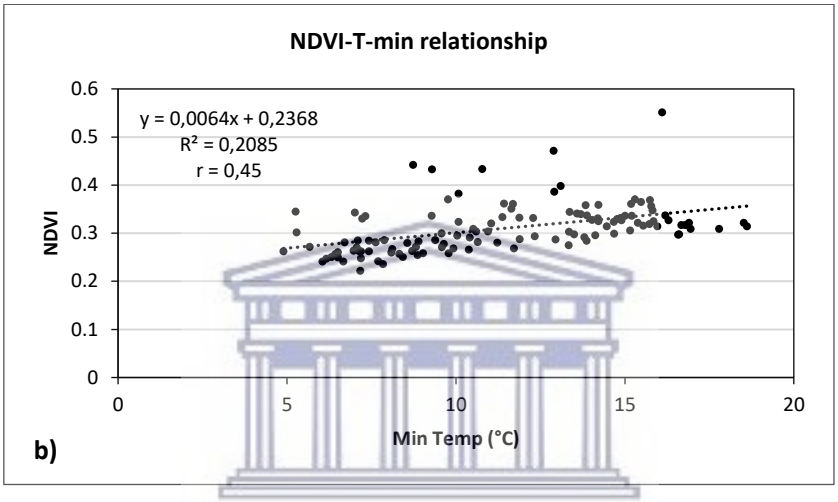

Figure 4.21: Correlation coefficient between monthly NDVI and monthly maximum temperatures (**a**); between monthly NDVI and monthly minimum temperatures (**b**) for the period 1984 -2017.

In a multiple regression model, minimum temperatures were excluded because these were correlated with maximum temperatures (i.e. multicollinearity). The results of the regression indicate that maximum temperatures explain 21.8% of the variance in NDVI and the combination of maximum temperatures and rainfall explains 26.4% of the variance in NDVI (Table 4.8). A significant regression equation was found (F (2.117) = 22.331, $p < 0.000$), with an R^2 of 0.276 (Table 4.9 and 4.10). This indicates that the influence of a linear combination of rainfall and maximum temperatures on NDVI is statistically significant. The NDVI increases by 0.005 for each additional degree in temperature and by 0.001 for each additional millimeter in rainfall (Table 4.10).

Table 4.8: Multiple regression model summary.

Model Summary [c]					
Model	**R**	**R Square**	**Adjusted R Square**	**Std. Error of the Estimate**	**Durbin-Watson**
1	.474[a]	.225	.218	.0446249	
2	.526[b]	.276	.264	.0433017	1.973

a. Predictors: (Constant), T-max
b. Predictors: (Constant), T-max, Rainfall
c. Dependent Variable: NDVI

Table 4.9: Multiple regression ANOVA.

ANOVA [a]						
Model		**Sum of Squares**	**df**	**Mean Square**	**F**	**Sig.**
1	Regression	.068	1	.068	34.217	.000[b]
	Residual	.235	118	.002		
	Total	.303	119			
2	Regression	.084	2	.042	22.331	.000[c]
	Residual	.219	117	.002		
	Total	.303	119			

a. Dependent Variable: NDVI
b. Predictors: (Constant), T-max
c. Predictors: (Constant), T-max, Rainfall

Table 4.10: Multiple regression coefficients.

Coefficients [a]										
Model		**Unstandardized Coefficients**		**Standardized Coefficients**	t	Sig.	**95,0% Confidence interval for B**		**Collinearity Statistics**	
		B	Std. Error	Beta			Lower Bound	Upper Bound	Tolerance	VIF
1	(Constant)	.195	.020		9.722	.000	.155	.235		
	T-max	.005	.001	.474	5.850	.000	.003	.006	1.000	1.000
2	(Constant)	.162	.023		7.133	.000	.117	.207		
	T-max	.005	.001	.532	6.555	.000	.004	.007	.939	1.065
	Rainfall	.001	.000	.234	2.885	.005	.000	.001	.939	1.065

a. Dependent Variable: NDVI

The *p*-values for regression coefficients (*b*) are statistically significant ($p < 0.001$ and < 0.005) for both maximum temperatures and rainfall respectively (Table 4.10). The standardized coefficient Beta suggests that maximum temperatures have the strongest relationship with NDVI (0.532), compared to rainfall (0.234).

4.1.7.2. | *Correlation by plant community in riparian and non-riparian area*

To observe how NDVI responds to rainfall and temperature in each plant community, a correlation coefficient was computed based on vegetation plots with a lag to consider the

influence of previous rainfall and temperature on current vegetation conditions. In both plant communities, temperatures are more statistically significant than rainfall.

Zero-month lag correlation

In the hillslope shrubland community, correlations are mostly strong in autumn and spring (Table 4.11). Rainfall has a strong correlation with NDVI during summer and the correlations are equally distributed between the riparian and non-riparian area in vegetation plot 1, 2 and 3. The correlations between NDVI and rainfall, NDVI and minimum temperatures are negative during summer but statistically significant. Maximum temperatures show insignificant correlation with NDVI in both areas (riparian and non-riparian) during summer. In other seasons (autumn, winter, and spring), rainfall shows insignificant correlation with NDVI in both areas. In the floodplain woodland community, both rainfall and temperature are not much of a factor for vegetation growth, and this is shown by fewer significant correlations. Most correlations (about 90%) are within the hillslope shrubland community, indicating that water availability and temperature are locally important in determining plant productivity. Rainfall is only significantly correlated with NDVI in the riparian area in vegetation plot 4 during summer and shows zero correlation in other seasons. This indicates that local rainfall is not a factor in determining immediate plant growth in such settings. Correlation between NDVI and temperature is mostly distributed between autumn and spring in both areas.

3-month lag correlation

The results of the 3-month lag correlation also display that 90% of correlations are distributed in the hillslope shrubland community (Table 4.12). However, rainfall shows a large correlation with NDVI in summer and autumn. During autumn, the correlation between rainfall and NDVI is statistically significant (mostly at 95% level; p <0.05) in most vegetation plots in the non-riparian area. In summer, the NDVI in the hillslope shrubland community is significantly correlated with rainfall and temperature, thus indicating that both climatic elements are a key factor for vegetation growth. In the floodplain woodland community, temperatures are more strongly correlated with NDVI than rainfall. Rainfall is only correlated with NDVI (r = -0.454; p < 0.01) in plot 4 in the riparian area.

Table 4.11: A zero-lag correlation matrix of NDVI versus rainfall and temperatures at a vegetation community scale.

Community and area		Plot	Seasons											
			Summer			Autumn			Winter			Spring		
			NDVI-rainfall	NDVI-t-max	NDVI-t-min	NDVI-rainfall	NDVI-t-max	NDVI-t-min	NDVI-rainfall	NDVI-t-max	NDVI-t-min	NDVI-rainfall	NDVI-t-max	NDVI-t-min
Hillslope shrubland	riparian area	P 1	**-0.477****	0.088	**-0.519****	0.022	**0.668****	**0.642****	-0.116	0.241	0.198	0.00	**0.614****	**0.704****
		P 2	**-0.441***	0.130	**-0.610****	-0.198	**0.696****	**0.493****	-0.046	0.302	0.300	-0.092	**0.595****	**0.616****
		P 3	**-0.427***	0.082	**-0.545****	-0.089	**0.486****	**0.531****	-0.112	0.047	**0.473****	0.152	**0.527****	**0.419***
		P 5	-0.094	-0.237	-0.171	0.331	**0.400***	**0.384***	-0.290	-0.270	0.174	-0.229	**0.480***	0.287
	non-riparian area	P 1	**-0.534****	0.191	**-0.591****	0.115	**0.616****	**0.583****	0.045	**0.401***	0.096	-0.097	**0.523****	**0.431***
		P 2	**-0.442***	0.321	**-0.601****	-0.163	0.350	0.280	-0.007	**0.410***	0.254	-0.042	**0.495***	**0.539****
		P 3	**-0.542****	-0.185	**-0.621****	0.018	**0.693****	**0.669****	-0.030	0.198	**0.480****	0.082	**0.489***	**0.622****
		P 5	-0.163	-0.250	**-0.414***	-0.175	**0.394***	**0.453***	-0.033	0.053	0.123	0.048	**0.413***	**0.580****
Floodplain woodland	riparian area	P 4	**-0.454****	-0.031	**-0.576****	-0.085	**0.357***	0.254	-0.13	-0.222	0.241	-0.032	**0.458***	0.376
		P 6	0.126	-0.032	0.231	0.098	**0.430***	**0.468****	-0.195	-0.175	0.130	0.167	0.248	**0.463***
		P 7	0.030	-0.302	-0.229	0.330	0.271	0.333	-0.123	-0.148	0.020	0.126	0.353	**0.466***
	non-riparian area	P 4	-0.280	0.234	-0.231	0.030	**0.503****	0.353	-0.08	-0.090	-0.232	0.136	**0.449***	0.338
		P 6	-0.158	0.211	-0.117	0.035	**0.568****	**0.475****	-0.019	0.298	**0.343***	0.384	**0.431***	**0.538****
		P 7	-0.005	**-0.433***	-0.167	0.238	0.007	0.281	-0.077	-0.251	0.310	0.082	**0.470***	**0.500***

Note: P for plot, t-max (maximum temperature), t-min (minimum temperature), * and ** statistically significant at 0.05 and 0.01 alpha level of significance respectively.

Table 4.12: A 3-month time lag correlation matrix of NDVI versus rainfall and temperatures at a vegetation community scale.

Community		Plot	Seasons											
			Summer			Autumn			Winter			Spring		
			NDVI-rainfall	NDVI-t-max	NDVI-t-min	NDVI-rainfall	NDVI-t-max	NDVI-t-min	NDVI-rainfall	NDVI-t-max	NDVI-t-min	NDVI-rainfall	NDVI-t-max	NDVI-t-min
Hillslope shrubland	riparian area	P 1	**-0.411***	**-0.375***	**-0.643****	**-0.391***	**0.638****	**0.367***	0.111	**-0.422****	**-0.353***	-0.10	**0.552****	**0.501***
		P 2	**-0.540****	**-0.363***	**-0.761****	**-0.652****	**0.627****	0.240	0.079	**-0.390***	**-0.371***	-0.228	**0.510****	0.394
		P 3	**-0.430***	-0.330	**-0.654****	-0.300	**0.436***	0.293	0.232	**-0.390***	-0.156	-0.196	**0.615****	**0.369***
		P 5	-0.176	-0.284	-0.151	0.135	**0.378***	0.345	0.165	**-0.423****	-0.174	**-0.427***	0.292	0.042
	non-riparian area	P 1	**-0.552****	**-0.370***	**-0.756****	**-0.372***	**0.575****	0.301	0.026	-0.281	-0.319	-0.221	**0.488***	0.273
		P 2	**-0.531****	**-0.438***	**-0.750****	**-0.441***	0.211	0.154	0.161	-0.318	-0.277	-0.103	**0.552****	**0.471***
		P 3	**-0.369***	**-0.494****	**-0.680****	**-0.356***	**0.655****	**0.418***	0.293	**-0.390***	-0.195	-0.054	0.313	**0.465***
		P 5	-0.255	**-0.446***	**-0.441***	**-0.465****	0.261	**0.362***	-0.096	0.119	0.168	-0.100	0.351	**0.453***
Floodplain woodland	riparian area	P 4	-0.230	-0.222	**-0.583****	-0.314	0.233	0.173	0.193	**-0.425****	-0.180	-0.341	**0.595****	0.349
		P 6	0.126	-0.021	0.203	-0.186	0.348	**0.409***	-0.181	-0.255	-0.044	-0.145	0.266	0.233
		P 7	-0.010	-0.316	-0.275	0.126	0.199	0.271	0.146	**-0.456****	-0.293	-0.088	0.215	0.139
	non-riparian area	P 4	**-0.381***	0.123	-0.218	-0.167	**0.521****	0.342	**0.327***	0.095	0.108	-0.124	**0.507****	0.246
		P 6	**-0.499****	-0.152	-0.224	-0.175	**0.599****	0.332	-0.006	0.258	0.247	0.022	**0.628****	0.330
		P 7	0.205	**-0.368***	-0.187	0.126	-0.213	0.282	0.157	**-0.387***	-0.099	0.221	0.271	0.377

Note: P for plot, t-max (maximum temperature), t-min (minimum temperature), * and ** statistically significant at 0.05 and 0.01 alpha level of significance respectively.

4.1.8. | The spatial range of Groundwater Dependent Ecosystems (GDEs)

In this section, an analysis of land cover classification is provided first. This is followed by an analysis of the indicators of groundwater discharge areas.

4.1.8.1. | *An overview of land cover classification results*

The land cover classification was performed using the object-based (supervised Nearest Neighbor) and pixel-based (supervised Maximum Likelihood) classification methods. The classification results of the three image datasets are shown below (Figure 4.22, 4.24 and 4.26). Each classified image is presented with an original pan-sharpened true colour image which was used to create training samples for classification (Figure 4.23, 4.25 and 4.27). This is to visualize the accuracy of the classification results. The classified results are also assessed quantitatively using an error matrix (Table 4.13).

4.1.8.2. | *Assessment of classification in July 2017*

Figure 4.22 display the classification results of SPOT 7 imagery taken in July of 2017. The healthy green vegetation dominates, more specifically along the river channels and in narrow valleys. The dominance of vegetation with high photosynthetic activity may be explained by the impact of rainfall, which normally rains during winter (July to August) in the study region (Le Maitre *et al*., 2009). The green patches on the hillslopes indicate individual tree species and misclassifications, which appear to be enormous as demonstrated by the overall accuracy of this image (Table 4.13). Water is mainly distributed in the central area and the south-eastern area of the map.

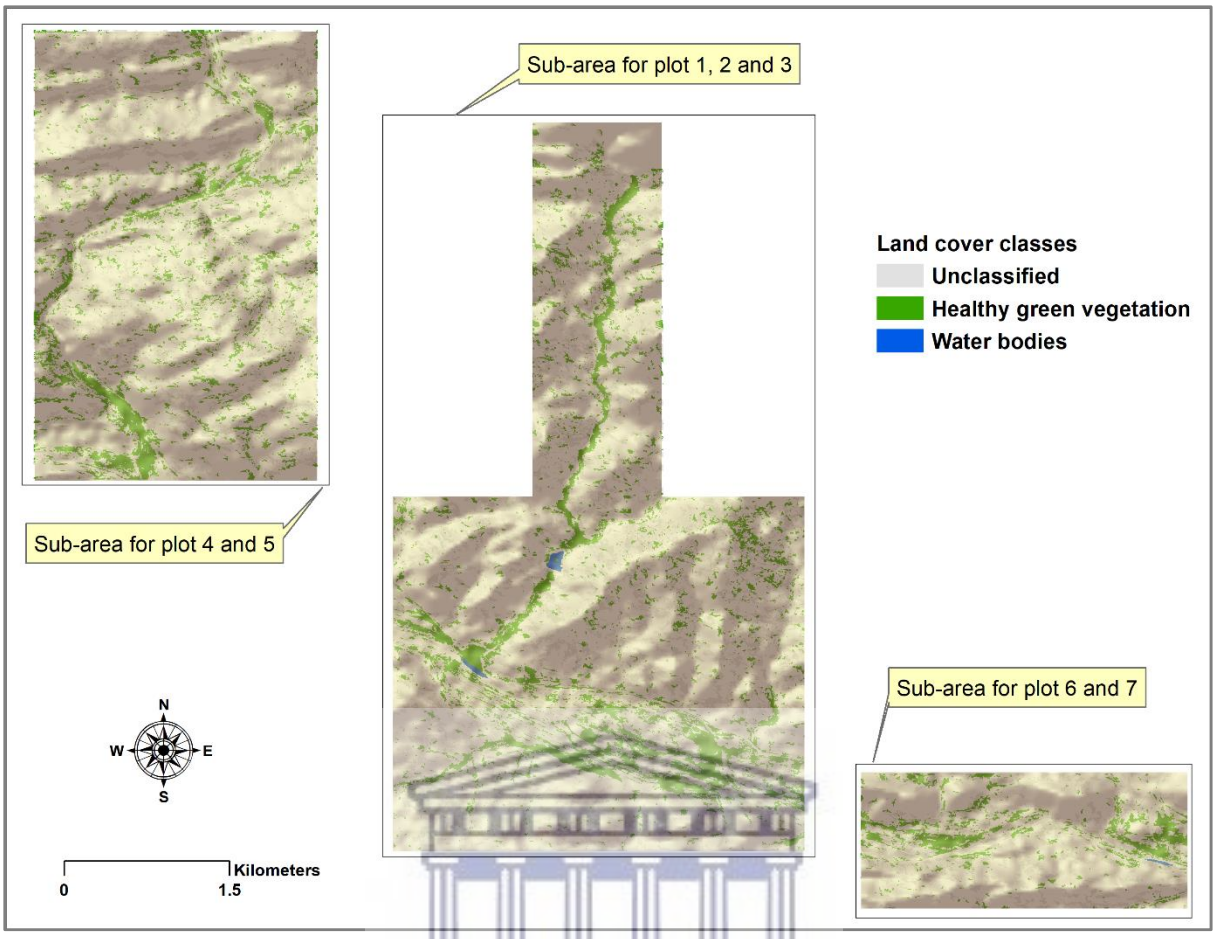

Figure 4.22: Land cover classification results of SPOT 7 imagery taken on the 17th of July 2017.

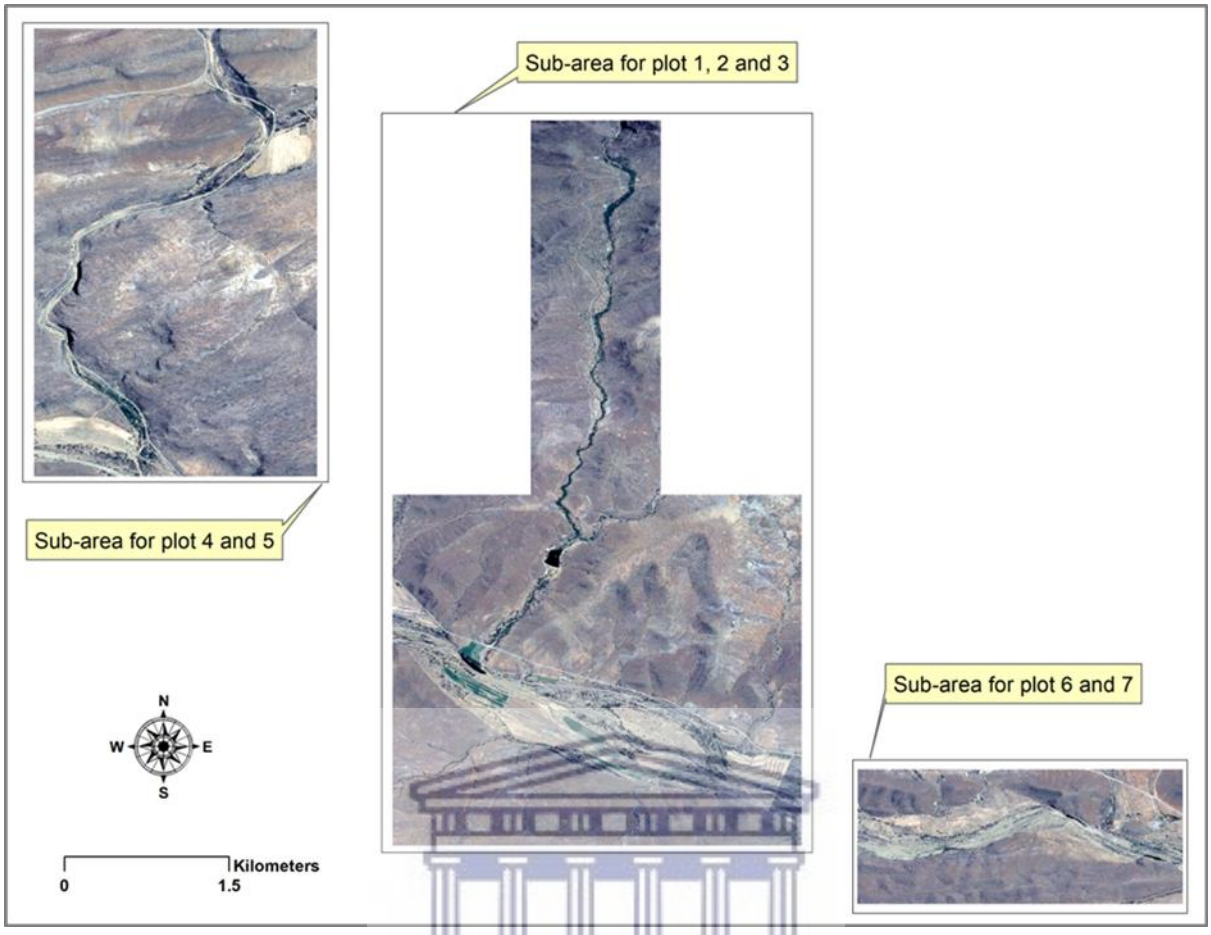

Figure 4.23: Sub-region of the pan-sharpened SPOT 7 image (17th July 2017).

4.1.8.3. | Assessment of classification in September 2017

In Figure 4.24 the quantity of healthy green vegetation has diminished and this can be detected along the river channels, in narrow valleys and in mountainous areas. This image was taken after the winter rainfall season, during which temperatures are below the required range of productivity. Water levels, as indicated by the dam and the river pools, have remained fairly static.

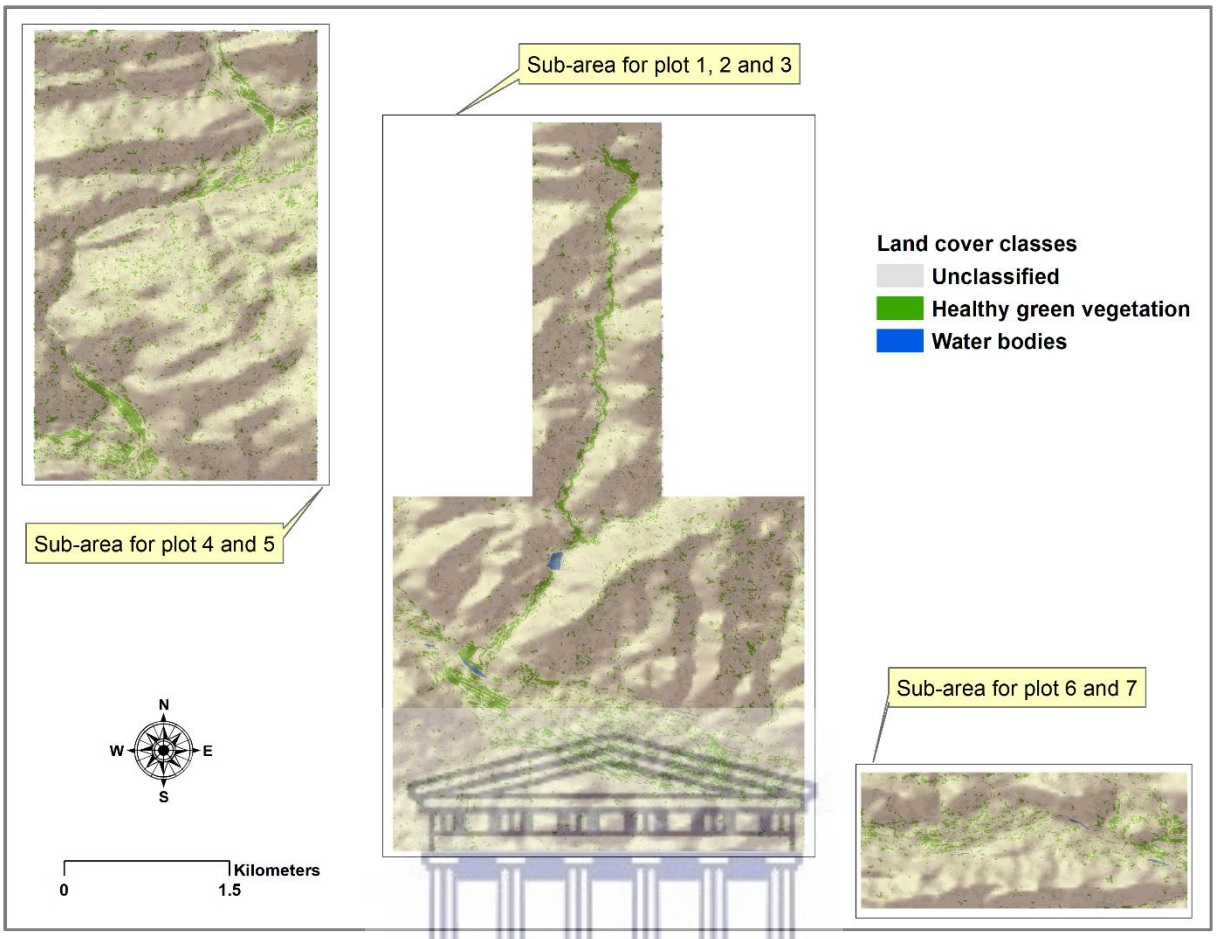

Figure 4.24: Land cover classification results of SPOT 7 imagery taken on the 13th of September 2017.

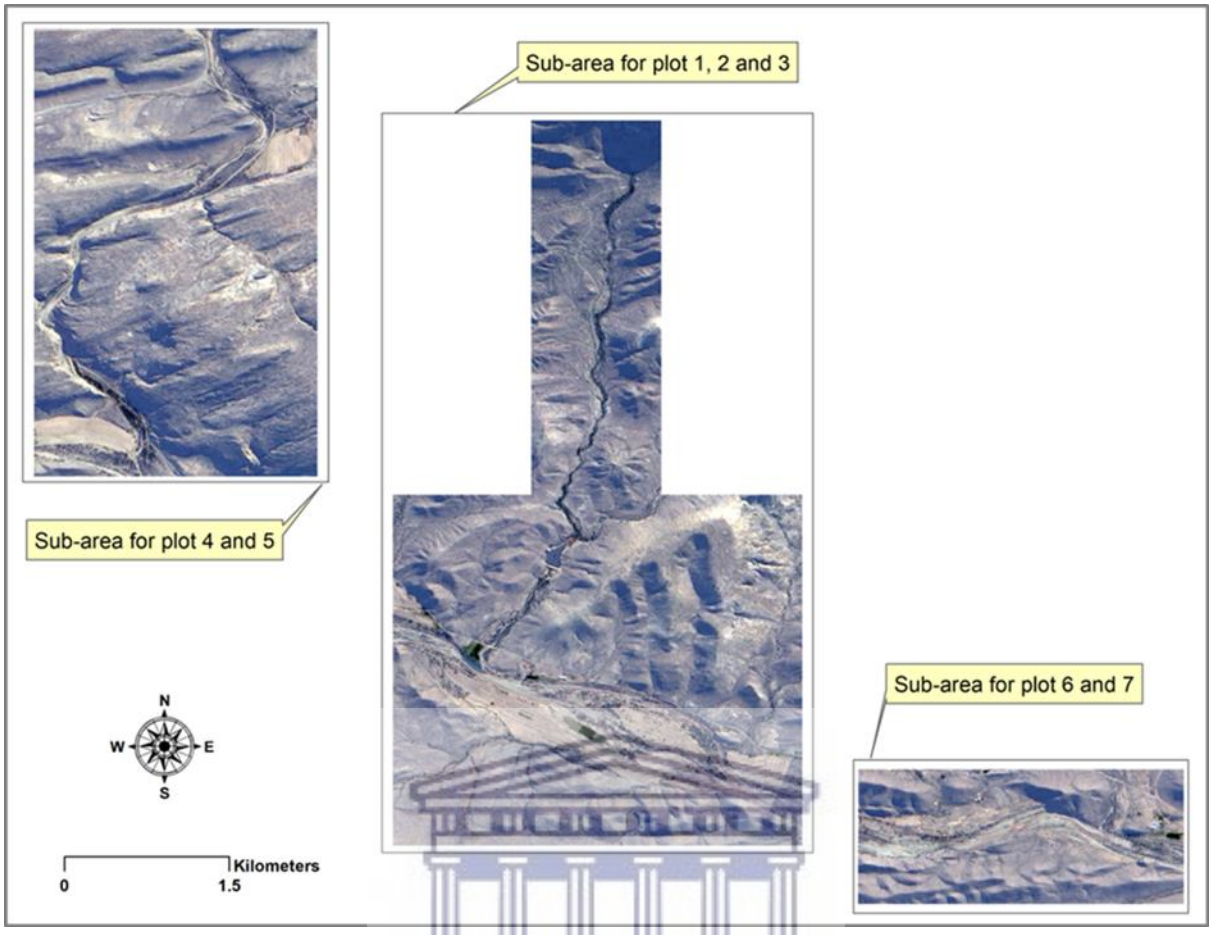

Figure 4.25: Sub-region of the pan-sharpened SPOT 7 image (13th September 2017).

4.1.8.4. | Assessment of classification in October 2017

In Figure 4.26 the misclassifications have significantly diminished. This is demonstrated by the reduced green patches on the hillslopes and high classification accuracy (Table 4.13). The healthy green vegetation has diminished remarkably in some areas. However, along the river channels and in the valleys, vegetation still display persistent amount of greenness. The water bodies are still visible in the central area, but have diminished in some parts of the south-eastern area. Therefore, this suggests the persistent healthy green vegetation, which include the irrigated pasture fields in the centre of the map and some water bodies are dependent on groundwater supply (i.e. GDEs).

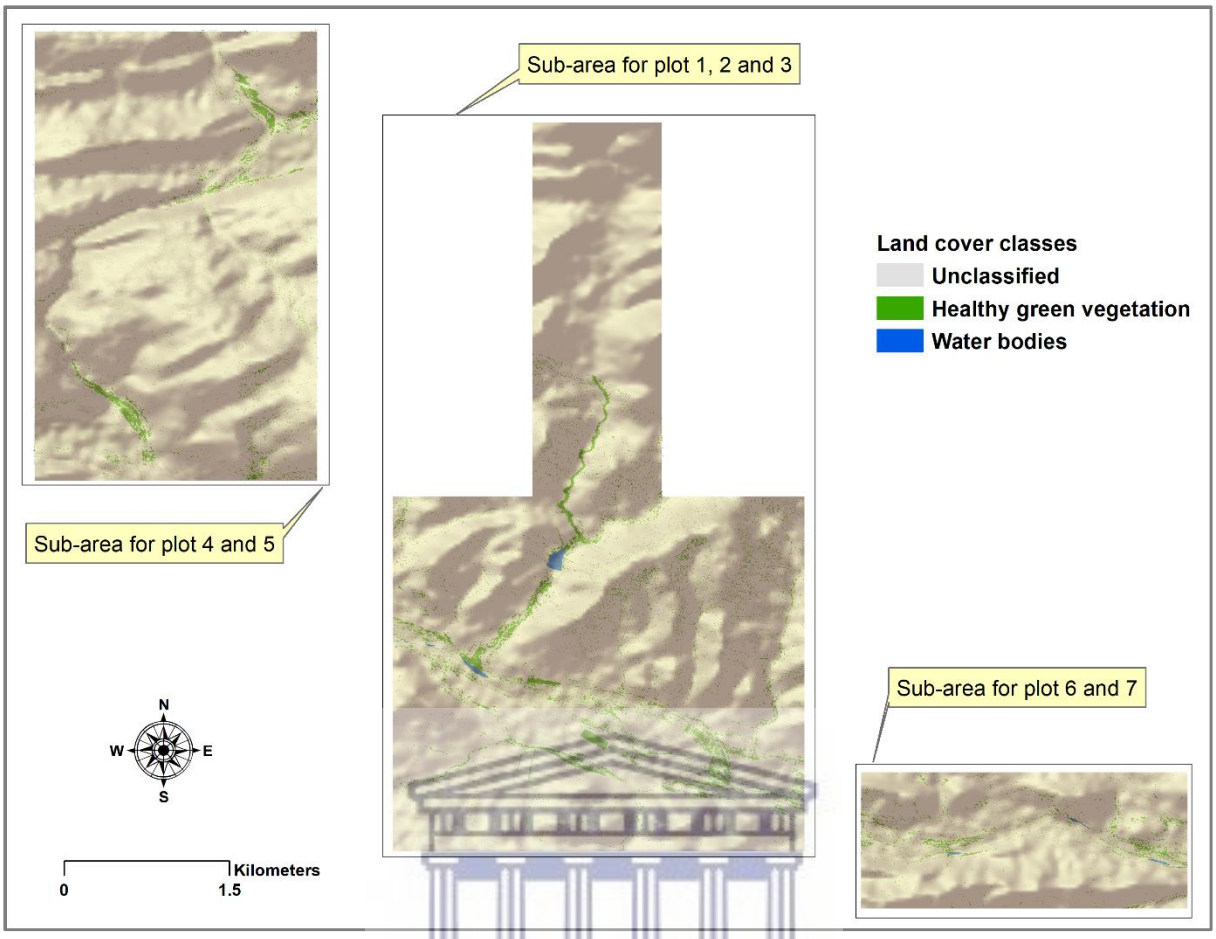

Figure 4.26: Land cover classification results of WorldView-2 imagery taken on the 28th of October 2017**.**

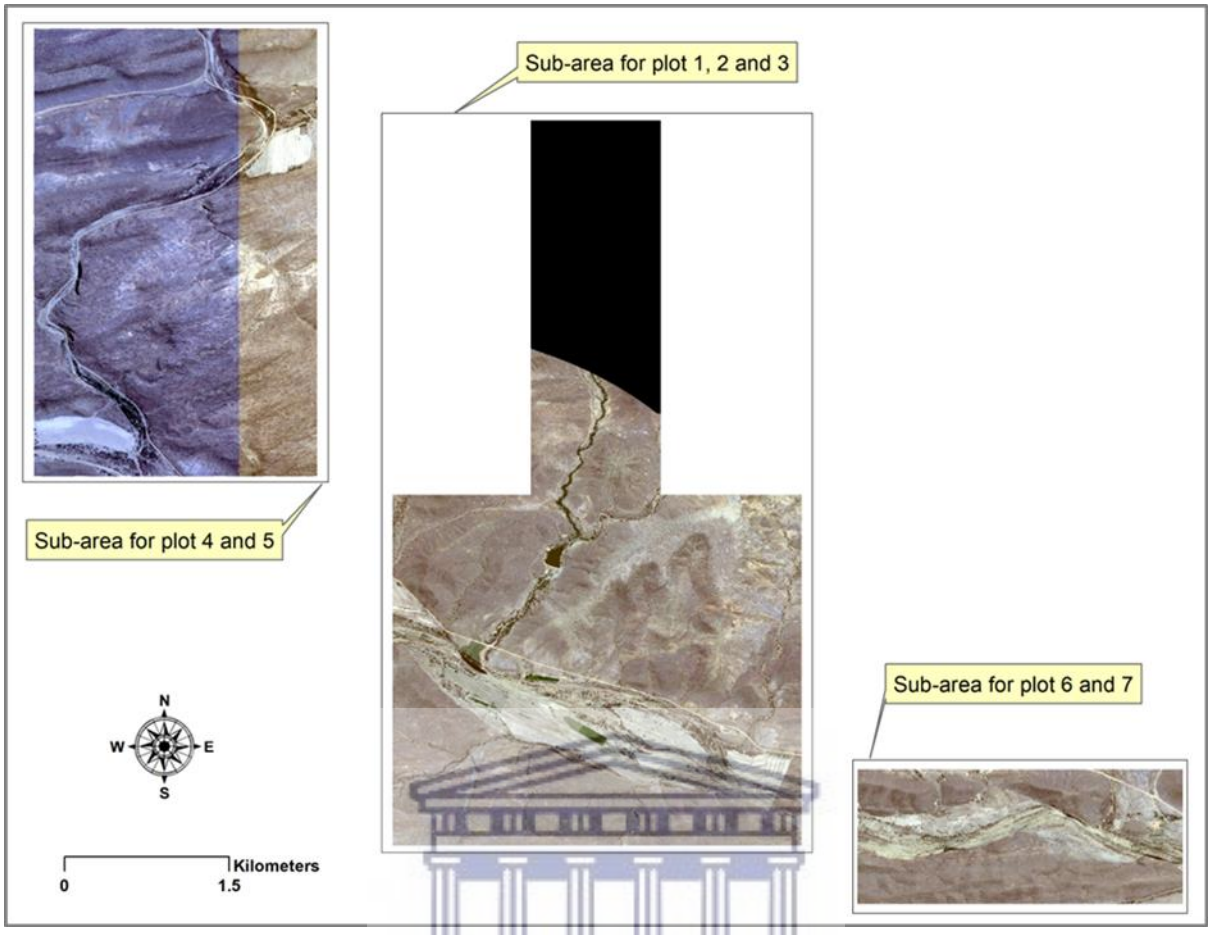

Figure 4.27: Sub-region of the pan-sharpened WorldView-2 image (28th October 2017).

4.1.8.5. | Quantitative assessment of classification results

The class 'water bodies' display high classification accuracy with a producer accuracy of 99.99% in October 2017 (Table 4.13). However, the error matrix demonstrate that both healthy green vegetation and water bodies produced high accuracies on both the SPOT 7 images and the WorldView-2 image. In comparing the overall accuracy of WorldView-2 and SPOT 7 images, Table 4.13 indicates that the pixel-based method produced better results with an overall accuracy of 96.07% and a Kappa coefficient of 0.93. The SPOT images yielded an overall accuracy of 69% and 72% respectively.

Table 4.13: Error matrix of land cover classification in eCognition for July and September 2017, and in ENVI for October 2017.

July 2017	**User/reference class**	**Healthy green vegetation**	**Water bodies**	**Total**
	Healthy green vegetation	13582	0	13582
	Water bodies	0	13582	13582
	Unclassified	135	18	153
	Total	13582	13582	27317
	Producer Accuracy	0.6512	0.9124	
	User accuracy	0.8012	1	
	Overall accuracy (%)	0.69		
September 2017	**User/reference class**	**Healthy vegetation**	**Water bodies**	**Total**
	Healthy green vegetation	13708	0	13708
	Water bodies	0	13708	13708
	Unclassified	80	9	89
	total	13708	13708	27505
	Producer accuracy	0.7521	0.8124	
	User accuracy	0.9122	1	
	Overall accuracy (%)	0.72		
October 2017	**Class**	**Water bodies**	**Healthy green vegetation**	
	Unclassified	0.01	5.39	
	Water bodies	99.99	0	
	Healthy green vegetation	0	94.61	
	Total	100	100	
	Producer accuracy	99.99	94.61	
	User accuracy	100	86.46	
	Overall accuracy (%)	96.07		
	Kappa coefficient	0.93		

4.1.8.6. | *Analysis of the indicators of groundwater discharge areas*

As indicated by Eamus *et al*. (2006) GDEs are most likely found in areas where groundwater is discharged to the surface. Therefore, having identified vegetation and water bodies that

rely on surface expression of groundwater, the mapping of groundwater discharge areas also served as means of validating the areas identified as GDEs.

Figure 4.28 display the results of the wetness index and the values range from -14.1 to 10.5. When the wetness index is high (i.e. greater than the threshold of 10), regions of topographic depressions are identified and therefore, potential groundwater discharge areas. Such areas are mainly located in gentle narrow valleys and in flat areas along the sides of the steeper mountain in the centre of the map. These are the areas where potential GDEs have been identified (topographic depression areas).

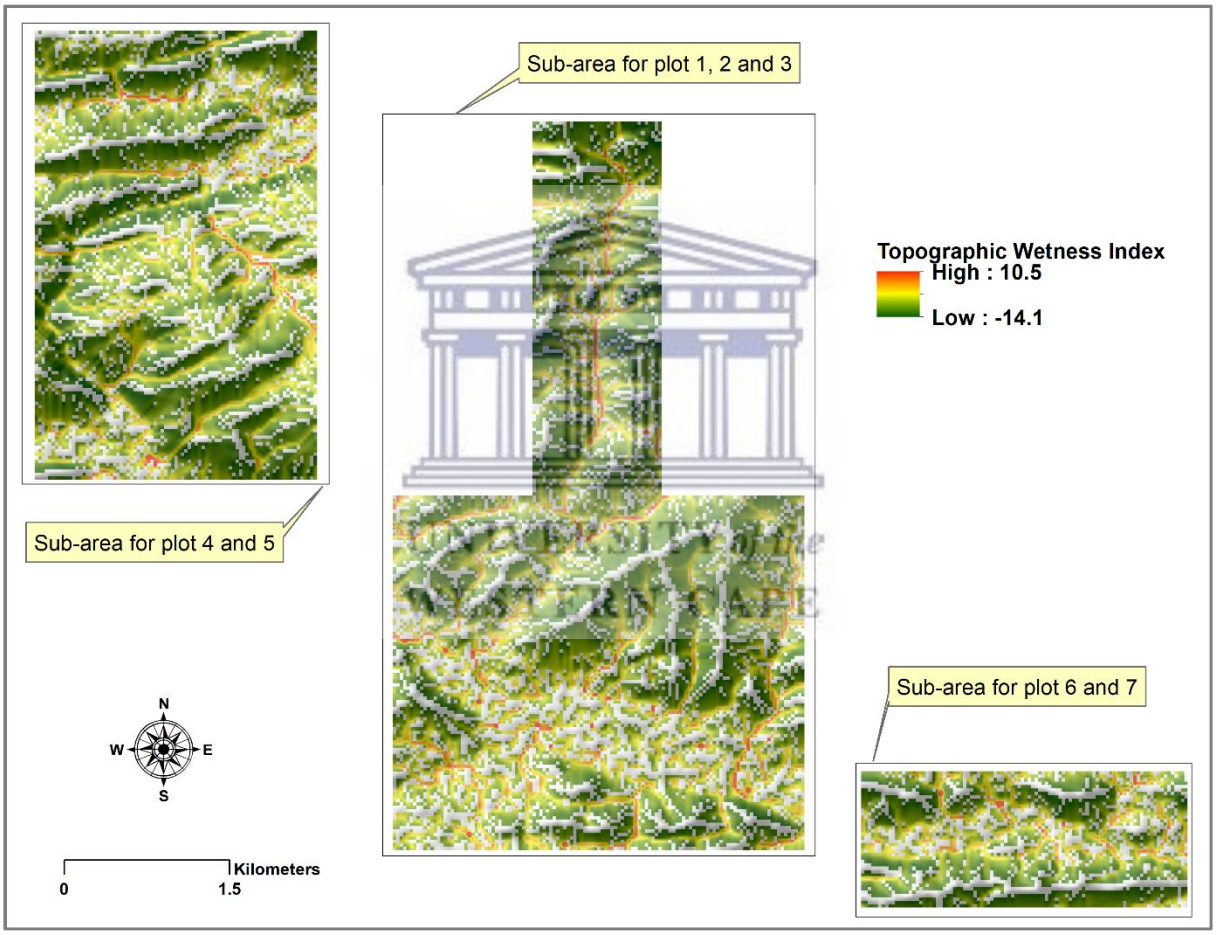

Figure 4.28: The Topographic Wetness Index (TWI) highlighting topographic depressions.

The curvature function in ArcGIS was used to compute the profile curvature map (Figure 4.29). The values of the profile curvature range from -4.5 to 4.3, and values greater than the threshold (0.01) were considered to indicate break of slope areas as potential groundwater discharge areas.

The results of profile curvature are comparable to those of the wetness index, where areas with a break of slope are frequently located along the valleys (i.e. concave slope) where healthy green vegetation dominates. The edges of the river channel in the north-eastern area and the central region also exhibit break of slope. However, it is worth noting that some areas with a break of slope do not perfectly match with the mapped potential GDEs in Figure 4.26.

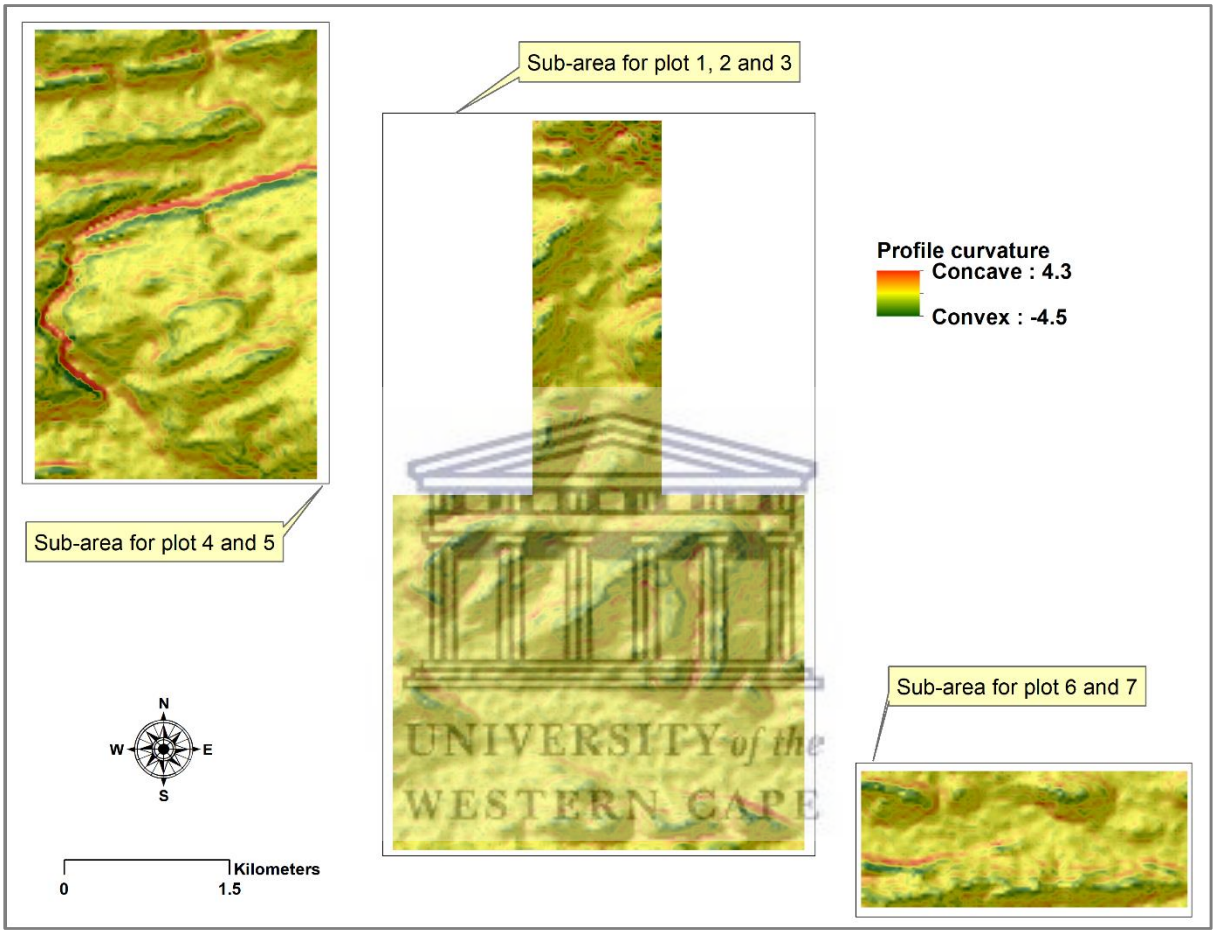

Figure 4.29: A profile curvature of mapped region showing break of slope areas.

Summary

The results in section 4.1.2 and 4.1.3 have shown that the study region is dominated by shrubs, which are drought-resistant and that the NDVI and rainfall patterns showed no clear relationship in most vegetation plots. Section 4.1.4 and 4.1.5 quantified the rainfall variability in the study region and observed rainfall and temperature trends. The results indicated that the region has experienced high variations in rainfall events (> 90%). Rainfall showed a decreasing trends over the years, with a long drought event from 2014 to 2017. Temperatures, on the other hand, showed an increasing trend. The relationship between

NDVI, rainfall and temperature was tested in a long-term inter-annual timescale and over seasonality in both plant communities. Results have shown that both maximum and minimum temperatures had a consistent and a positive association with NDVI. The significance of correlation between NDVI and rainfall was statistically insignificant. However, both climatic elements demonstrated to be the main factors for vegetation growth when a linear combination tested to be statistically significant. The zero-lag and 3-month lag correlations differed over four seasons (summer, autumn, winter and spring) between the floodplain woodland and the hillslope shrubland plant communities. These are further detailed in the following section. Section 4.1.8 mapped potential GDEs. The results have shown that the healthy green vegetation and water bodies in riparian zones maintain persistent levels of greenness and wetness even during dry seasons. The TWI and profile curvature indicated that potential GDEs are likely to occur in lowlands and in areas of break of slope, where groundwater is discharged to the surface. These results are discussed in more detail in the following section and in chapter 5.

4.2. | Discussion

4.2.1. | Analysis of plant species

The plant samples collected during the survey (see Appendix A) and field observations suggest the study region is dominated by shrubs (Figure 4.30). This is consistent with Vlok *et al*. (2005) who observed that shrubs dominate the floodplain vegetation in the Little Karoo and that plant species in different plant communities within the Succulent Karoo biome change rapidly from one patch to the next. Dean *et al*. (1995) also argue that the Karoo is dominated by dwarf shrubland vegetation and that dwarf deciduous shrubs such as the Asteraceae family are most common.

Figure 4.30: The dominance of shrubland in the study region mostly located in hilly slopes (right image), with woodland vegetation located along the river channel or in a valley forming a linear shape (central image).

4.2.2. | The influence of rainfall and temperature on vegetation productivity

The study assessed the influence of rainfall and temperature on vegetation productivity. This was achieved by comparing time-series data of NDVI, rainfall, and temperature over the study period (1984-2017). What emerged strongly from the analysis was that the NDVI and rainfall showed no clear relationship in most vegetation plots (1, 2, 4 and 6), and this was indicated by high NDVI variability but relatively low rainfall levels. However, in plot 3 vegetation productivity was comparable to rainfall conditions, thus indicating a relationship between rainfall and NDVI. In addition, vegetation plot 5 and 7 demonstrated that vegetation productivity has declined over the years. This might be explained by moisture stress caused by the declining rainfall in the study region (Figure 4.11) and high evaporation rates in the Klein Karoo (Le Maitre *et al*., 2009). Du Toit and O'Connor (2014) and Roux and Vorster (1983) have also suggested that rainfall has decreased in the Klein Karoo over the years.

Previous studies have confirmed that southern Africa is characterized by increasing rainfall variability since the late 1960s, which is suggested to be accompanied by widespread and intense drought events (Fauchereau *et al*., 2003). In this study, rainfall variability was quantified in each vegetation plot and an SPI-12 was calculated to measure drought. The results showed that the study region experienced high variations in rainfall events in both plant communities (> 90%). This is in agreement with Le Maitre *et al*. (2009) who observed that variability in rainfall increases as the rainfall decreases in the Klein Karoo. The results of the drought index demonstrated that the study region experienced the longest drought from 2014 to 2017 (Figure 4.14). Therefore, excessive variations in rainfall may result in droughts which consequently can alter the composition of vegetation. This provides an understanding of the dominance of shrubs in the region which have adapted to dry conditions by accessing saturated soil water (Letts *et al*., 2010).

The relationship between NDVI, rainfall and temperature was tested over a long-term inter-annual timescale and over seasonality in the hillslope shrubland and floodplain woodland plant communities. In a long-term inter-annual timescale the correlation and model results indicated that trends in vegetation productivity were positively associated with temperature, with the best correlation (r = 0.47 and r = 0.45) for both maximum and minimum temperatures respectively. The relationship between NDVI and rainfall was statistically

insignificant (r = 0.10). The influence of a linear combination of rainfall and maximum temperatures on NDVI was statistically significant. This suggests both climatic elements emerge as contributing factors in vegetation growth in a long-term inter-annual timescale.

At a plant community level, a zero-lag and 3-month lag correlations were carried out over four seasons (summer, autumn, winter, and spring). In the hillslope shrubland plant community temperatures plays a key role on vegetation productivity during autumn and spring. In a 3-month lag correlation (Table 4.12) vegetation demonstrate immediate response to rainfall during autumn, specifically in non-riparian areas. The study region receives rainfall predominantly in winter (Le Maitre *et al*., 2009). However, the correlation between rainfall and NDVI in winter (Table 4.11 and 4.12) indicate that there is no vegetation growth because it is too cold and temperatures are too low to reach a desired species optimum level for plant development - which is highlighted by Hatfield and Prueger (2015).

In summer, the availability of moisture is significant for vegetation productivity and this is displayed by statistically significant correlations between rainfall and NDVI. The correlation between NDVI and maximum temperatures indicates that excessively high temperatures are a limiting factor for vegetation growth. This has been previously indicated by Hatfield and Prueger (2015) and Whitecross *et al*. (2012) who asserted that exposure to extreme temperatures during plant development will reduce production quantity and quality. In a 3-month lag correlation matrix (Table 4.12), maximum temperatures are significantly correlated with NDVI during summer. However, the correlations are not excessively higher to indicate improvements compared to the zero-lag correlations.

In the floodplain woodland plant community temperatures also play a key role on vegetation productivity in autumn, winter and spring (Table 4.11 and 4.12). The significance of temperatures on vegetation growth in winter could be explained by the fact that this community has permanent access to water (Zaimes *et al*., 2007) and, therefore, productivity almost occurs throughout seasons. Rainfall is only statistically significant in explaining NDVI variance at one vegetation plot in summer (plot 4) in zero-lag correlation, and in plot 4 and 6 during summer and winter in a 3-month lag correlation. This suggest that immediate rainfall is not important in explaining plant growth and that vegetation in this community respond to through flow and may be GDEs. Le Maitre *et al*. (1999) have also argued that plants in riparian

areas have root systems that remain in contact with saturated soil layers and are able to tap groundwater that is discharging into the stream. The River Health Programme (2007) also states that vegetation in riparian zones grows in greater densities than the surrounding terrestrial vegetation in the Karoo.

4.2.3. | The occurrence of probable Groundwater Dependent Ecosystems (GDEs)

Image classification was used to map two potential GDE classes (i.e. healthy green vegetation and water bodies) through change detection over a single dry year. The technique has been previously used to map GDEs (Barron *et al*., 2012; Dresel *et al*., 2010; Munch and Conrad, 2007). The classification results demonstrated that the healthy green vegetation and water bodies in lowlands maintain consistent amount of greenness and wetness during dry seasons (Figure 4.22, 4.24 and 4.26). This is more visible in the WorldView-2 image (Figure 4.26), which has a higher classification accuracy than the SPOT images. According to Barron et al. (2012), such invariant vegetation and water are likely to be groundwater dependent, specifically in the absence of other water sources. This is consistent with field observations where surface water flow was non-existent but water and vegetation along the valleys and in riparian areas exhibited strong productivity and high levels of wetness. Bestland *et al*. (2017) also discovered that surface water pools are dependent on groundwater for their supply of water in dry seasons. Groeneveld and Griepentrog (1985) argue that groundwater is an essential source of supply to maintain the riparian zone, particularly in climatic regions with seasonal precipitation. However, during field data collection farmers indicated that the depth to groundwater when drilling boreholes was typically 60-100 m. In measuring groundwater levels at selected sites in the Gouritz WMA, the DWS (2015) also highlighted that the deepest groundwater level is more than 100 m. Therefore, it seems unlikely that the mapped potential GDEs are connected to the regional aquifer, but are likely receiving water from interflow (Figure 5.1).

In comparing the results of image classification and indicators of groundwater discharge areas (TWI and profile curvature), the mapped probable GDEs occur in topographic depressions and in some areas of break of slope where groundwater is discharged to the surface (Figure 4.28 and 4.29). Similar findings have been highlighted in the literature. Brydsten (2006) argues that groundwater discharge can occur in existing surface waters and at low angle slopes. Tweed

et al. (2007) used the standard deviation of the NDVI (SDVI) and also discovered that vegetation with stable photosynthetic activity indicates potential groundwater discharge areas.

4.2.3.1. Uncertainties

There is uncertainty with the proposed method of mapping potential GDEs. According to Barron *et al*. (2012) the use of remote sensing observations in measuring the dependency of systems to groundwater is relatively indirect. Therefore, hydrogeological information and groundwater dataset in addition to remote sensing indicators can be used to infer groundwater dependency. In this study, the validation of the identified GDEs was essentially limited by the inaccessible groundwater dataset and extensive field verification techniques associated with cost implications. However, the proposed method has produced probable GDE classes that are consistent with surface features in a true colour high-resolution WorldView-2 multispectral image.

CHAPTER 5: GENERAL DISCUSSION, CONCLUSION AND RECOMMENDATIONS

5.1. | General discussion

5.1.1. | The response of plant communities to rainfall and temperature

The correlation matrix (Table 4.11 and 4.12) between NDVI, rainfall, and temperature showed that responses to rainfall and temperature differed between the floodplain woodland and the hillslope shrubland plant communities. The hillslope shrubland community had a strong response to both rainfall and temperature, while the floodplain woodland community only showed a strong response to temperature in most vegetation plots. The high response of the floodplain woodland community to temperature can be explained by the need of temperature for plant growth and development (Hatfield and Prueger, 2015), while the low response to rainfall can be explained by the already existing water and moisture in riparian areas and along the valleys through groundwater. This is in accordance with a study by Zaimes *et al*. (2007) which indicated that riparian vegetation grows in greater densities than vegetation in terrestrial uplands because the former has more sources and greater amounts of water (Figure 5.1 and 5.2). In a study of vegetation response to climate variability, Rishmawi *et al*. (2016) also discovered that vegetation in wetter areas does not directly respond to rainfall variations.

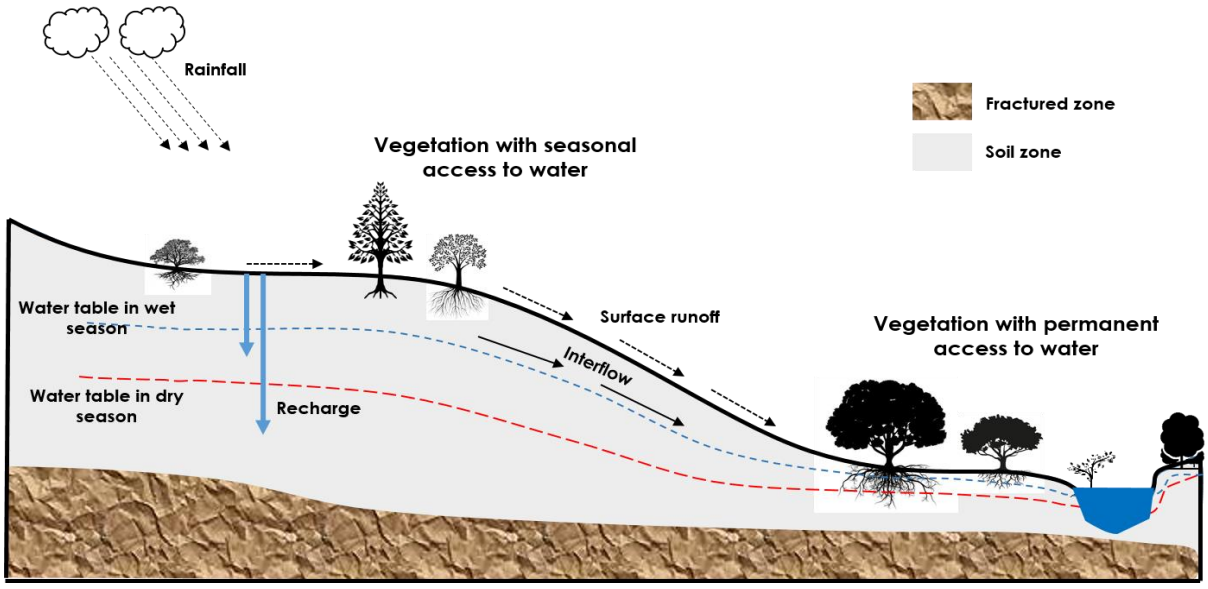

Figure 5.1: Delineating the response and water availability for riparian and non-riparian vegetation.

In the hillslope shrubland community, vegetation depends significantly on overland flow and responds immediately to rainfall, particularly when groundwater levels are low (Figure 5.1). Zaimes *et al*. (2007) have also indicated that rainfall is the primary source of water for vegetation in terrestrial uplands. The hillslope shrubland community also responds significantly to minimum temperatures. This analysis is similar to Esler and Rundel (1999), who also found that minimum temperatures allow continued growth of the Succulent Karoo vegetation following summer rainfall.

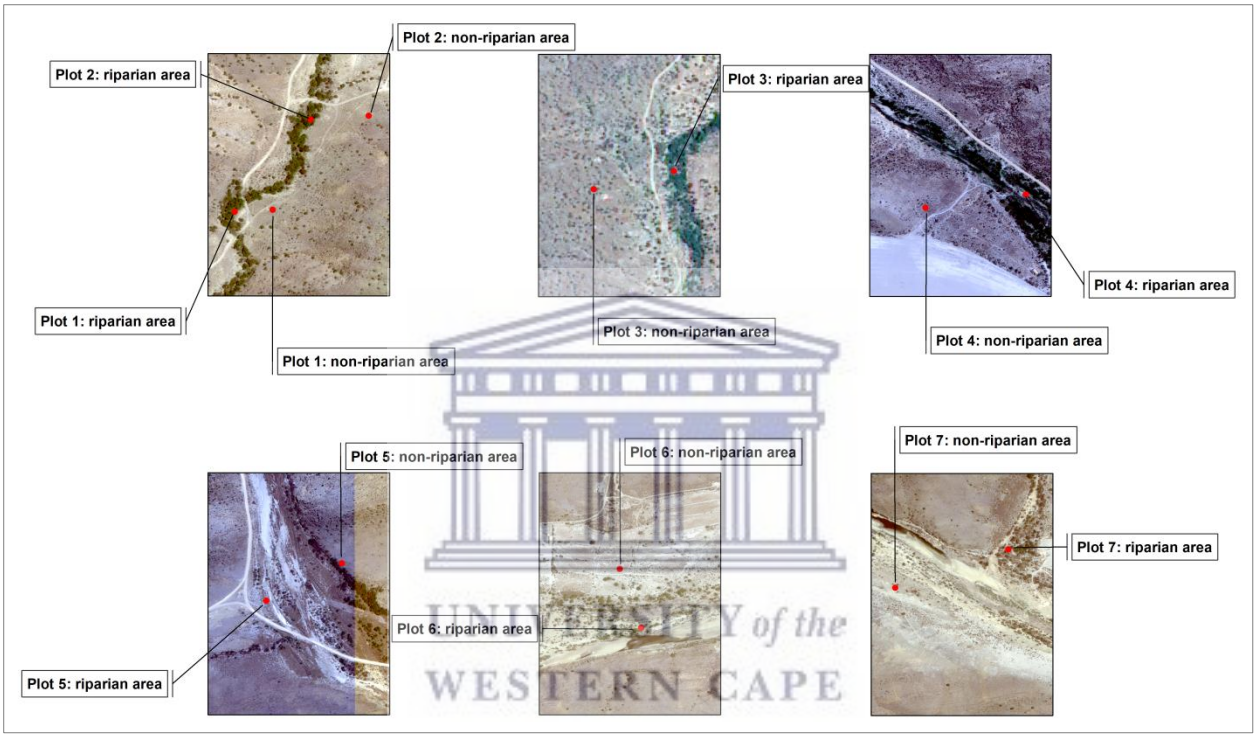

Figure 5.2: The sampled vegetation plots highlighting the location of riparian and non-riparian areas in the study region.

5.1.2. | Riparian vs non-riparian areas, and potential GDEs

The riparian areas in both the floodplain woodland and the hillslope shrubland communities comprise the dominant plant species; *Pteronia pallens, Euclea undulata* and *Vachellia karroo*. *Pteronia pallens* and *Euclea undulata* have been classified as evergreen woody shrubs by Vorster (2017), and the *Vachellia karroo* is considered to grow where groundwater is available along drainage lines and sources groundwater with a long taproot system (Barnes *et al*., 1996). However, Vlok *et al*. (2005) found the *Vachellia karroo* to be also present in the hillslopes. The authors also found that vegetation in the Succulent Karoo biome changes from

one patch to another. Similar findings were detected in this study where all three dominant species were also found in non-riparian areas (Table 4.1).

Within the riparian areas, a GDE with permanent access to water (Figure 5.1 and 5.2) was identified (i.e. healthy green vegetation – see Section 4.1.8). In mapping vegetation in the Klein Karoo, Vlok *et al*. (2005) also found that aquatic habitat (which include riverine and floodplain vegetation) in the Klein Karoo is restricted to lowland landscapes. These vegetation units were found to be dependent on water and occur alongside permanent or seasonal water drainage zones, thus highlighting areas where water is available through subsurface flow or overland flow during rainfall seasons. In this study, there was no overland flow as the survey was conducted during a dry period. Therefore, the high vegetation productivity in riparian areas can be explained by the availability of water and high level of surface moisture through subsurface flow, probably delivered by interflow processes (Figure 5.1).

The non-riparian areas are characterized by the dominance of the low *Rhigozum obovatum* shrub and the succulent *Ruschia muricata* species. Both plant species have been classified as terrestrial vegetation by Vlok *et al*. (2005) and grow in arid regions, and are thus resistant to drought conditions (Mucina and Rutherford, 2006). This is because humid air during winter prevents frost from damaging plant species, while sunlight plays a pivotal role in maintaining plant species during dry seasons in the Succulent Karoo biome (Vlok *et al*., 2005). This explains the persistent green tree species on the hillslopes (Figure 4.22, 4.24 and 4.26). However, some plant species perish and these are mostly non-drought tolerant and are assumed to have short root systems, thus incapable of sourcing groundwater in dry periods (Figure 5.1). Esler and Rundel (1999) also discovered that plant species with shallow root systems in the Succulent Karoo biome source near-surface groundwater after a rainfall event, and productivity decreases as rainfall decreases in late spring.

The water bodies in Section 4.1.8 and in vegetation plot 6 and 7 (Figure 5.2) have been identified as groundwater dependent. These are manly situated in the river channel, occur in groundwater discharge areas (Figure 4.28 and 4.29) and remain in contact with groundwater during wet and dry seasons as demonstrated in Figure 5.1. This might be explained by the underlying geological formation of the mapped area, which is composed of the TMG and the Bokkeveld group (Figure 1.5). Because of folding and faulting in the Cape Fold belt, the TMG

and Bokkeveld group were fractured and therefore, water is able to move in voids between the rock particles (Roets, 2008). Such types of geological formations have been categorized as secondary fractured aquifers (Le Maitre *et al*., 2009) and are potential zones of groundwater discharge or recharge.

5.2. | Conclusion

The study showed that the Touws quaternary catchments are characterized by a decreasing highly variable rainfall. The rainfall trends and the SPI-12 showed the study region is characterized by a cycle of wet and dry periods (4 to 6-year cycle), with more frequent drought seasons than wet seasons. Temperatures showed an increasing trend, particularly maximum temperatures. The identified climatic trends are also documented in the literature (Le Maitre *et al*., 2009). Analysis of vegetation plots showed that the trend between NDVI and rainfall is inconsistent, with the former responding a few months after a major rainfall event. However, the study region is dominated by shrubs, most of which are drought resistant, thus, indicating that some areas are persistently green throughout seasons. Correlation analysis and a multiple regression model between NDVI, rainfall, and temperature showed that both climate elements emerge as contributing factors in vegetation dynamics, particularly in a 3-month lag relationship. However, the correlations differed between the floodplain woodland community and the hillslope shrubland community. The latter showed a strong correlation with rainfall and temperature, while the former only showed a strong correlation with temperature in most vegetation plots.

In determining the ability of land cover classification and indicators of groundwater discharge areas in mapping potential GDEs, the spatial mapping of three image dates illustrated the location of vegetation with consistent photosynthetic activity and water. These were significantly located in the river channels, in narrow valleys and in riparian areas of the floodplain woodland and the hillslope shrubland communities where vegetation grows in greater densities due to permanent access to water through subsurface flow. The non-riparian areas in both plant communities were largely dominated by drought-resistant plant species with seasonal access to water and more responsive to overland flow during rainfall seasons. In addition to the error matrix and groundwater discharge areas, analysis of the characteristics of plant species and the literature were used to validate the identified

probable GDEs. In overall, the study showed that climatic trends (rainfall and temperature) are the main factors of vegetation change and the dependence of vegetation on groundwater can be potentially assessed by mapping surface change.

5.3. | Recommendations

The influence of climate on vegetation productivity as well as the dependence of vegetation on groundwater could be further expanded. The study recommends the following for future research:

- Remote sensing such as hyperspectral remote sensing can be used to help environmental scientists to better observe changes in vegetation productivity and mitigate measures to overcome severe impacts on vegetative landscapes caused by climate variability.
- The consideration of the range of variability in NDVI as a discriminator of GDEs.
- The inclusion of more fine resolution satellite images in mapping vegetation of the semi-desert areas can help to discriminate and identify plant species with small sizes. This can further improve land cover classification, specifically in areas where land surface features have similar reflectance properties.
- The addition of high-resolution DEM such as LiDAR and hydrogeological information can help improve the mapping of groundwater discharge areas as a means of locating GDEs. In addition, the break of slope technique may be highly suitable for regions with large-scale changes in topographic relief.
- Prospective research work in the study area could use the sap flow technique to understand the uptake of groundwater by vegetation and the use of groundwater level measurements can provide means to estimate transpiration originating from groundwater.

References

Acocks, J.P.H. 1953. Veld Types of South Africa. In: *Memoirs of the Botanical Survey of South Africa* 28*,* pp 1-192.

Adam, H.E., Csaplovics, E. and Elhaja, M.E. 2016. A comparison of pixel-based and object-based approaches for land use land cover classification in semi-arid areas, Sudan. In *IOP Conference Series: Earth and Environmental Science* (Vol. 37, No. 1, pp 012061). IOP Publishing.

Agapiou, A., Alexakis, D. and Hadjimitsis, D. 2014. Spectral sensitivity of ALOS, ASTER, IKONOS, LANDSAT and SPOT satellite imagery intended for the detection of archaeological crop marks. *International Journal of Digital Earth,* 7(5), pp 351-372.

Alimuddin, I., Sumantyo, J.T.S. and Kuze, H. 2012. Assessment of pan-sharpening methods applied to image fusion of remotely sensed multi-band data. *International Journal of Applied Earth Observation and Geo-information,* 18, pp 165-175.

Allen R.B. and Platt, K.H. 1990. Annual seedfall variation in Nothofagus solandri (Fagaceae), Canterbury, New Zealand. *Oikos*, pp 199–206.

Ambrosino, C., Chandler, R.E. and Todd, M.C. 2011. Southern African monthly rainfall variability: An analysis based on generalized linear models. *Journal of climate,* 24(17), pp 4600-4617.

Barbeta, A. and Peñuelas, J. 2017. Relative contribution of groundwater to plant transpiration estimated with stable isotopes. *Scientific reports*, 7(1).

Barbosa, H.A. and Kumar, T.L. 2016. Influence of rainfall variability on the vegetation dynamics over Northeastern Brazil. *Journal of Arid Environments,* 124, pp 377-387.

Barlow, K.M., Christy, B.P., O'leary, G.J., Riffkin, P.A. and Nuttall, J.G. 2015. Simulating the impact of extreme heat and frost events on wheat crop production: a review. *Field Crops Research,* 171, pp 109-119.

Barnes, R.D., Filer, D.L. and Milton, S.J. 1996. Acacia Karroo: monograph and annotated bibliography (No. 32). Oxford Forestry Institute, Department of Plant Sciences, University of Oxford.

Barron, O.V., Emelyanova, L., Van Niel, T.G., Pollock, D. and Hodgson, G. 2012. Mapping groundwater dependent ecosystems using remote sensing measure of vegetation and moisture dynamics. *Hydrological Processes*, 28(2), pp 372-385.

Beck, P.S., Atzberger, C., Hogda, K.A., Johansen, B. and Skigmore, A.K. 2006. Improved monitoring of vegetation dynamics at very high altitudes: A new method using MODIS NDVI. *Remote sensing of Environment,* 100(3), pp 321-334.

Benz, U.C., Hofmann, P., Willhauck, G., Lingenfelder, I. and Heynen, M. 2004. Multi-resolution, object-oriented fuzzy analysis of remote sensing data for GIS-ready information. ISPRS *Journal of photogrammetry and remote sensing,* 58(3-4), pp 239-258.

Bestland, E., George, A., Green, G., Olifent, V., Mackay, D. and Whalen, M. 2017. Groundwater dependent pools in seasonal and permanent streams in the Clare Valley of South Australia. *Journal of Hydrology: Regional Studies*, 9, pp 216-235.

Blaschke, T., Burnett, C. and Pekkarinen, A. 2004. Image segmentation methods for object-based analysis and classification. In *Remote sensing image analysis: Including the spatial domain* (pp 211-236). Springer, Dordrecht.

Blaschke, T. 2010. Object based image analysis for remote sensing. *ISPRS journal of photogrammetry and remote sensing,* 65(1), pp 2-16.

Bock, M., Xofis P., Mitchley, J., Rossner, G. and Wissen, M. 2005. Object-oriented methods for habitat mapping at multiple scales – case studies from northern Germany and Wye Downs, UK. *Journal for Nature Conservation* 13, pp 75-89.

Brooks, C., Schaub, D., Powell, R., French, N. and Shuchman, R. 2006. *Multi-temporal and multiplatform agricultural land cover classification in south-eastern Michigan,* Proceedings of the ASPRS 2006 Annual Conference, 01-05 May, Reno, Nevada.

Brydsten, L. 2006. *Modelling groundwater discharge areas using only digital elevation models as input data*. Umea University, Technical Report TR-06-39.

Büttner, S.H., Reid, W.K. and Erasmus, R. 2016. Late Permian tectonics and associated fluid influx during the Cape Orogeny: evidence from fault-bound quartz veins in the Witteberg Group (Cape Supergroup, South Africa). *South African Journal of Geology,* 119(2), pp 379-398.

Campbell, J.B. and Wynne, R.H. 2011. *Introduction to remote sensing*. Guilford Press.

Chamaille-Jammes, S., Fritz, H. and Murindagomo, F. 2006. Spatial patterns of the NDVI–rainfall relationship at the seasonal and inter-annual time scales in an African savanna. *International Journal of Remote Sensing,* 27(23), pp 5185-5200.

Chen, J., Wu, X., Finlayson, B.L., Webber, M., Wei, T., Li, M. and Chen, Z. 2014. Variability and trend in the hydrology of the Yangtze River, China: annual precipitation and runoff. *Journal of Hydrology,* 513, pp 403-412.

Cissé, S., Eymard, L., Ottlé, C., Ndione, J.A., Gaye, A.T. and Pinsard, F. 2016. Rainfall intra-seasonal variability and vegetation growth in the Ferlo Basin (Senegal). *Remote Sensing*, 8(66), 24 pp.

Coetzee, J.A. 1967. Pollen analytical studies in east and southern Africa. *Palaeoecology of Africa*, 3, pp 1-146.

Colvin, C., Le Maitre, D. and Hughes, S. 2002. *Assessing Vegetation Ecosystem Dependence on Groundwater.* WRC Report 1092.

Colvin, C., Le Maitre, D., Saayman, I. and Hughes, S. 2007. *Aquifer dependent ecosystems in key hydrogeological type settings in South Africa*. WRC project K5/1330.

Cowling, R.M., Richardson, D.M. and Pierce, S.M. (eds) 2003. *Vegetation of southern Africa*. Cambridge University Press.

Curtis, O. and Bond, W.G. 2013. What is renosterveld? Feature. *Veld and Flora,* 99, pp 180-183.

Dean, W.R.J., Hoffinan, M.T., Meadows, M.E. and Milton, S.J. 1995. Desertification in the semi-arid Karoo, South Africa: review and reassessment. *Journal of Arid Environments,* 30(3), pp 247-264.

Definiens imagine 2007. *eCognition Developer 8.64.1 tour guide*. Munchen: Trimble Germany GmbH.

Department of Environmental Affairs. 2018, Pretoria. Available online at: https://www.egis.environment.gov.za/gis_data_downloads (Accessed 28/10/2018).

Department of Water and Sanitation (DWS). 2015. *Reserve Determination Studies for the Selected Surface Water, Groundwater, Estuaries and Wetlands in the Gouritz Water Management Area*: Groundwater Report. Prepared by Exigo Sustainability for Scherman Colloty & Associates cc. Report no. RDM/WMA16/02/CON/0413.

Dieppois, B., Pohl, B., Rouault, M., New, M., Lawler, D. and Keenlyside, N. 2016. Inter-annual to inter-decadal variability of winter and summer Southern African rainfall and their teleconnections. *Journal of Geophysical Research: Atmospheres*, 121(11), pp 6215-6239.

DigitalGlobe (2013b) - Standard Imagery. Available online at: http://www.geosoluciones.cl/documentos/worldview/DigitalGlobe-Core-Imagery-Products-Guide.pdf (Accessed 3/06/2018).

Doody, T.M., Barron, O.V., Dowsley, K., Emelyanova, I., Fawcett, J., Overton, I.C., Pritchard, J.L., Van Dijk, A.I. and Warren, G. 2017. Continental mapping of groundwater dependent ecosystems: A methodological framework to integrate diverse data and expert opinion. *Journal of Hydrology: Regional Studies,* 10, pp 61-81.

Dresel, P. E., Clark, R. Cheng, X., Reid, M., Fawcett, J., and Cochraine, D. 2010. *Mapping Terrestrial Groundwater Dependent Ecosystems: Method Development and Example Output*. Victoria Department of Primary Industries, Melbourne VIC. 66 pp.

Duah, A.A. 2010. *Sustainable utilization of Table Mountain Group aquifers*. PhD Thesis, University of the Western Cape, Bellville.

Dube, T. and Mutanga, O. 2016. The impact of integrating WorldView-2 sensor and environmental variables in estimating plantation forest species aboveground biomass and carbon stocks in uMgeni Catchment, South Africa. *ISPRS Journal of Photogrammetry and Remote Sensing,* 119, pp 415-425.

Dube, T., Mutanga, O., Elhadi, A. and Ismail, R. 2014. Intra-and-inter species biomass prediction in a plantation forest: testing the utility of high spatial resolution spaceborne multispectral RapidEye sensor and advanced machine learning algorithms. *Sensors*, 14(8), pp 15348-15370.

du Toit, J.C. and O'Connor, T.G. 2014. Changes in rainfall pattern in the eastern Karoo, South Africa, over the past 123 years. *Water SA,* 40(3), pp 453-460.

Eamus, D., Froend, R., Loomes, R., Hose, G. and Murray, B. 2006. A functional methodology for determining the groundwater regime needed to maintain the health of groundwater-dependent vegetation. *Australian Journal of Botany, 54* (2), pp 97-114.

Enroth, C. 2014. Garden Tips from Knox County Master Gardeners. *How Weather Affects Plants*.

Esler, K.J. and Rundel, P.W. 1999. Comparative patterns of phenology and growth form diversity in two winter rainfall deserts: the Succulent Karoo and Mojave Desert ecosystems. *Plant Ecology,* 142(1-2), pp 97-104.

Fauchereau, N., Trzaska, S., Rouault, M. and Richard, Y. 2003. Rainfall variability and changes in southern Africa during the 20th century in the global warming context. *Natural Hazards,* 29(2), pp 139-154.

Feizizadeh, B., Blaschke, T., Tiede, D. and Moghaddam, M.H.R. 2017. Evaluating fuzzy operators of an object-based image analysis for detecting landslides and their changes. *Geomorphology,* 293*,* pp 240-254.

Feng, Y., Lu, D., Chen, Q., Keller, M., Moran, E., dos-Santos, M.N., Bolfe, E.L. and Batistella, M. 2017. Examining effective use of data sources and modeling algorithms for improving biomass estimation in a moist tropical forest of the Brazilian Amazon. *International Journal of Digital Earth*, 10(10), pp 996-1016.

Fox, J. 1997. *Applied regression analysis, linear models, and related methods*. Sage Publications, Inc.

Funk, C., Peterson, P., Landsfeld, M., Pedreros, D., Verdin, J., Shukla, S., Husak, G., Rowland, J., Harrison, L., Hoell, A. and Michaelsen, J. 2015. The climate hazards infrared precipitation with stations--a new environmental record for monitoring extremes. *Scientific data*, 2, pp 1-21.

Gao, B.C. 1996. NDWI—A normalized difference water index for remote sensing of vegetation liquid water from space. *Remote sensing of environment,* 58(3), pp 257-266.

Geel, C., Schulz, H.M., Booth, P. and Horsfield, B. 2013. Shale gas characteristics of Permian black shales in South Africa: results from recent drilling in the Ecca Group (Eastern Cape). *Energy Procedia,* 40, pp 256-265.

Glanville, K., Ryan, T., Tomlinson, M., Muriuki, G., Ronan, M. and Pollett, A. 2016. A Method for Catchment Scale Mapping of Groundwater-Dependent Ecosystems to Support Natural Resource Management (Queensland, Australia*). Environmental management,* 57(2), pp 432-449.

Gordon, N.D., McMahon, T.A., Finlayson, B.L. and Gippel, C.J. 2004. *Stream hydrology: an introduction for ecologists.* John Wiley and Sons.

Govender, M., Chetty, K., Naiken., V. and Bulcock, H. 2008. A comparison of satellite hyperspectral and multispectral remote sensing imagery for improved classification and mapping of vegetation. *Water SA*, 34(2), pp 147-154.

Groeneveld, D.P. and Griepentrog, T.E. 1985. *Interdependence of groundwater, riparian vegetation, and streambank stability: a case study*. USDA Forest Service General Technical Report RM, 120, pp 44-48.

Groundwater dependent ecosystems, WetlandInfo 2014, Queensland Government, Queensland. Available online at: https://wetlandinfo.des.qld.gov.au/wetlands/ecology/aquatic-ecosystems-natural/groundwater-dependent (Accessed 25/04/2018).

Hare, W. 2003. *Assessment of knowledge on impacts of climate change-contribution to the specification of art. 2 of the UNFCCC: Impacts on ecosystems, food production, water and socio-economic systems.*

Hatfield, J.L. and Prueger, J.H. 2015. Temperature extremes: Effect on plant growth and development. *Weather and climate extremes*, 10, pp 4-10.

Hatton, T., Evans, R. and Merz, S.K. 1997. *Dependence of ecosystems on groundwater and its significance to Australia*. Sinclair Knight Merz.

Hayes, M.J., Svoboda, M.D., Wiihite, D.A. and Vanyarkho, O.V. 1999. Monitoring the 1996 drought using the standardized precipitation index. *Bulletin of the American meteorological society,* 80(3), pp 429-438.

Hiller, N. and Dunlevey, J.N. 1978. The Bokkeveld-Witteberg boundary in the Montagu—Touws River area, Cape Province. *Trans. Geol. Soc. S. Aft*, 81, pp 101-104.

Hodgson, D.M., Flint, S.S., Hodgetts, D., Drinkwater, N.J., Johannessen, E.P. and Luthi, S.M. 2006. Stratigraphic evolution of fine-grained submarine fan systems, Tanqua depocenter, Karoo Basin, South Africa. *Journal of Sedimentary Research,* 76(1), pp 20-40.

Holding, D.R. and Streich, A.M. 2013. Plant Growth Processes: Transpiration, Photosynthesis, and Respiration. *University of Nebraska, Lincoln*, NE, 10 pp.

Huntington, J., McGwire, K., Morton, C., Snyder, K., Peterson, S., Erickson, T., Niswonger, R., Carroll, R., Smith, G. and Allen, R. 2016. Assessing the role of climate and resource management on groundwater dependent ecosystem changes in arid environments with the Landsat archive. *Remote sensing of Environment*, 185, pp 186-197.

Huxman, T.E., Cable, J.M., Ignace, D.D., Eilts, J.A., English, N.B., Weltzin, J. and Williams, D.G. 2004. Response of net ecosystem gas exchange to a simulated precipitation pulse in a semi-arid grassland: the role of native versus non-native grasses and soil texture. *Oecologia*, 141(2), pp 295-305.

IPCC, 2013: Technical Summary. In: *Climate Change 2013 – The Physical Science Basis: Working Group I Contribution to the Fifth Assessment Report of the Intergovernmental Panel on Climate Change.* Cambridge: Cambridge University Press, pp 31-116.

IPCC, 2018: Summary for Policymakers. In: *Global warming of 1.5°C. An IPCC Special Report on the impacts of global warming of 1.5°C above pre-industrial levels and related global greenhouse gas emission pathways, in the context of strengthening the global response to the threat of climate change, sustainable development, and efforts to eradicate poverty* [V. Masson-Delmotte, P. Zhai, H. O. Pörtner, D. Roberts, J. Skea, P. R. Shukla, A. Pirani, W. Moufouma-Okia, C. Péan, R. Pidcock, S. Connors, J. B. R. Matthews, Y. Chen, X. Zhou, M. I. Gomis, E. Lonnoy, T. Maycock, M. Tignor, T. Waterfield (eds.)]. World Meteorological Organization, Geneva, Switzerland, 32 pp.

Jackson, R.D. and Huete, A.R. 1991. Interpreting vegetation indices. *Preventive veterinary medicine*, 11(3-4), pp 185-200.

Johnson, M.R., Anhaeusser, C.R. and Thomas, R.J. (Eds.) 2006. *The Geology of South Africa*, Geological Society of South Africa and Council for Geoscience, Pretoria.

Jumaat, N.F.H., Ahmad, B. and Dutsenwai, H.S. 2018, June. Land cover change mapping using high resolution satellites and unmanned aerial vehicle. In *IOP Conference Series: Earth and Environmental Science* (Vol. 169, No. 1, p. 012076). IOP Publishing.

Kerle, N., Janssen, L.L. and Huurneman, G.C. 2004. Principles of remote sensing. *ITC, Educational textbook series*, 2, 540 pp.

Khosravi, H., Haydari, E., Shekoohizadegan, S. and Zareie, S. 2017. Assessment the effect of drought on vegetation in desert area using landsat data. *The Egyptian Journal of Remote Sensing and Space Science,* 20, pp S3-S12.

Klak, C. & Raimondo, D. 2006. Drosanthemum micans (L.) Schwantes. National Assessment: Red List of South African Plants version 2017.1. (Accessed on 11/09/2018).

Klove, B., Ala-Aho, P., Bertrand, G., Boukalova, Z., Ertürk, A., Goldscheider, N., Ilmonen, J., Karakaya, N., Kupfersberger, H., Kvœrner, J. and Lundberg, A. 2011. Groundwater dependent ecosystems. Part I: Hydroecological status and trends. *Environmental Science & Policy*, 14(7), pp 770-781.

Kongo, E. and Pavlique, U. 2015. *Urban land cover classification from high resolution Geoeye-1 imagery using a Lidarbased digital surface model.* MSc Thesis, Stellenbosch University, Stellenbosch.

Kotzé, I.J. and Fairall, N. 2006. Using Landsat TM imagery to map fynbos plant communities: a case study. *South African Journal of Wildlife Research-24-month delayed open access,* 36(1), pp 75-87.

Kraaij, T. and Milton, S.J. 2006. Vegetation changes (1995–2004) in semi-arid Karoo shrubland, South Africa: effects of rainfall, wild herbivores and change in land use. *Journal of Arid Environments,* 64(1), pp 174-192.

Laliberte, A.S., Koppa, J., Fredrickson, E.L. and Rango, A. 2006, July. Comparison of nearest neighbor and rule-based decision tree classification in an object-oriented environment. In *Proceedings of IEEE international Geoscience and Remote Sensing Symposium, Denver, Colorado, USA* (pp 3923-3926).

Lanfri, S. 2010. *Vegetation analysis using remote sensing*. M.A. Cordoba National University.

Langley, S.K., Cheshire, H.M. and Humes, K.S. 2001. A comparison of single date and multi-temporal satellite image classifications in a semi-arid grassland. *Journal of Arid Environments,* 49(2), pp 401-411.

Le Maitre, D.C., Scott, D.F. and Colvin, C. 1999. A review of information on interactions between vegetation and groundwater. *Water SA*, Vol 25, No 2. pp 137-152.

Le Maitre, D., Colvin, C. and Maherry, A. 2009. Water resources in the Klein Karoo: the challenge of sustainable development in a water-scarce area. *South African Journal of Science*, 105(1-2), pp 39-48.

Letts, M.G., Johnson, D.R. and Coburn, C.A. 2010. Drought stress ecophysiology of shrub and grass functional groups on opposing slope aspects of a temperate grassland valley. *Botany,* 88(9), pp 850-866.

Levin, N. 1999. Fundamentals of remote sensing; 1st hydrographic data management course. *IMO—International Maritime Academy: Trieste, Italy*, pp 85-86.

Low, A.B. and Rebelo, A.G. 1996. Vegetation of South Africa, Lesotho and Swaziland. DEAT, Pretoria.

MacKellar, N., New, M. and Jack, C. 2014. Observed and modelled trends in rainfall and temperature for South Africa: 1960-2010. *South African Journal of Science,* 110(7-8), pp 1-13.

Masek, J.G., Vermote, E.F., Saleous N.E., Wolfe, R., Hall, F.G., Huemmrich, K.F., Gao, F., Kutler, J., and Lim, T-K. 2006. A Landsat surface reflectance dataset for North America, 1990–2000. *IEEE Geoscience and Remote Sensing Letters* 3(1), pp 68-72. http://dx.doi.org/10.1109/LGRS.2005.857030.

Masubelele, M.L., Hoffman, M.T., Bond, W.J. and Gambiza, J. 2014. A 50 year study shows grass cover has increased in shrublands of semi-arid South Africa. *Journal of Arid Environments,* 104, pp 43-51.

Matongera, T.N., Mutanga, O., Dube, T. and Sibanda, M. 2017. Detection and mapping the spatial distribution of bracken fern weeds using the Landsat 8 OLI new generation sensor. *International journal of applied earth observation and geo-information,* 57, pp 93-103.

Maxwell, T. 2005. *Object-oriented classification: Classification of Pan-Sharpened QuickBird imagery and a fuzzy approach to improving image segmentation efficiency*. M.Sc.E. thesis, Department of Geodesy and Geomatics Engineering Technical Report No. 233, University of New Brunswick, Federiction, New Brunswick, Canada, 157 pp.

McKee, T.B., Doesken, N.J. and Kleist, J. 1993, January. The relationship of drought frequency and duration to time scales. *In Proceedings of the 8th Conference on Applied Climatology*, 17(22), pp 179-183. Boston, MA: American Meteorological Society.

Midgley, G.F., Chapman, R.A., Hewitson, B., Johnston, P., De Wit, M., Ziervogel, G., Mukheibir, P., Van Niekerk, L., Tadross, M., Van Wilgen, B.W. and Kgope, B. 2005. *A status quo, vulnerability and adaptation assessment of the physical and socio-economic effects of climate change in the Western Cape.* CSIR Report No. ENV-S-C 2005-073, Stellenbosch.

Midgley, G., Rutherford, M. and Bond, W.J. 2001. The Heat is on: Impacts of Climate Change on Plant Diversity in South Africa. *National Botanical Institute, Cape Town, South Africa*.

Milton, S.J., Dean, W.R.J. and Ellis, R.P. 1998. Rangeland health assessment: a practical guide for ranchers in arid Karoo shrublands. *Journal of Arid Environments,* 39(2), pp 253-265.

Moore, I.D., Grayson, R.B. and Ladson, A.R. 1991. Digital terrain modelling: a review of hydrological, geomorphological, and biological applications. *Hydrological processes,* 5(1), pp 3-30.

Mucina, L. and Rutherford, M.C. (eds) 2006. The vegetation of South Africa, Lesotho and Swaziland. *Strelitzia* 19, National Biodiversity Institute, Pretoria.

Münch, Z. and Conrad, J. 2007. Remote sensing and GIS based determination of groundwater dependent ecosystems in the Western Cape, South Africa. *Hydrogeology Journal*, 15(1), pp 19-28.

Murray, A.L. 2015. *A socio-ecological analysis of environmental change in the Kannaland Municipality of the Klein Karoo, South Africa, over the last 100 years*. MSc, University of Cape Town, Cape Twon.

O. Mutanga, T. Dube. and F. Ahmed. 2016. Progress in remote sensing: vegetation monitoring in South Africa. *South African Geographical Journal,* 98(3), pp 461-471, DOI: 10.1080/03736245.2016.1208586.

Parage, V., Vajsova, B., Faget, N. and Astrand, P.J. 2014. *New sensors benchmark report on SPOT 7*. Joint Research Centre and European Commission, Luxembourg, Report EUR 27063 and JRC 93987.

Pauw, T. 2012. *Assessment of SPOT 5 and ERS-2 OBIA for mapping wetlands*. MSc Thesis, Stellenbosch University, Stellenbosch.

Pérez Hoyos, I., Krakauer, N., Khanbilvardi, R. and Armstrong, R. 2016. A review of advances in the identification and characterization of groundwater dependent ecosystems using geospatial technologies. *Geosciences*, 6(2), pp 1-20.

Petersen, C.R., Jovanovic, N.Z., Le Maitre, D.C. and Grenfell, M.C. 2017. Effects of land use change on streamflow and stream water quality of a coastal catchment. *Water SA*, 43(1), pp 139-152.

Peters, D.P., Yao, J., Sala, O.E. and Anderson, J.P. 2012. Directional climate change and potential reversal of desertification in arid and semiarid ecosystems. *Global Change Biology,* 18(1), pp 151-163.

Richardson, S., Ervine, E., Froend, R., Boon, P., Barber, S. and Bonneville, B. 2011. Australian Groundwater-dependent Ecosystem Toolbox Part 1: AssessmentFramework, Waterlines Report. National Water Commission, Canberra http://nwc.gov.au/ data/assets/pdf file/0006/19905/GDE-toolbox-part-1.pdf.

Richard, Y., Martiny, N., Fauchereau, N., Reason, C., Rouault, M., Vigaud, N. and Tracol, Y. 2008. Inter-annual memory effects for spring NDVI in semi-arid South Africa. *Geophysical Research Letters*, 35(13), pp L13704.

Rishmawi, K., Prince, S.D. and Xue, Y. 2016. Vegetation responses to climate variability in the northern arid to sub-humid zones of Sub-Saharan Africa. *Remote Sensing,* 8(11).

River Health Programme. 2007. *State of Rivers Report: Rivers of the Gouritz Water Management Area*. Department of Water Affairs and Forestry, Pretoria ISBN No: 0-620-38676-0.

Roets, W. 2008. *Groundwater Dependence of Aquatic Ecosystems Associated with the Table Mountain Group Aquifer*. PhD Thesis, University of the Western Cape, Bellville.

Rohde, M.M., Froend, R. and Howard, J. 2017. A global synthesis of managing groundwater dependent ecosystems under sustainable groundwater policy. *Groundwate*r, 55(3), pp 293-301.

Rouault, M. & Richard, Y. 2003. Intensity and spatial extension of drought in South Africa at different time scales. *Water SA*, 29(4), pp 489-500.

Roux, P.W. and Vorster, M. 1983. Vegetation change in the Karoo. *Proceedings of the Annual Congresses of the Grassland Society of Southern Africa*, 18(1), pp 25-29.

Rutherford, M.C. and Powrie, L.W. 2013. Impacts of heavy grazing on plant species richness: A comparison across rangeland biomes of South Africa. *South African Journal of Botany,* 87, pp 146-156.

Rutherford, M.C. and Westfall, R.H. 1994. Biomes of southern Africa: an objective characterization. *Memoirs of the botanical survey of South Africa*, 54, pp 1-98.

Sánchez, N., González-Zamora, Á., Piles, M. and Martínez-Fernández, J. 2016. A new Soil Moisture Agricultural Drought Index (SMADI) integrating MODIS and SMOS products: A case of study over the Iberian Peninsula. *Remote Sensing*, 8(287), 25 pp.

Schulze, R.E. 2007. *Coefficient of Variation of Annual Precipitation*. In: Schulze, R.E. (Ed). 2007. South African Atlas of Climatology and Agrohydrology. Water Research Commission, Pretoria, RSA, WRC Report 1489/1/06, Section 6.3.

Schulze, R.E. 2011. *Climate Change and the South African Water Sector: Terminology*. In: Schulze, R.E. 2011. A 2011 Perspective on Climate Change and the South African Water Sector. Water Research Commission, Pretoria, RSA, WRC Report TT 518/12, Chapter 1.3, pp 13 -17.

Scott, D.F. and Le Maitre, D.C. 1998. *The interaction between vegetation and groundwater: Research Priorities for South Africa.* WRC Report No 730/1/98.

Smith, R.M.H. 1990. A review of stratigraphy and sedimentary environments of the Karoo Basin of South Africa. *Journal of African Earth Sciences (and the Middle East),* 10(1-2), pp 117-137.

Thenkabail, P.S., Enclona, E.A., Ashton, M.S., Legg, C. and De Dieu, M.J. 2004. Hyperion, IKONOS, ALI, and ETM+ sensors in the study of African rainforests. *Remote Sensing of Environment,* 90(1), pp 23-43.

Truc, L., Chevalier, M., Favier, C., Cheddadi, R., Meadows, M.E., Scott, L., Carr, A.S., Smith, G.F. and Chase, B.M. 2013. Quantification of climate change for the last 20,000 years from Wonderkrater, South Africa: implications for the long-term dynamics of the Intertropical Convergence Zone. *Palaeogeography, Palaeoclimatology, Palaeoecology,* 386, pp 575-587.

Turyahikayo, A.K. 2014. *Analyzing multi-temporal vegetation density in the upper Molopo river catchment using remote sensing techniques*. MSc, North-West University.

Tweed, S.O., Leblanc, M., Webb, J.A. and Lubczynski, M.W. 2007. Remote sensing and GIS for mapping groundwater recharge and discharge areas in salinity prone catchments, south-eastern Australia. *Hydrogeology Journal,* 15(1), pp 75-96.

Tyler, G. 2001. Relationships between climate and flowering of eight herbs in a Swedish deciduous forest. *Annals of Botany,* 87(5), pp 623-630.

Vermote, E., Justice, C., Claverie, M. and Franch, B. 2016. Preliminary analysis of the performance of the Landsat 8/OLI land surface reflectance product. *Remote Sensing of Environment,* 185, pp 46-56.

Vinod, K.V.K. and Kamal, J. 2010. Development of Spectral Signatures and Classification of Sugarcane using ASTER Data. *International Journal of Computer Scince & Communication*, 1, pp 245-251.

Visser, J.N.J. 1986. Lateral lithofacies relationships in the glacigene Dwyka Formation in the western and central parts of the Karoo Basin. *Transactions of the Geological Society of South Africa*, 89, pp 373-383.

Vlok, J.H.J., Cowling, R.M. & Wolf, T. 2005. *A vegetation map for the Little Karoo*. Unpublished maps and report for a SKEP project supported by CEPF grant no 1064410304.

Vorster, L. 2017. *Current status and impact (2004-2015) of indigenous ungulate herbivory on the vegetation of Sanbona Wildlife Reserve in the Little Karoo.* MSc Thesis, University of Cape Town, Cape Town.

Wei, W., Chen, X. and Ma, A. 2005, July. Object-oriented information extraction and application in high-resolution remote sensing image. In *Geoscience and Remote Sensing Symposium, 2005. IGARSS'05. Proceedings. 2005 IEEE International* (Vol. 6, pp 3803-3806). IEEE.

Wessels, K. 2008. Modelling vegetation phenology from 20 years' daily satellite data: statistical modelling. *CSIR Science Scope,* 2(4), pp 58-59.

Whitecross, M.A., Archibald, S. and Witkowski, E.T.F. 2012. Do freeze events create a demographic bottleneck for Colophospermum mopane? *South African Journal of Botany*, 83, pp 9-18.

World Meteorological Organization, 2012: *Standardized Precipitation Index User Guide* (M. Svoboda, M. Hayes and D. Wood). (WMO-No. 1090), Geneva.

Xie, Y., Sha, Z. and Yu, M. 2008. Remote sensing imagery in vegetation mapping: a review. *Journal of plant ecology*, 1(1), pp 9-23.

Xue, J. and Su, B. 2017. Significant remote sensing vegetation indices: A review of developments and applications. *Journal of Sensors*, 2017, pp 1-17.

Xu, X., Yang, D. and Sivapalan, M. 2012. Assessing the impact of climate variability on catchment water balance and vegetation cover. *Hydrology and Earth System Sciences*, 16(1), pp 43-58.

Zaimes, G., Nichols, M., Green, D. and Crimmins, M. 2007. *Understanding Arizona's riparian areas*. College of Agriculture and Life Sciences, University of Arizona (Tucson, AZ).

Zargar, A., Sadiq, R., Naser, B. and Khan, F.I. 2011. A review of drought indices. *Environmental Reviews,* 19(NA), pp 333-349.

Zencich, S.J., Froend, R.H., Turner, J.V. and Gailitis, V. 2002. Influence of groundwater depth on the seasonal sources of water accessed by Banksia tree species on a shallow, sandy coastal aquifer. *Oecologia,* 131(1), pp 8-19.

Zhou, Y., Wenninger, J., Yang, Z., Yin, L., Huang, J., Hou, L., Wang, X., Zhang, D. and Uhlenbrook, S. 2013. Groundwater–surface water interactions, vegetation dependencies and implications for water resources management in the semi-arid Hailiutu River catchment, China–a synthesis. *Hydrology and Earth System Sciences,* 17(7), pp 2435-2447.

APPENDIX A – Sample plant species collected during the survey.

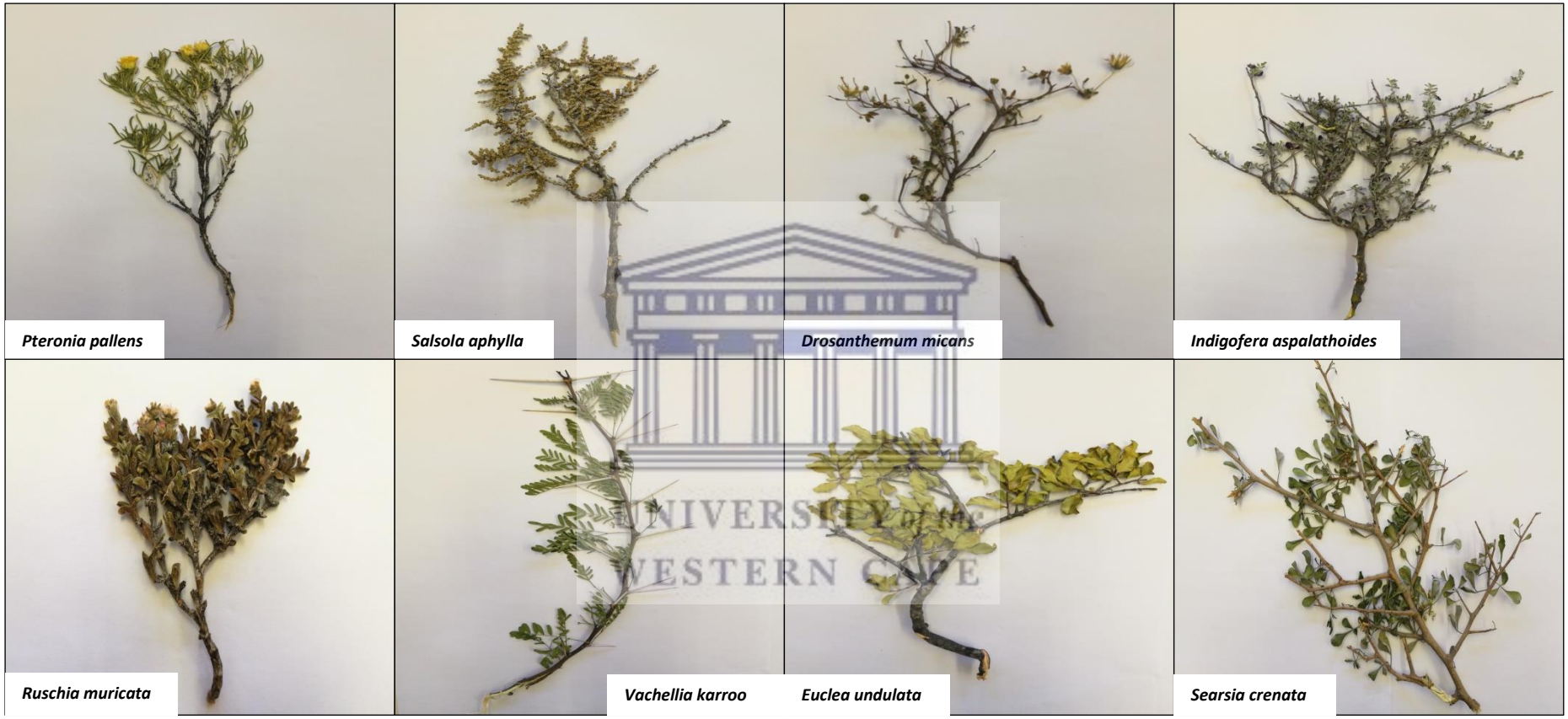

Figure A1: The dominant plant species identified during the field survey in each sample plot.

* *Anchusa capensis* sample faded shortly after the survey period and therefore could not be photographed. The image above was obtained from the SANBI webpage.

APPENDIX B – Spectral and spatial characteristics of the used satellite sensors with acquisition dates.

Table B1: Characteristics of the satellite sensors and scene dates.

Satellite Sensor	Scene ID	Projection	Datum	Date Acquired	Cloud Cover%	Path & Row	Bands used	Resolution (m)	Wavelength (Micrometers)
Landsat TM	LT51740831996315JSA00	UTM	WGS84	1996-11-10	0.00	174/83	3	30	0.63-0.69
	LT51740831997013JSA00			1997-01-13	0.00		4	30	0.76-0.90
	LT51740831997029JSA00			1997-01-29	5.00				
	LT51740831997045JSA00			1997-02-14	0.00				
	LT51740831997061JSA00			1997-03-02	1.00				
	LT51740831997141JSA00			1997-05-21	6.00				
	LT51740831997189JSA00			1997-07-08	0.00				
	LT51740831997253JSA00			1997-09-10	0.00				
	LT51740831997269JSA00			1997-09-26	0.00				
	LT51740831997349JSA00			1997-12-15	0.00				
	LT51740831998032JSA00			1998-02-01	0.00				
	LT51740831998080JSA00			1998-03-21	8.00				
	LT51740831998192JSA00			1998-07-11	4.00				
	LT51740831999019JSA01			1999-01-19	1.00				
	LT51740831999035JSA00			1999-02-04	1.00				
	LT51740831999131JSA00			1999-05-11	0.00				
	LT51740831999163JSA00			1999-06-12	0.00				
	LT51740832000022JSA00			2000-01-22	21.00				
	LT51740832000134JSA00			2000-05-13	0.00				
	LT51740832000294JSA00			2000-10-20	4.00				
	LT51740832000310JSA00			2000-11-05	4.00				
	LT51740832000358JSA00			2000-12-23	0.00				
	LT51740832004033JSA00			2004-02-02	0.00				
	LT51740832004081JSA03			2004-03-21	0.00				
	LT51740832004161JSA00			2004-06-09	4.00				
	LT51740832004177JSA00			2004-06-25	0.00				
	LT51740832004193JSA00			2004-07-11	1.00				
	LT51740832005195JSA00			2005-07-14	12.00				
	LT51740832005323JSA02			2005-11-19	0.00				
	LT51740832006102JSA00			2006-04-12	0.00				

	LT51740832006118JSA00			2006-04-28	0.00				
	LT51740832006182JSA00			2006-07-01	0.00				
	LT51740832006230JSA00			2006-08-18	1.00				
	LT51740832006278JSA00			2006-10-05	11.00				
	LT51740832006310JSA00			2006-11-06	0.00				
	LT51740832006358JSA00			2006-12-24	3.00				
	LT51740832007153JSA00			2007-06-02	0.00				
	LT51740832007185JSA00			2007-07-04	0.00				
	LT51740832007217JSA00			2007-08-05	0.00				
	LT51740832008044JSA01			2008-02-13	0.00				
	LT51740832009126JSA01			2009-05-06	0.00				
	LT51740832009142JSA01			2009-05-22	8.00				
	LT51740832010097JSA00			2010-04-07	4.00				
	LT51740832011100JSA00			2011-04-10	2.00				
	LC81740832013249LGN01			2013-09-06	0.13				
	LC81740832013265LGN01			2013-09-22	0.26				
	LC81740832013297LGN01			2013-10-24	16.04				
	LC81740832013329LGN01			2013-11-25	0.83				
	LC81740832014076LGN01			2014-03-17	0.57				
	LC81740832014108LGN01			2014-04-18	0.90				
	LC81740832014172LGN01			2014-06-21	0.02				
	LC81740832014188LGN01			2014-07-07	0.97				
	LC81740832014236LGN01			2014-08-24	0.04				
	LC81740832014268LGN01			2014-09-25	0.20				
Landsat OLI	LC81740832014284LGN01	UTM	WGS84	2014-10-11	1.08	174/83	4 5	30 30	0.64-0.67 0.85-0.88
	LC81740832014348LGN01			2014-12-14	8.05				
	LC81740832015015LGN01			2015-01-15	0.05				
	LC81740832015079LGN01			2015-03-20	0.03				
	LC81740832015127LGN01			2015-05-07	0.17				
	LC81740832015159LGN01			2015-06-08	0.01				
	LC81740832015191LGN01			2015-07-10	16.05				
	LC81740832015239LGN01			2015-08-27	27.70				
	LC81740832015335LGN01			2015-12-01	6.39				
	LC81740832015351LGN01			2015-12-17	0.00				
	LC81740832016002LGN02			2016-01-02	0.04				

	LC81740832016098LGN01			2016-04-07	11.60				
	LC81740832016146LGN01			2016-05-25	0.01				
	LC81740832016242LGN01			2016-08-29	2.17				
	LC81740832016258LGN01			2016-09-14	7.87				
	LC81740832016338LGN01			2016-12-03	0.00				
	LC81740832017004LGN01			2017-01-04	5.82				
	LC81740832017084LGN00			2017-03-25	0.16				
	LC81740832017100LGN00			2017-04-10	1.23				
	LC81740832017164LGN00			2017-06-13	11.24				
	LC81740832017180LGN00			2017-06-29	1.04				
	LC81740832017244LGN00			2017-09-01	0.01				
	LC81740832017276LGN00			2017-10-03	5.56				
	LC81740832017340LGN00			2017-12-06	2.22				
SPOT 7	P_201707170813440_ORT_SPOT7_20180806			2017-07-17				1.5	
	MS_201707170813440_ORT_SPOT7_20180806							6.0	
	P_201711300820370_ORT_SPOT6_20180806			2017-09-13				1.5	
	MS_201711300820370_ORT_SPOT6_20180806							6.0	
WorldView-2	057595185010_01_P001_MUL	UTM	WGS84	2017-10-28	0.00		1-4	2.0	
	057595185010_01_P001_PAN							50 cm	
	057595185010_01_P002_MUL							2.0	
	057595185010_01_P002_PAN							50 cm	
	057595185010_01_P003_MUL							2.0	
	057595185010_01_P003_PAN							50 cm	